Check for updates

Reviews of Geophysics

REVIEW ARTICLE
10.1029/2020RG000711

Key Points:

- Almost two decades are available of satellite measurements of multiple carbon and water tracers for quantifying tropical carbon and water states, fluxes, and interactions
- Substantial progress has been made in quantifying the role of water variability on carbon variability in the wet and dry tropics
- Satellite data provide evidence of the role of vegetation on the water cycle
- New measurements are needed of key states and fluxes controlling C/W interactions (e.g. soil moisture, evapotranspiration, soil carbon and respiration) to reduce uncertainty in the tropical carbon sink and its evolution
- Models that can integrate this wealth of data are needed to infer the hidden processes controlling carbon and water

Correspondence to:
J. Worden,
john.r.worden@jpl.nasa.gov

Citation:
Worden, J., Saatchi, S., Keller, M., Bloom, A., Liu, J., Parazoo, N., et al. (2021). Satellite observations of the tropical terrestrial carbon balance and interactions with the water cycle during the 21st century. *Reviews of Geophysics*, *59*, e2020RG000711. https://doi.org/10.1029/2020RG000711

Received 6 MAY 2020
Accepted 13 JAN 2021

Author Contributions:
Conceptualization: John Worden, Sassan Saatchi, Michael Keller, David Schimel
Data curation: John Worden

© 2021. Jet Propulsion Laboratory, California Institute of Technology. Government sponsorship acknowledged.
This is an open access article under the terms of the Creative Commons Attribution-NonCommercial License, which permits use, distribution and reproduction in any medium, provided the original work is properly cited and is not used for commercial purposes.

Satellite Observations of the Tropical Terrestrial Carbon Balance and Interactions With the Water Cycle During the 21st Century

John Worden[1], Sassan Saatchi[1], Michael Keller[1,2,3], A. Anthony Bloom[1], Junjie Liu[1], Nicholas Parazoo[1], Joshua B. Fisher[1], Kevin Bowman[1,12], John T. Reager[1], Kristen Fahy[1], David Schimel[1], Rong Fu[4], Sarah Worden[4], Yi Yin[5], Pierre Gentine[6], Alexandra G. Konings[7], Gregory R. Quetin[7], Mathew Williams[8], Helen Worden[9], Mingjie Shi[4,10], and Armineh Barkhordarian[1,11]

[1]Jet Propulsion Laboratory, California Institute of Technology, Pasadena, CA, USA, [2]U.S. Department of Agriculture Forest Service, International Institute of Tropical Forestry, Campinas, Brazil, [3]EMBRAPA Agricultural Informatics, Campinas, Brazil, [4]University of California Los Angeles, Los Angeles, CA, USA, [5]California Institute for Technology, Geological and Planetary Science, Pasadena, CA, USA, [6]Columbia University, New York, NY, USA, [7]Department of Earth System Science, Stanford University, Stanford, CA, USA, [8]University of Edinburgh and National Centre for Earth Observation, Edinburgh, UK, [9]National Center for Atmospheric Research, Boulder, CO, USA, [10]Pacific Northwest National Labs, [11]University of Hamburg, Hamburg, Germany, [12]Joint Institute for Regional Earth System Science and Engineering (JIFRESSE), University of California, Los Angeles, USA

Abstract A constellation of satellites is now in orbit providing information about terrestrial carbon and water storage and fluxes. These combined observations show that the tropical biosphere has changed significantly in the last 2 decades from the combined effects of climate variability and land use. Large areas of forest have been cleared in both wet and dry forests, increasing the source of carbon to the atmosphere. Concomitantly, tropical fire emissions have declined, at least until 2016, from changes in land-use practices and rainfall, increasing the net carbon sink. Measurements of carbon stocks and fluxes from disturbance and recovery and of vegetation photosynthesis show significant regional variability of net biosphere exchange and gross primary productivity across the tropics and are tied to seasonal and interannual changes in water fluxes and storage. Comparison of satellite based estimates of evapotranspiration, photosynthesis, and the deuterium content of water vapor with patterns of total water storage and rainfall demonstrate the presence of vegetation-atmosphere interactions and feedback mechanisms across tropical forests. However, these observations of stocks, fluxes and inferred interactions between them do not point unambiguously to either positive or negative feedbacks in carbon and water exchanges. These ambiguities highlight the need for assimilation of these new measurements with Earth System models for a consistent assessment of process interactions, along with focused field campaigns that integrate ground, aircraft and satellite measurements, to quantify the controlling carbon and water processes and their feedback mechanisms.

Plain Language Summary Changes to the carbon sequestered in tropical forests and soils, as a result of human activities and changes in rainfall, temperature, and CO_2 concentrations, have a substantial impact on Earth's climate. This review summarizes recent results highlighting how the constellation of satellites now in orbit are providing new understanding of the tropical carbon cycle and how it interacts with climate variability through the water cycle, and how satellite data can be used to improve our process description of the Earth System.

1. Introduction

The distribution of temperature and precipitation of the Earth system depends on atmospheric CO_2 concentrations, which in turn are related to the amount of fossil emissions and the amount of CO_2 taken up by the terrestrial and oceanic carbon sinks. The tropical biosphere, being the largest above-ground reservoir of carbon (Houghton, 2005), is therefore intrinsically coupled to the fate of the Earth system. Prior to the 21st century, most changes in tropical forests were dominated by land use (Nobre et al., 1991; Santilli et al., 2005; Skole & Tucker, 1993). However, moving into the 21st century, a series of large-scale droughts caused by

Funding acquisition: John Worden, Sassan Saatchi, Kevin Bowman
Project administration: John Worden, Sassan Saatchi, Michael Keller, Kristen Fahy
Software: Armineh Barkhordarian, Mingjie Shi
Supervision: John Worden, Sassan Saatchi, Michael Keller
Visualization: Armineh Barkhordarian, Mingjie Shi
Writing – original draft: John Worden, Sassan Saatchi, Michael Keller, Anthony Bloom, Junjie Liu, Nicholas Parazoo, Joshua B. Fisher, Kevin Bowman, John T. Reager, Rong Fu, Sarah Worden, Yi Yin, Pierre Gentine, Alexandra G. Konings, Gregory R. Quetin, Mathew Williams, Helen Worden
Writing – review & editing: John Worden, Sassan Saatchi, Michael Keller, Anthony Bloom, Junjie Liu, Nicholas Parazoo, Joshua B. Fisher, Kevin Bowman, John T. Reager, Kristen Fahy, David Schimel, Rong Fu, Sarah Worden, Yi Yin, Pierre Gentine, Alexandra G. Konings, Gregory R. Quetin, Mathew Williams, Helen Worden, Mingjie Shi, Armineh Barkhordarian

sea surface temperature (SST) anomalies of the El Niño Southern Oscillation (1997–1998, 2015–2016), and in the Tropical North Atlantic (2005, 2010; Marengo et al., 2005, 2010, 2015) have increased the role of climate variability on tropical forest change. Observations therefore suggest that climate change and variability are as important as land use, and possibly fertilization effects from increasing atmospheric CO_2, in defining the current and future state of the tropical biosphere (Exbrayat et al., 2017; Gentine et al., 2019; Schimel et al., 2015).

As these changes are impacting the current state and function of tropical forests, Earth System models (ESMs) are predicting an intensification of hydrological and biogeochemical cycles (e.g., Fung et al., 2005; Green et al., 2019; Neelin et al., 2006), largely due to feedbacks between the carbon, water, and energy cycles (Bonan, 2008; Bonan & Doney, 2018; Davidson et al., 2012; Kurz et al., 2008; Pires & Costa, 2013). However, these predictions have significant uncertainty because the full complexity of interactions and feedback mechanisms between biogeochemical cycles is not adequately represented or constrained with observations in terrestrial biosphere models (e.g., Risi et al., 2013; Sellers et al., 2018 and references therein). A consequence of poorly understood feedbacks and lack of observations is that ESMs predict a range of possible trajectories in carbon stocks and fluxes varying not only in magnitude but even in sign, suggesting tropical CO_2 sinks with both positive and negative future trends (e.g., Friedlingstein et al., 2006, 2014a).

Our understanding of the underlying processes controlling these feedbacks has been primarily informed by sparse measurements of surface flux data used directly in the models or upscaled to the whole tropics using temperature and rainfall data (e.g., M. Jung et al., 2017; W. Wang et al., 2013). A constellation of satellites are now in orbit with measurements that allow us to infer the fluxes and states of carbon and water at a variety of spatio-temporal scales (Figure 1 and Appendices). These measurements, provide a 10–20-year record of the changing tropical carbon and water cycles and are providing new insights into how these changes impact tropical forest structure, productivity, and net exchange of carbon and water with the atmosphere. Examining the covariations of these data provide understanding of how climatic (e.g., anomaly and trends of rainfall and temperature) and anthropogenic (e.g., land use) changes controls these processes, their interactions, and feedbacks.

Our objective in this review is to evaluate how satellite observations have informed our understanding of tropical forests' carbon cycle and its link to climate in general and the water cycle in particular. We choose the period of 2001–2016 as it spans the period with the largest number of satellite observations, although different satellites have different start and end times within this period. We examine changes in the moist and dry tropics between 30°S and 25°N across the three continents during this period (Figure 2). As part of this review we summarize unresolved processes at global scales that continue to contribute large uncertainties to the global carbon cycle. There is also now an important opportunity to enhance the calibration of ESM parameters and quantify their errors using the wealth these satellite records in order to reduce uncertainties of the underlying processes and improve predictive skill. The data assimilation methods needed to undertake such calibrations are now available and in part demonstrated in this review.

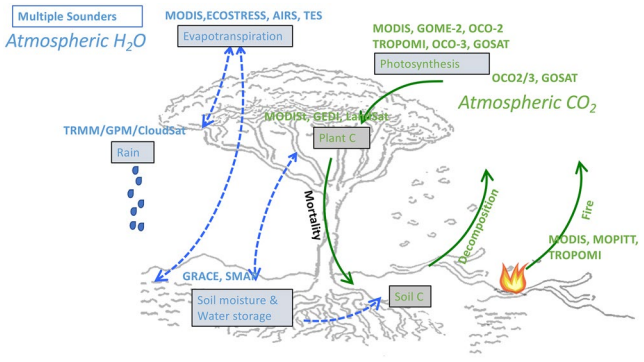

Figure 1. Schematic of the flow of carbon (green) and water (blue) in the terrestrial biosphere and different satellite instruments that can place constraints on these fluxes.

The paper is divided into five sections. Section 1 is the introduction. Section 2 focuses on recent results on carbon storage, productivity, and fluxes from climate variability, land use activities, and fire both from bottom-up and top-down remote sensing techniques. Section 3 summarizes recent results demonstrating the links between the tropical carbon and water cycles as well as discussing changes in key water states observed by satellite and how they might affect tropical carbon balance. In Section 4, we discuss a number of additional underlying processes and feedbacks that remain poorly observed and hence have large uncertainty. In Section 5, we discuss how integrating and assimilating satellite observations into terrestrial biosphere models may better constrain these processes to ensure consistency in the inferred feedback mechanisms. This section also provides examples for combining observations with a new class of models that can assimilate these data for quantifying carbon/water interactions (e.g., Bloom et al., 2020; T. Schneider et al., 2017). Finally, we make recommendations on new observations, joint satellite/aircraft/ground field campaigns and model/assimilation development in Section 6.

19449208, 2021, 1, Downloaded from https://agupubs.onlinelibrary.wiley.com/doi/10.1029/2020RG000711, Wiley Online Library on [10/11/2025]. See the Terms and Conditions (https://onlinelibrary.wiley.com/terms-and-conditions) on Wiley Online Library for rules of use; OA articles are governed by the applicable Creative Commons License

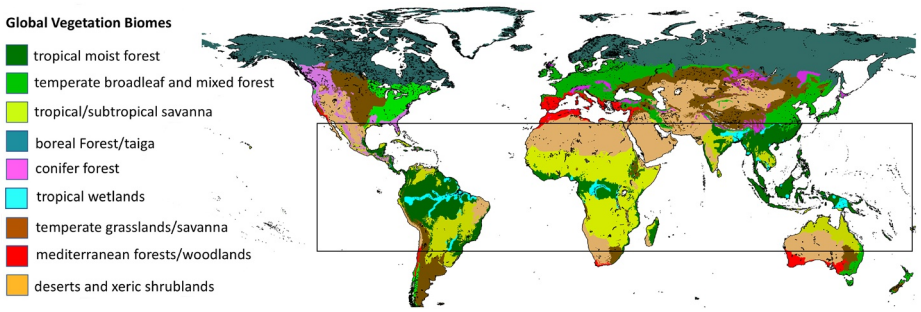

Figure 2. The global biome distribution. The tropical region discussed in this paper is highlighted by the rectangle.

This review pays less attention to several important processes that impact carbon and water cycling of tropical forests in order to keep the length and scope of the paper reasonable because the topics are well-covered by other reviews, or because there is only limited information from remote sensing. We neglect the energy and nutrient cycles, except when discussing their links to the carbon and water cycles (e.g., Cleveland et al., 2011, 2013 and refs therein). Aerosols from biogenic emissions and fires also have substantive effects on water cycling and radiation (e.g., Andreae et al., 2004; Rosenfeld et al., 2014, Poeschi et al., 2015). Tropical methanogenesis processes and resulting methane fluxes from large-scale permanently are an important component of carbon/water cycling and these processes are discussed in a number of articles (Ganeson et al., 2019; Melack et al., 2004; Richey et al., 2002; Parker et al., 2018). Phenology has been studied using different remote sensing techniques across the tropics and the influence of climate, composition, structure and light conditions, and nutrients have been explored at local to regional scales (Myneni et al., 2007; Saleska et al., 2003; Wu et al., 2016; L. Xu et al., 2015). Other components of water and carbon fluxes such as the lateral flow of carbon through tropical aquatic systems, peatlands or soil carbon fluxes are not discussed in the review due to the difficulty of using existing remote sensing approaches, although we highlight the uncertainties in these fluxes in Section 4.

2. Satellite Based Estimates of Carbon Stocks, Photosynthesis, and Net Biosphere Exchange

Atmospheric CO_2 records suggest that the land surface has acted as a strong global carbon sink over the recent decades, mitigating about 30% of fossil fuel emissions (e.g., Friedlingstein et al., 2019 and refs therein). A substantial fraction of this sink is located in the tropics (Brienen et al., 2015; Stephens et al., 2007). However, it is uncertain how the terrestrial carbon sink evolves as climate and atmospheric composition continue to change because of anthropogenic emissions (Friedlingstein et al., 2006). In fact, the recent changes in climate across tropical forests, with increasing extreme dry and wet conditions accompanied by large-scale deforestation and degradation may have significantly impacted the tropical ecosystem carbon storage and fluxes (Lewis et al., 2011; O. L. Phillips et al., 2009; Y. Yang et al., 2018). Nevertheless, there is a large uncertainty in quantifying the carbon balance in tropical forests, which in turn is believed to be the largest uncertainty in the global terrestrial carbon budget (Houghton, 2005; Houghton & Nassikas, 2017). The sources of these uncertainties are attributed to: (1) difficulties in estimating carbon stored in tropical forests, (2) inaccuracy in predicted rates of forest disturbance in the form of human induced deforestation, degradation (including fires), and climate driven loss of carbon from droughts, and (3) difficulties in predicting rates of carbon uptake due to post-disturbance recovery, changes in soil moisture, or increased atmospheric CO_2. The relative importance of each of these components is not known, but it is assumed that all three sources of uncertainty contribute about equally to the difficulties in estimating carbon budgets in the tropics (Houghton et al., 2009). Complicating our understanding of this partitioning of the carbon balance of tropical forests are the significant seasonal and inter-annual variations that have been attributed to regional climate variability in the form of droughts and floods which adversely impacts tree mortality and productivity (Brienen et al., 2015; Kim et al., 2012; Restrepo-Coupe et al., 2013). Satellite observations of tropical forests have contributed significantly to reducing these uncertainties, as discussed next.

19449208, 2021, 1, Downloaded from https://agupubs.onlinelibrary.wiley.com/doi/10.1029/2020RG000711, Wiley Online Library on [10/11/2025]. See the Terms and Conditions (https://onlinelibrary.wiley.com/terms-and-conditions) on Wiley Online Library for rules of use; OA articles are governed by the applicable Creative Commons License

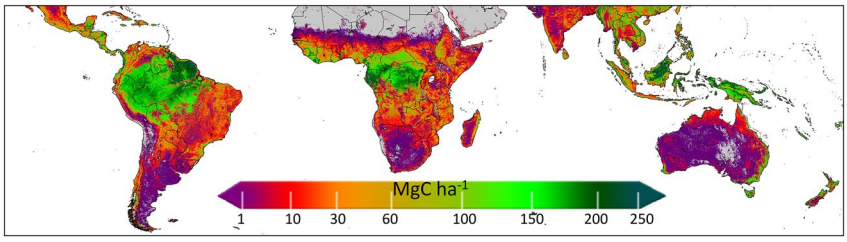

Figure 3. Distribution of above ground live biomass carbon density and uncertainty. (see Appendix A for description of data used to generate this map).

2.1. Carbon Stored in Tropical Forests

Estimates of above-ground carbon stored in live tropical forests vary between 180 and 300 Pg C (Baccini et al., 2012; Bar-On et al., 2018; Malhi et al., 2010; S. S. Saatchi et al., 2011), depending on the period of the data, variations of the extent of forest cover, models for converting remote sensing measurements of forest structure to biomass, and the contribution from soil carbon. However, one of the largest source of uncertainty in the estimates is due to the lack of forest inventory data, unlike in most temperate forest ecosystems (Schimel et al., 2015). Tropical regions are therefore grossly under-sampled by comparison to forests in mid-latitudes, suggesting a potentially large bias in estimating global carbon storage and fluxes. In the absence of systematic national forest inventory data over tropical forests, there have been several attempts in using remote sensing data along with existing networks of research plots to estimate forest above-ground biomass and its spatial distribution. Recent published estimates using this approach, have different spatial resolutions, cover different periods, (e.g., Hansen et al., 2010; Baccini et al., 2012; S. S. Saatchi et al., 2011; Carreiras et al., 2017), and exhibit some differences in spatial patterns (Mitchard et al., 2013). Nevertheless, they converge in providing, for the first time, regional estimates of carbon stored in the live vegetation (above and below ground) across all tropical forests. These maps have used spaceborne light detection and ranging (LIDAR) observations from the Geoscience Laser Altimeter System (GLAS) onboard the ICESAT-1 satellite to sample forest structure distributed across the tropics. The methodologies differ in their use of other satellite imagery for mapping and a variety of parametric or non-parametric algorithms in estimating the spatial distribution of carbon stocks (Mitchard et al., 2013; L. Xu et al., 2016). Spaceborne LIDAR samples are considered the most reliable source of information for quantifying forest structure and estimating above-ground biomass. The GLAS LIDAR provided more than eight million cloud-free samples from 2003 to 2008 in a relatively systematic sampling of vertical structure of forests along its orbital tracks (S. Saatchi et al., 2015).

Figure 3 presents a map of forest stock to demonstrate how these different measurements can be used with machine learning approaches to advance our knowledge of above ground biomass. This map of forest stock is developed from a synthesis of existing methodologies and an extensive set of *in-situ* measurements for calibration of remote sensing data to above-ground biomass and total vegetation carbon stock. This carbon map of tropical vegetation improves upon previous similar products by including wood density variations across tropical forests in modeling the LIDAR to biomass, integrating L-band radar measurements (ALOS PALSAR) in spatial modeling that improves biomass estimation in woodlands and dry forests, and adding a large number of recently acquired airborne LIDAR data to improve the potential systematic errors in spatial patterns of biomass. The map is global and provides a significant improvement over previous products in terms of spatial resolution (100 m) to allow assessment of carbon emissions and uptakes at the scale where land use and other disturbances occur (See Appendix A.1). A coarser-resolution (1 km), static version of this carbon map has been used in several studies for quantifying carbon fluxes directly or as a constraint in earth system models (Carlson et al., 2017; L. Fan et al., 2019; Wei et al., 2017).

However, in most cases, these maps may have a systematic error in areas of very high biomass in the tropics due to the limited sensitivity of existing satellite observations. With the new observations from NASA's Global Ecosystem Dynamics Investigation (GEDI) satellite LIDAR sensor, with more than three orders of magnitude improvements in sample size and sample quantity compared to GLAS LIDAR (Hancock et al., 2018), estimates of tropical forest carbon distribution will improve significantly in near future.

19449208, 2021, 1, Downloaded from https://agupubs.onlinelibrary.wiley.com/doi/10.1029/2020RG000711, Wiley Online Library on [10/11/2025]. See the Terms and Conditions (https://onlinelibrary.wiley.com/terms-and-conditions) on Wiley Online Library for rules of use; OA articles are governed by the applicable Creative Commons License

19449208, 2021, 1, Downloaded from https://agupubs.onlinelibrary.wiley.com/doi/10.1029/2020RG000711, Wiley Online Library on [10/11/2025]. See the Terms and Conditions (https://onlinelibrary.wiley.com/terms-and-conditions) on Wiley Online Library for rules of use; OA articles are governed by the applicable Creative Commons License

NASA-ISRO Synthetic Aperture Radar (NISAR) mission to be launched in 2022 and the European Space Agency BIOMASS radar mission (Quegan et al., 2019) to be launched in 2022–2023 will also provide systematic measurements and estimates of carbon stock and changes across tropics in future and will be able to monitor net carbon fluxes from above-ground disturbance and recovery processes.

2.2. Carbon Emissions from Tropical Forest Loss

Studies focused on the carbon balance in tropical regions are concerned with estimating carbon emissions due to deforestation, timber harvesting, and disturbances associated with fire or droughts. The most common approach is based on carbon book-keeping models that track net carbon emissions based on statistics on approximate information of land use and land cover (LULC) activities reported by countries to United Nations Framework on Climate Change (UNFCCC) or Food and Agricultural Organization (FAO; R. A. Houghton et al., 2000; Houghton, 2007; Le Quéré et al., 2018; Hansis et al., 2015). The book-keeping models focus on land use activities and mostly ignore the impact of climate. These models use many broad assumptions about the fate of cleared lands and their respective carbon stocks to estimate the net carbon impacts (Harris et al., 2012). Recent advances in remote sensing monitoring of forest cover change and maps of carbon stocks has introduced a more direct approach for quantifying emissions from different sources (Harris et al., 2012, 2017). The methodology referred to as the *gain-loss* approach provides estimates of net emissions by multiplying the land use change area estimates, characterized as *activity data*, and estimates of emissions per unit area, characterized by carbon stocks as *emission factors*. This approach requires carbon stocks estimates at the beginning of reference period, and LULC changes during the reference period. At the pantropical scale, recent studies using spatial carbon maps and spatial deforestation monitoring from remote sensing data have improved on estimates of gross emissions by overlaying the deforestation, fire, and any disturbance data on continuous maps of carbon density (Harris et al., 2012). However, these estimates are based on coarse resolution data (18.5 km) derived from the Moderate Resolution Imaging Spectroradiometer (MODIS) time series imagery. With the new Landsat based forest clearing (Hansen et al., 2013) method, the analysis can be performed at 1-km spatial resolution using the pan-tropical carbon stock map for the year 2000 (S. S. Saatchi et al., 2011), improving the estimate of gross emissions from deforestation across tropical forests and their changes (Figure 4). These results suggest that the spatial information on the carbon stocks and forest cover change can readily reduce the uncertainty associated with gross assumptions of average carbon stocks and rates of deforestation that were used in pre-satellite carbon budget calculations (Houghton, 1999). With improvements of the resolution of satellite data on carbon stocks and forest cover change, it is expected that such bottom-up estimation of emissions from land use change in tropics will improve significantly.

In contrast, it is much harder to estimate the area affected by forest degradation, and resulting carbon losses, from satellite observations. This is partly because degradation is caused by a wide variety of processes with different effects, including commercial logging, fuelwood extraction, sub-canopy cultivation, grazing, fire, and edge effects caused by nearby deforestation (Ordway & Asner, 2020; Putz & Redford, 2010). Current estimates of carbon loss from forest degradation in tropical countries can be as large as from deforestation annually (~0.55 PgC/year), from which 53% are from logging, 30% from wood fuel harvest, and 17% from forest fire (Pearson et al., 2017). This large carbon loss is currently obscured from satellite observations and can introduce a significant uncertainty on the tropical forest carbon balance. This large uncertainty points toward the need of satellite observations that permit direct observations of biomass change, as opposed to the combination of activity data and emissions factors, to greatly improve our estimate of carbon losses from degradation and moreover for the recovery of carbon in forests that regenerate following degradation.

Tropical forests have also been losing carbon from tree mortality resulting from extreme water stress from climate anomalies and long-term changes in temperature and rainfall (Lewis et al., 2011; O. L. Phillips et al., 2009). Although moist tropical forests are not considered as a water-limited ecosystem, episodic water stress from droughts have shown to introduce large scale tree mortality, and reduce the net primarily production, leading to a weaker forest carbon sink (Brienen et al., 2015). For instance, in 2010, a drought in Amazonia turned the forest from a net sink to a net source of carbon of approximately 0.5 PgC/year (van der et al., 2015). Dry tropical forests and savanna ecosystems in tropical regions also add significantly to

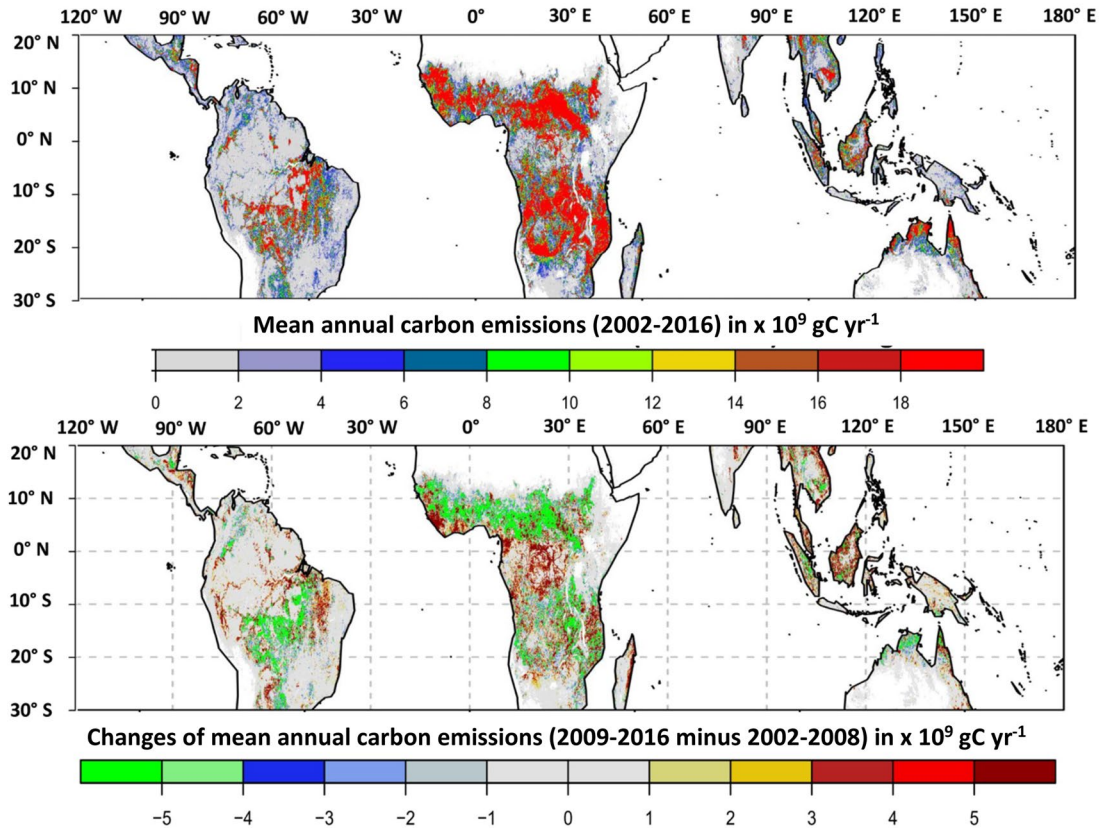

Figure 4. (Top Panel) Total emissions from forest disturbance by combining the land use activities and fires derived from the Landsat time series (Hansen et al., 2013) and MODIS burned area (van der Werf et al., 2017) products. White areas are regions with biomass changes below detection levels. The emissions are calculated at 10 km spatial resolution using the pan-tropical forest carbon map multiplied by annual forest disturbance maps aggregated from high resolution burned areas (500 m) and forest cover change (30 m) data. The global emissions calculated at 10 km and for the period of 2002–2016 were aggregated to develop the mean annual emissions. (Bottom Panel) the average difference between two periods. MODIS, Moderate Resolution Imaging Spectroradiometer.

the interannual variability of the carbon dynamics due to moisture availability, fire, and land use change (Ahlsthrom et al., 2015; Humphrey et al., 2018; Pelletier et al., 2018).

Satellite observations have been able to quantify the carbon loss of both dry and wet tropical forests from water stress and droughts. The methodology has focused on the direct quantification of changes of carbon from drought-induced canopy disturbance and mortality (S. Saatchi et al., 2012; Y. Yang et al., 2018), monitoring the canopy browning or green-up from optical measurements (Saleska et al., 2016; L. Zhou et al., 2014), or quantifying the carbon dynamics from microwave radiometric measurements of vegetation optical depth (Brandt et al., 2018; L. Fan et al., 2019). Top-down approaches from airborne and satellite observations of carbon dioxide and monoxide have also shown the decline in carbon uptake of tropical forests during drought years (Gatti et al., 2014; van der et al., 2015). Aside from changing growth rates, water stress can also increase the rates of tree mortality (e.g., Rowland et al., 2015). Some mortality from water stress lags one or more years after a drought (Doughty et al., 2015; Ito et al., 2012; Y. Yang et al., 2018). However, vulnerability varies among species, sizes, ages, growth rates, and locations, with tree vigor the best predictor of individual mortality. At most sites, large, long-lived trees are at the greatest risk (Bennett et al., 2015; O. L. Phillips et al., 2010) of water stress.

2.3. Carbon Emissions from Fires

Fire is an important disturbance agent in the terrestrial ecosystem, particularly in the dry tropics (e.g., Andela et al., 2017; Brando et al., 2019 and refs therein) and is tightly coupled with vegetation, climate, biogeochemical cycles, and human activities. Satellite based detections of forests fire and emissions have advanced

19449208, 2021, 1, Downloaded from https://agupubs.onlinelibrary.wiley.com/doi/10.1029/2020RG000711, Wiley Online Library on [10/11/2025]. See the Terms and Conditions (https://onlinelibrary.wiley.com/terms-and-conditions) on Wiley Online Library for rules of use; OA articles are governed by the applicable Creative Commons License

19449208, 2021, 1, Downloaded from https://agupubs.onlinelibrary.wiley.com/doi/10.1029/2020RG000711, Wiley Online Library on [10/11/2025]. See the Terms and Conditions (https://onlinelibrary.wiley.com/terms-and-conditions) on Wiley Online Library for rules of use; OA articles are governed by the applicable Creative Commons License

significantly in recent years (Y. Chen et al., 2017; van der Werf et al., 2017). Emissions are often estimated using two complementary approaches - bottom up and top-down. The bottom-up approaches rely on satellite-derived burned area (Giglio et al., 2013), together with modeled or data-constrained fuel abundances, combustion completeness, and the emission factor of a specific tracer (van der Werf et al., 2017). The Global Fire Emissions Database (GFED, van der Werf et al., 2010) is one such database that models fire emissions with these inputs. Fire radiative power has also been used to quantify fire occurrences (Kaiser et al., 2012).

The top-down approach, using bottom-up estimates as the prior knowledge, seeks to optimize the emission estimates by fitting modeled trace gas mixing ratios (mainly CO_2 and CO) with atmospheric observations while accounting for the uncertainty of each information piece in a Bayesian framework (Appendix A.2). Numerous satellites (e.g., MOPITT, TROPOMI, AIRS, and TES, as shown in Figure 1) measure atmospheric carbon monoxide (CO) and these have been used extensively as a tracer for fire carbon emission estimates because CO has a relatively simple source structure; direct emissions are mainly from fossil fuel combustion and biomass burning, with relatively small spatial colocations between the two. The atmospheric lifetime of CO is only a few weeks, allowing satellite observations to track transport of CO from its source regions (Jiang et al., 2017; Pechony et al., 2013; Pfister et al., 2005; Shindell et al., 2006; Yin et al., 2015, 2016; Zheng et al., 2019). Combining the information of the burned area and fire carbon emissions informs estimates of fuel availability and combustion factors, helping to refine our process-based understanding (Bloom et al, 2015, 2016; Y. Yin et al., 2020).

As shown in Figures 5 and 6, both burned area and CO emissions attributed to fire, indicate a net decline in tropical fire occurrences in the past decades, at least until 2016 (Jiang et al., 2017; J. R. Worden et al., 2017; Aragão et al., 2018). Andela et al. (2017) showed a 25% decline in the global burned area from 1997 to 2015 combining multiple optical and thermal satellite data sets such as from the MODIS, with the most significant decreases in the savannas of Africa. While we show burned area and CO here, we note that total carbon derived from either burned area or CO emissions are in surprisingly good agreement, at least at the pan-tropical scale. Estimates agree within ~15% (Appendix A.2) and both CO and BA based Carbon emissions show declines of ~15% for the 2002 through 2016 time period.

Alternative burned area data sets that are also based on MODIS reflectance and thermal anomaly data using a different algorithm (Chuvieco et al., 2018) show similar pan-tropical declines. This product disagrees with GFED in southern Africa finding an increase in burned where GFED shows a decline (Forkel et al., 2019). Comparing these two products show that regional trends (~1,000 km) between the two data sets can be poorly correlated, and trend in the burned area is strongly affected by the start and the end years of the analysis, so care must be taken when using these different satellite data sets to explore regional changes.

Agricultural expansion and intensification have been suggested as the primary drivers of global declining fire (Andela and van der Werf 2014; Andela et al., 2017). However, a further regional analysis suggested that one-third of the African fire reduction occurred in croplands, and climate factors relating to biomass productivity and aridity explained about 70% of the burned area decline in natural land cover (Zubkova et al., 2019). These studies therefore highlight the importance of both land-use and changes in dryness in controlling fire emissions.

Despite the decline in the tropical burned area up until 2016, anomalously large fires occurred during El Niño droughts, emitting not only large amounts of carbon but also causing negative health, ecological, and economic impacts (Marlier et al., 2013). During a normal year, when air dryness in the forest understory is low (VPD < 0.75 kPa) and fuel moisture content is high (>23%), fire rarely extends to the intact forest areas (Brando et al., 2019; Dadap et al., 2019; Nepstad et al., 2004). However, in El Nino years, these two factors change significantly, increasing the flammability across tropical forests, particularly near forest edges. In addition, the large peat fire emissions from Indonesia during the 2015 El Nino (Jiang et al., 2017; Liu et al., 2017) resulted from nonlinear responses to regional drought. In the future, droughts associated with El Nino may act as a positive feedback to future climate warming and projected enhancement of ENSO events (Field, 2016; Y. Yin et al., 2016). Observed changes in fire dynamics are estimated to impact the global carbon cycle through both direct fire emissions (Andela et al., 2017; Arora & Melton, 2018); as well as indirectly through vegetation growth rate changes under different fire frequencies (e.g., Arora & Melton, 2018).

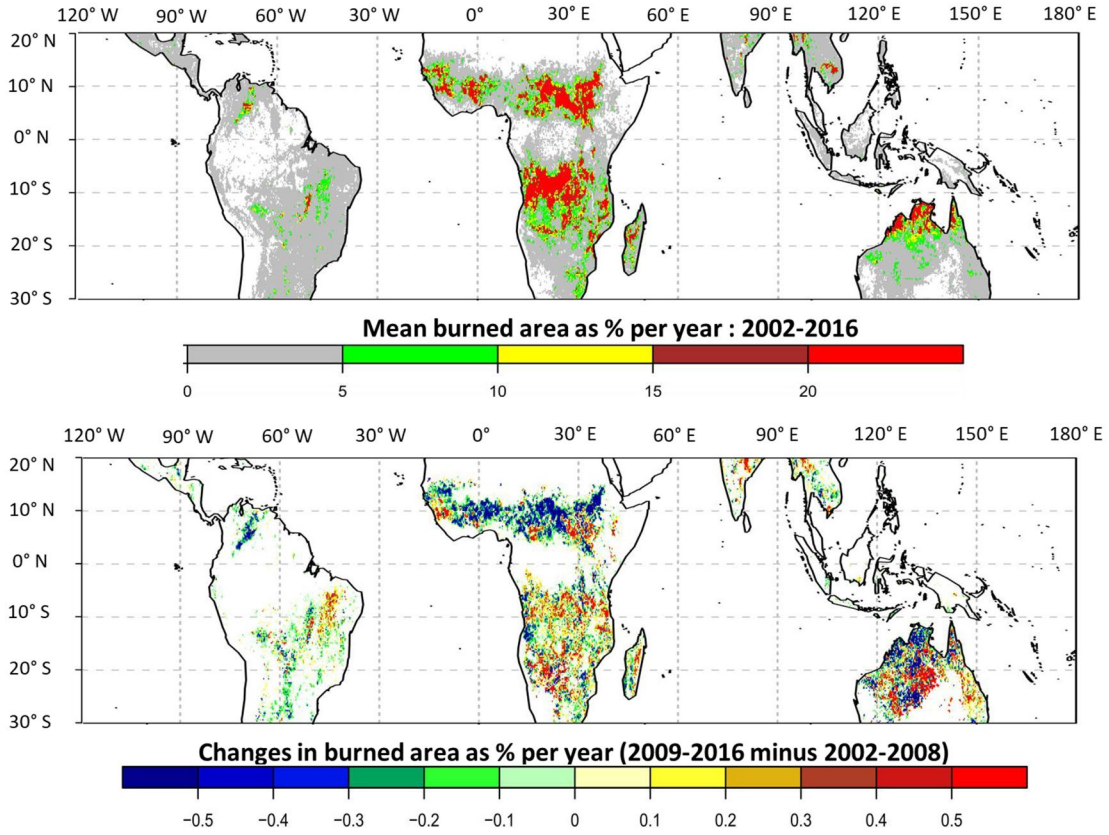

Figure 5. (top) Area (percentage) burned each year for the years between 2002 and 2016 as measured from MODIS. (bottom) The change in burned area for this time period. Areas in white are below detection. MODIS, Moderate Resolution Imaging Spectroradiometer.

Future studies aimed at quantifying burned area and fire emissions with higher resolution and accuracy are needed to reduce the uncertainty in current data sets. It is also critical to improve our understanding of the complex interplay among fire, vegetation, climate, and human activities in the context of climate warming where increased fire risks are projected (Andela, et al., 2019; Forkel et al, 2019; Knorr et al., 2016; Pechony & Shindell, 2010).

2.4. Carbon Uptake from Tropical Forest Gain

Tropical forests are not a static storage of carbon and account for one-third of the total metabolic activity of the Earth's vegetation associated with the gross primary production (Beer et al., 2010; Myneni et al., 1995; Zhao et al., 2005). These forests capture more than 50–70 PgC per year through photosynthesis (as discussed in the next section) and releasing a near similar amount back to the atmosphere through autotrophic and heterotrophic respiration (Malhi, 2011). The gain of carbon in tropical wet and dry forests, like most forests globally, occur after disturbance and through a recovery process. Regrowth of tropical secondary forests following a complete removal of forest or partial extraction of trees can partially and significantly counterbalance carbon emissions (Poorter et al., 2016; Y. Pan et al., 2011). The process of carbon gain in these forests depend strongly on a combination of nutrient availability in the soil that may be depleted due to past land use activities and moisture availability (Poorter et al., 2016). Furthermore, regenerating forests may also be subject to atmospheric CO_2 fertilization effects that may enhance their recovery process and biomass gain (Besnard et al., 2018; Cleveland et al., 2011; Phillips et al., 2014; van der Sleen et al., 2014).

Direct observations of tropical forest biomass and biomass gain from past disturbances have evolved in recent years (L. Fan et al., 2019; S. S. Saatchi et al., 2011; Y. Yang et al., 2018). However, the methodologies for detecting biomass gain are limited in areas of younger sencondary forests (Englhart et al., 2011; Morel et al.,

19449208, 2021, 1, Downloaded from https://agupubs.onlinelibrary.wiley.com/doi/10.1029/2020RG000711, Wiley Online Library on [10/11/2025]. See the Terms and Conditions (https://onlinelibrary.wiley.com/terms-and-conditions) on Wiley Online Library for rules of use; OA articles are governed by the applicable Creative Commons License

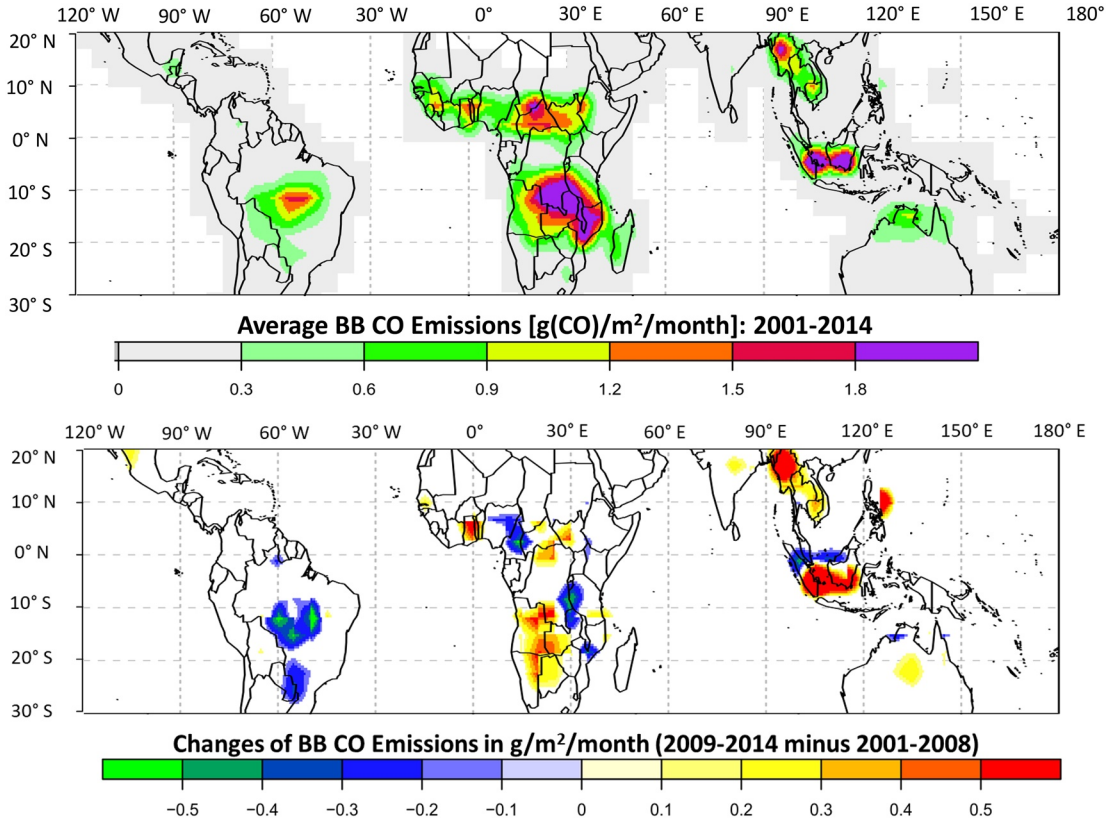

Figure 6. Same as Figure 5 but now for CO emissions as measured by the Terra MOPITT instrument. CO, carbon monoxide; MOPITT, Measurement of Pollution in The Troposphere.

2011; Yu et al., 2016) or at local scales with the aid of advanced airborne observations (Dubayah et al., 2010; Kent et al., 2015; Meyer et al., 2014; S. S. Saatchi et al., 2011).

Quantifying net carbon gain from secondary regeneration has been difficult because of the lack of systematic observations of secondary forest biomass accumulation (Barbosa et al., 2014). The rate of secondary forest regeneration depends upon the type and intensity of disturbance, subsequent land use, and the processes of forest regeneration, as well as the characteristics of the regenerating landscape (Chazdon et al., 2008; Poorter et al., 2016). Secondary forests can be highly productive, having an average recovery rate of about 3.05 Mg C ha^{-1} yr^{-1} approximately 11–20 times the uptake rate of an old growth forest (Poorter et al., 2016).

Most recent satellite techniques have mainly focused on identifying areas of secondary forests after the last disturbance (Almeida et al., 2016; Carreiras, Quegan et al., 2017; Hansen et al., 2013), and using other ancillary data such as ground plots or age-biomass models to estimate the carbon uptake. Satellite radar sensors have been able to directly estimate secondary forest age-biomass relationship and allow monitoring carbon uptakes of up to 20 years with reliable uncertainty (Cassol et al., 2019; Yu & Saatchi, 2016). However, the ability to provide these estimates systematically from space at annual or sub-annual frequency requires dedicated satellite missions such as NASA's NISAR and ESA's Biomass that are planned to be launched in 2022.

2.5. Forest Gross Primary Production

Observational estimates based on vegetation index imagery have revolutionized our understanding of the spatial distribution of Gross Primary Production (GPP; e.g., X. Zhou et al., 2005; Ryu et al., 2019 and references therein). For example, the MODIS satellite visible data can be used to quantify GPP, using a number of inputs from re-analysis and vegetation models, providing a record of GPP changes since 2002 (e.g., Y. Zhang et al., 2017 and references therein). However, these data are limited by different atmospheric and

19449208, 2021, 1, Downloaded from https://agupubs.onlinelibrary.wiley.com/doi/10.1029/2020RG000711, Wiley Online Library on [10/11/2025]. See the Terms and Conditions (https://onlinelibrary.wiley.com/terms-and-conditions) on Wiley Online Library for rules of use; OA articles are governed by the applicable Creative Commons License

19449208, 2021, 1, Downloaded from https://agupubs.onlinelibrary.wiley.com/doi/10.1029/2020RG000711, Wiley Online Library on [10/11/2025]. See the Terms and Conditions (https://onlinelibrary.wiley.com/terms-and-conditions) on Wiley Online Library for rules of use; OA articles are governed by the applicable Creative Commons License

surface scattering effects which degrades the accuracy of GPP estimates, their seasonality, and trends in the cloudy tropics (e.g., Maeda et al., 2016). New satellite based measurements of solar induced chlorophyll fluorescence (SIF) represent a major breakthrough for quantifying photosynthesis beyond the leaf scale (e.g., Sun et al., 2017). Chlorophyll fluorescence originates from the core of photosynthetic light reactions, in which a small fraction (roughly 2%) of photosynthetic active radiation absorbed by chlorophyll is re-emitted at longer wavelengths (660–850 nm) as fluorescence, in competition with two other de-excitation pathways, photochemical and non-photochemical quenching. These measurements have typically been made at leaf scale via pulse-amplitude modulation fluorescence (Baker, 2008; Genty et al., 1989; Krause & Weis et al., 1991; Moya et al., 2004), but are now possible at canopy and ecosystem scale using passive remote sensing (Mohammed et al., 2019 and refs therein). SIF, as measured by satellites, places constraints on large scale photosynthetic activity, and has potential to offer more mechanistic understanding of ecosystem carbon dynamics (Flexas et al., 2002; Frankenberg et al., 2011; Magney et al., 2019).

As with visible light data, spatial sampling remains a problem for constructing GPP based on SIF, especially in regions with persistent deep convective clouds such as the tropics. Temporal sampling may also be an issue as uncertainties remain on the relationship between measurements of SIF at one particular time of day and the diurnal cycle of photosynthesis due to changes in SIF yield with changing light conditions (Magney et al., 2019; X. Yang et al., 2015). Non-linearities exist in the relationship between the SIF radiance signature and photosynthesis for high and low light conditions, which can be difficult to quantify when integrated over the entire forest canopy layer compared to the leaf understanding. Despite these problems, a strength of SIF is its ability to capture photosynthetic variation as a function of season and in response to episodic drought, which is problematic using reflectance-based vegetation metrics (LAI, EVI) whose seasonality is not directly correlated with GPP, especially in evergreen forests such as the tropics and high-latitudes (Frankenberg et al., 2009). SIF has now been retrieved from multiple overlapping satellites since 1995, providing a long-term decadal record of global photosynthetic change (Parazoo et al., 2019). Figure 7 (top panel) shows estimates of GPP constrained by SIF observations from the Orbiting Carbon Observatory 2 (OCO-2; Parazoo et al., 2014; Y. Zhang et al., 2018, see Appendix A.3). These SIF based GPP estimates, which compare well to upscaled estimates based on site data and satellite imagery (e.g., Frankenberg et al., 2011), can also be used to quantify the relative importance of GPP variations in the wet and dry tropics across the Amazon and highlight model challenges in capturing the timing and amplitude of dry and wet season photosynthesis (Parazoo et al., 2014). Figure 7 (bottom panel) shows the seasonality of GPP derived from SIF assimilated into a terrestrial carbon cycle model (e.g., Parazoo et al., 2014) for the three regions of the pan-tropics, highlighting the importance of the water cycle on GPP (e.g., Green et al., 2017; 2019) as GPP effectively co-varies with precipitation (next section). The data assimilation approach used in Figure 7 is also further described in Section 5.

2.6. Top-Down Observations of NBE and its Relationship to the CO_2 Growth Rate

With the advent of satellites that can quantify XCO_2 globally (e.g., Eldering et al., 2017; Palmer et al., 2018 and refs therein), global fluxes of CO_2 (Appendix A.4) can be quantified and net biosphere exchange (NBE) can be derived from these fluxes. These flux estimates typically have a very coarse spatial resolution between 500 and 1,000 km (e.g., Liu et al., 2017; Bowman et al., 2017) and uncertainties that vary from region to region (Appendix A.4). Consideration must be given over which regions and time periods are large enough to reduce these uncertainties to make comparisons between years or with other data sets meaningful. For example, while mean NBE values can have bias errors that reduce confidence in their interpretation, NBE differences, or anomalies, are useful for evaluating changes in carbon balance, their relationship with climate variability, and the CO_2 growth rate. Figure 8 shows a comparison in the NBE anomaly from year to year derived from the OCO-2 and Greenhouse Observation SATellite (GOSAT) satellites, and the global CO_2 growth rate. This comparison confirms the nearly one-to-one (R^2 value is 0.94) relationship showing how the tropical biosphere affects the interannual variability of atmospheric CO_2. As discussed in the next section, these regional estimates of NBE, when combined with measurements of photosynthesis (Section 2.5) and water can be used to quantify how climate drivers affect carbon balance at much finer scales than previous estimates using surface measurements alone (e.g., Cox et al., 2013).

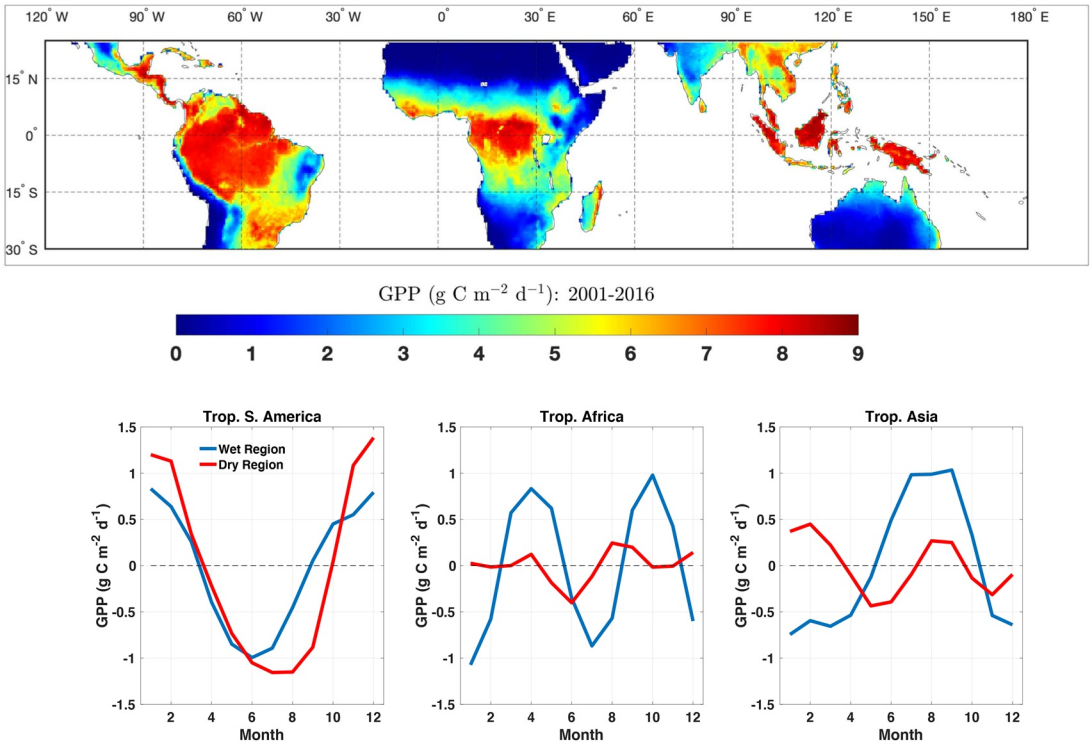

Figure 7. (top) Mean tropical gross primary production for the time period between 2002 and 2016 based on integrating OCO-2 SIF data into an ensemble of terrestrial carbon cycle models. (bottom) The seasonality of GPP for the three tropical regions. OCO-2, Orbiting Carbon Observatory 2; SIF, solar induced chlorophyll fluorescence.

3. Carbon and Water Interactions and Feedbacks

3.1. Direct Impact of Water Cycle Variability on Carbon Fluxes and Stocks

Over yearly to decadal time scales, variations in SST related to ENSO alters oceanic moisture fluxes over the tropical continents and corresponding humidity, rainfall, and temperature (Anber et al., 2015). These temperature and moisture changes (e.g., Wang & Schimel et al., 2003) in turn modulate the carbon balance as observed in NBE, GPP, and the respiration component from fires as discussed in Section 2 (e.g., Y. Chen et al., 2011; Sellers et al., 2018). Increases in fire emissions across the tropics are related to moisture variability and transport modulated by ENSO (e.g., Y. Chen et al., 2017). Large decreases in humidity and rainfall associated with ENSO and coupled to human activities can also create larger fire emissions as observed in Indonesia (Field et al., 2009, 2016) in which very low water tables result in the burning of both vegetation and ancient peat; this non-linear behavior potentially provides a preview of "tipping point" behavior in which large changes in the water cycle substantively alter the carbon balance (e.g., Lenton et al., 2008), releasing carbon with long residence times (e.g., Bloom et al., 2016) into the atmosphere. Similarly, both site measurements and satellite-based measurements suggest the other component carbon fluxes such as GPP are strongly affected by varying moisture. Lee et al. (2013) used SIF and canopy water content measurements to show the impact of water stress on the Amazon forest. Guan et al. (2015) uses SIF and EVI measurements with rainfall to show that rainfall amounts larger than 2000 mm/year are needed to sustain tropical evergreen forests in the dry season. S. Saatchi et al. (2013) showed that repeated droughts in the Amazon have a lasting effect on forest carbon and forest stock using satellite-based estimates of rainfall and canopy water content. Satellite

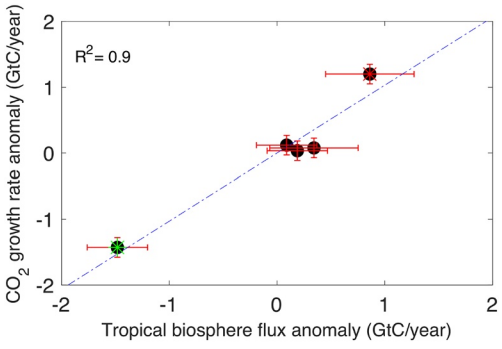

Figure 8. The relationship between atmospheric CO_2 growth rate anomaly (GtC/year) and the tropical biosphere flux anomaly (GtC/year) constrained by satellite column CO_2 observations, GOSAT data (red/black symbols) are shown for 2010–2013 and OCO-2 data (green hash symbols) is for 2015. GOSAT, Greenhouse Observation SATellite; OCO-2, Orbiting Carbon Observatory 2; SIF, solar induced chlorophyll fluorescence.

19449208, 2021, 1, Downloaded from https://agupubs.onlinelibrary.wiley.com/doi/10.1029/2020RG000711, Wiley Online Library on [10/11/2025]. See the Terms and Conditions (https://onlinelibrary.wiley.com/terms-and-conditions) on Wiley Online Library for rules of use; OA articles are governed by the applicable Creative Commons License

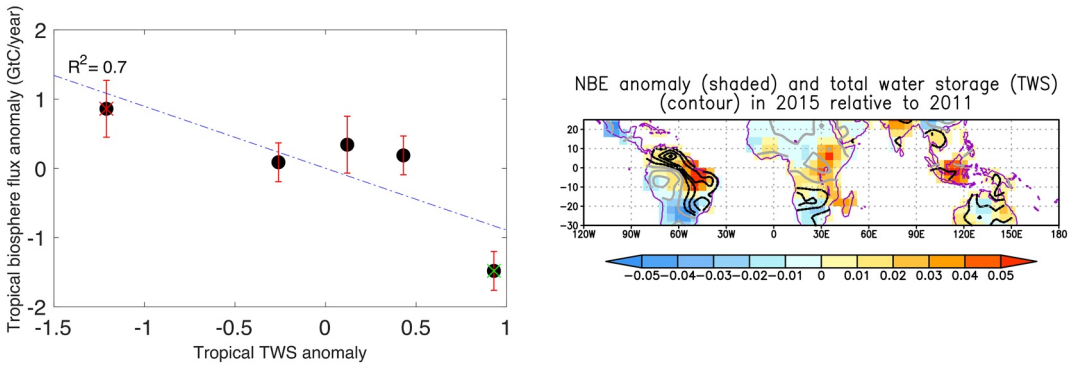

Figure 9. (left) The tropical biosphere flux anomaly from the previous figure as a function of GRACE TWS. (right) NBE (unit: GtC/box) (shaded) from atmospheric flux inversion and total water equivalent (TWS) (contour) from GRACE in 2015 relative 2011. Black dashed contours have negative TWS values in 2015 relative to 2011, while the gray solid lines have positive TWS values in 2015 relative to 2011. GRACE, Gravity Recovery and Climate Experiment; NBE, Net biosphere exchange; TWS, terrestrial water storage.

based estimates of rainfall and vegetation color indices show that decreasing rainfall over several years on the Congo forest results in vegetation browning (L. Zhou et al., 2014).

However only recently can we observe how these local and regional stresses affect atmospheric CO_2 at pan-tropical scales and relate them back to their component carbon and water fluxes. Humphrey et al. (2018) found a global relationship between terrestrial water storage (TWS) as observed by the Gravity Recovery and Climate Experiment (GRACE) instrument and the CO_2 growth rate. However, Liu et al. (2017) showed that this bulk effect between water and carbon is more nuanced across the tropics. Liu et al. (2017) used new regional scale (Section 2.6 and A.4) carbon fluxes as derived from total column measurements of CO_2 from the GOSAT and OCO-2 satellites, satellite based estimates of fire emissions (Section 2.3) and GPP as derived from SIF (Section 2.5), along with water vapor and rainfall measurements to show how the tropical carbon balance responds to moisture changes across the tropics and that changes in the terrestrial carbon balance was different across each of the main regions. Each of the three tropical regions (S. America, Africa, and Maritime) had a net flux of ~0.8 PgC; however, these changes result from a decrease in GPP in S. America, an increase in respiration in Africa and both an increase in fire emissions and decrease in GPP in the maritime region. These landmark studies show that carbon balance does not uniformly respond to climate variability but instead responds to different stresses depending on the ecosystem.

Ideally changes in NBE are compared to changes in soil moisture as that is a more immediate representation of the water available to plants and hence how water affects carbon (e.g., Fung et al., 2005; Green et al., 2019). Recent satellite measurements from the Soil Moisture Active Passive (SMAP) and Soil Moisture Ocean Salinity (SMOS) missions use microwave measurements to estimate surface soil moisture. Unfortunately, radar based soil moisture estimates over the tropics are difficult to interpret due to attenuation of the signal within thick vegetation or forest canopies (e.g., Babaeian et al., 2019 and refs therein). However, we do have 15+ years of satellite-based measurements of rainfall and TWS, which can be used to inform about variations in soil moisture (e.g., Gentine et al., 2019). For example, tropical biosphere flux anomalies have a close relationship with TWS anomalies measured by the GRACE satellites, as shown in Figure 9a (left panel). The NBE is positive (i.e., more carbon is released into the atmosphere) when the water storage has a negative anomaly, and vice versa. TWS explains more than 67% of the tropical biosphere flux anomalies. However, it is unclear how this relationship between NBE and TWS varies between wet and dry tropics because of the spatial resolution of NBE data. Spatially, NBE is positive when the TWS anomaly is negative (indicating a drought condition) in the Amazon and maritime region (Figure 9b right panel). In contrast, NBE and TWS are somewhat spatially correlated in Africa, which may indicate a large influence from heterotrophic respiration (Liu et al., 2017) although the exact mechanism for this behavior is unclear and may be unrelated to carbon/water exchanges (e.g., Palmer et al., 2019). Coupling top-down NBE and TWS constraints such as these with models of the carbon and water cycles may help to resolve these remaining

19449208, 2021, 1, Downloaded from https://agupubs.onlinelibrary.wiley.com/doi/10.1029/2020RG000711, Wiley Online Library on [10/11/2025]. See the Terms and Conditions (https://onlinelibrary.wiley.com/terms-and-conditions) on Wiley Online Library for rules of use; OA articles are governed by the applicable Creative Commons License

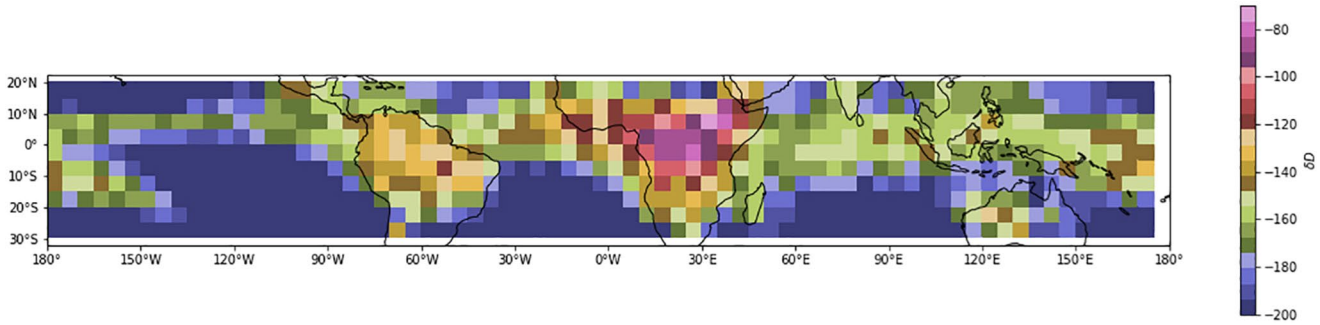

Figure 10. The mean deuterium content of water vapor for the tropics for the years 2005–2010 from the Aura TES instrument (see Appendix A.8). The units (δD) are in parts per thousand relative to the isotopic composition of ocean water, or per mil/SMOW. TES, Troposphere Emission Spectrometer.

uncertainties and can also be used to elucidate how water affects other carbon cycle fluxes such as GPP, forest stocks and fires. These model-data fusion approaches are further discussed in Section 5.

3.2. Interactions and Feedbacks Between Vegetation and Water

Feedbacks between vegetation, soil moisture, and rainfall are also of critical importance for understanding tropical carbon balance as vegetation modulates rainfall which in turn affects water availability as vegetation contributes 30%–50% to the overall atmospheric moisture in the wet tropics (Salati et al., 1979). These feedbacks can have substantive effects over short and long time scales. Green et al. (2017) used measurements of SIF and rainfall to show that variations in photosynthesis can explain up to 30% of the variations in rainfall in the dry tropics. At interannual timescales, severe droughts can affect forest composition and subsequent ET. S. Saatchi et al. (2013) used microwave-based measurements to show that forest structure shows persistent degradation 3–4 years after the 2005 Amazon drought (e.g. Yang et al., 2018); hypothesizing that this could result from feedbacks into the water cycle through changes in ET (e.g. Zemp et al., 2017). In turn, Shi et al. (2019) used satellite-based ET and deuterium content of water vapor to provide evidence that a decrease in Amazonian ET in the dry-to-wet transition phase (~September to November) occurred in 2006 as a result of the 2005 drought. The Southern Amazon dry season length is also observed to be increasing (e.g., Fu et al., 2013; Sena et al., 2018) and one explanation may be due to loss of vegetation and corresponding ET from logging, agriculture, and repeated droughts.

In addition to new satellite observations of SIF (Section 2.5), remote sensing observations of the deuterium content of water vapor, vapor pressure deficit, and ET have the potential for evaluating vegetation atmosphere interactions and feedbacks (e.g. Good et al., 2015; Wright et al., 2017). Measurements of the deuterium content of water vapor (e.g., the HDO/H_2O ratio) are now made by several satellite instruments (e.g., J. Worden et al., 2007; Frankenberg et al., 2009; J. R. Worden et al., 2019; Appendix 8). This data allows us to look at how different moisture sources and processes affect atmospheric water vapor, since water vapor from the ocean has a different isotopic signature than water vapor from tropical transpiration. Risi et al. (2013) demonstrates how these data are directly sensitive to the relative contribution of vegetation versus oceanic moisture on lower-tropospheric humidity, a key indicator for precipitation. Figure 10 shows a map of the global mean value of the isotopic composition (or deuterium content) of water vapor for 2006–2010 time period in the lower troposphere between 800 and 500 hPa. The units are in parts per thousand (δ-D, or per mil) relative to the isotopic composition of ocean water. For example, the isotopic composition of the vapor that evaporates from tropical land generally has a value between 0 and -75 per mil and vapor originating from the ocean ranges between −75 and −100 per mil in the tropics (e.g., Risi et al., 2013; Rahul et al., 2018 and refs therein). Water vapor associated with rainfall and deep convection will usually be depleted relative to ocean vapor, due to recycling of vapor in the convective system (J. Worden et al., 2007) and entrainment of isotopically depleted air from the free troposphere (e.g., Risi et al., 2008). The Congo is typically more enriched than the Amazon; however, this could indicate that there is more deep convection in the Amazon than the Congo, as opposed to less transpiration because deep convection is more efficient at removing (or depleting) the heavier water from water vapor than normal rainfall processes (e.g., Galewsky

19449208, 2021, 1, Downloaded from https://agupubs.onlinelibrary.wiley.com/doi/10.1029/2020RG000711, Wiley Online Library on [10/11/2025]. See the Terms and Conditions (https://onlinelibrary.wiley.com/terms-and-conditions) on Wiley Online Library for rules of use; OA articles are governed by the applicable Creative Commons License

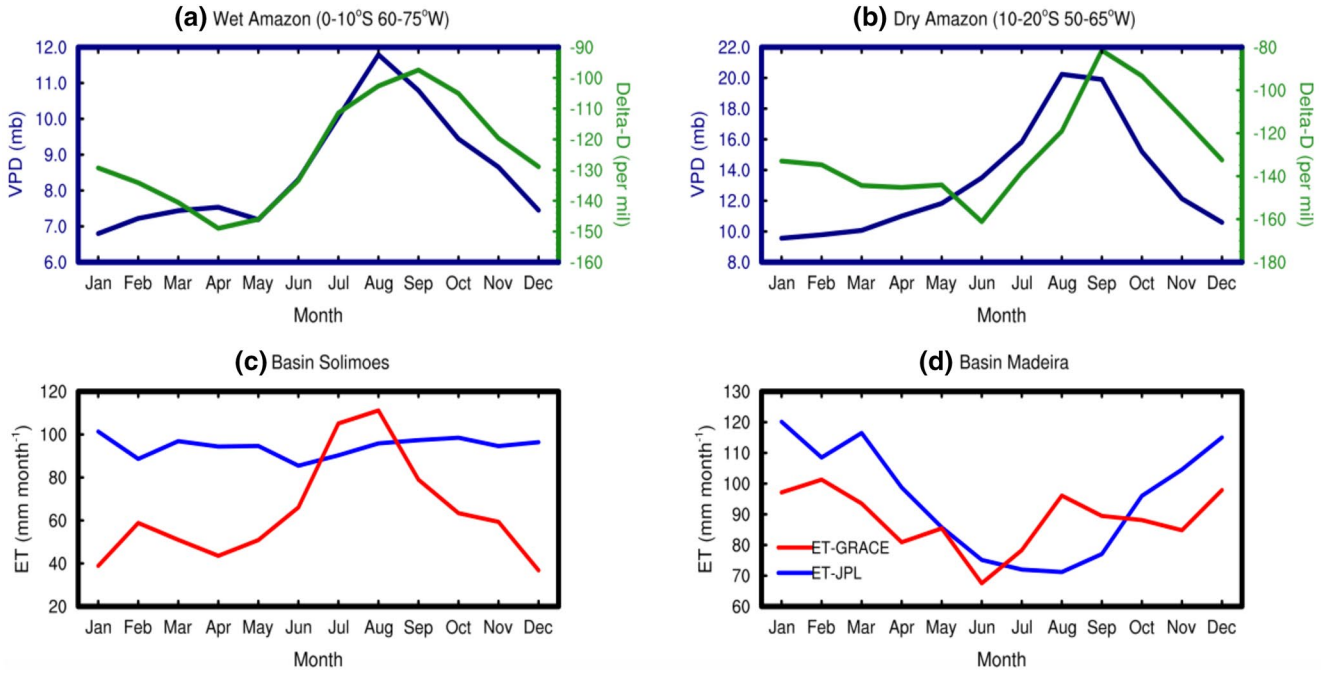

Figure 11. (top) Seasonality of the Amazon VPD (Appendix A.7) and deuterium content of tropospheric water vapor (Appendix A.8) for the wet Amazon (left) and dry Amazon (right). (bottom) Seasonality of ET (Appendix A.6) as derived from a residual of GRACE, TRMM, and river runoff (red) and satellite surface measurements (blue). Basin maps for Solimoes (left) and Madeira (right) are used to grid ET for the bottom figures to ensure the comparisons between data sets are consistent. ET, evapotranspiration; GRACE, Gravity Recovery and Climate Experiment; TRMM, Tropical Rainfall Monitoring Mission; VPD, vapor pressure deficit.

et al., 2016 and refs therein). Care must therefore be taken in using these data to attribute vapor to specific sources and processes.

Wright et al. (2017) looked at the variation of the deuterium content of water vapor using data from the Aura Tropospheric Emission Spectrometer (Appendix A.7) to show increasing relative contribution of transpiration to the water vapor in the Southern Amazon, prior to the wet season, and that this transpiration helped to initiate the Amazon monsoon. An important caveat is that the isotopic composition of water vapor describes the relative contribution of ET to oceanic water during the dry season but not the absolute amount of ET fluxes. Unfortunately, there is not enough TES deuterium data to create a difference plot similar to Figure 4–6 to determine if there has been a large scale re-balancing of tropical moisture sources. New deuterium measurements from the AIRS instrument (J. R. Worden et al., 2019) have the potential to create this satellite record.

The question of what drives seasonal changes to ET arises from the Wright et al. (2017) paper. Here we can use satellite measurements of vapor pressure deficit (VPD) from the AIRS instrument (Barkhordarian et al., 2017; Appendix A.7) to infer one possible explanation. VPD is the difference between the amount of vapor at the near surface relative to 100% humidity. VPD is controlled by both atmospheric and surface conditions and therefore reflects the amount of water in the surface available for evaporation, the water use efficiency of the plants, and the atmospheric demand on surface moisture, as well as large scale atmospheric fluxes (e.g., Seager et al., 2015; Massman et al., 2019). As shown in Figure 11, there is a seasonal increase in VPD that corresponds to the increase in δ-D and suggests that seasonal evaporative demand is partly driving the source of the atmospheric water vapor during this time period. These comparisons of deuterium content and VPD can be made against seasonal ET estimates using vegetation based measurements (e.g., J. B. Fisher et al., 2009; Maeda et al., 2017) and as a residual observation of rainfall, gravity, and river runoff (e.g., Swann & Koven, 2017) as shown in the bottom part of Figure 11. The gravity derived ET estimates (Appendix A.6.2) suggest that ET can be important during the dry and dry-to-wet seasons in the humid tropics as suggested by the ET over the Solimoes Basin, and also during the dry to wet transition season in the dry tropics as suggested by the ET over the Madeira Basin (Maeda et al., 2017). However, these large seasonal differences

19449208, 2021, 1, Downloaded from https://agupubs.onlinelibrary.wiley.com/doi/10.1029/2020RG000711, Wiley Online Library on [10/11/2025]. See the Terms and Conditions (https://onlinelibrary.wiley.com/terms-and-conditions) on Wiley Online Library for rules of use; OA articles are governed by the applicable Creative Commons License

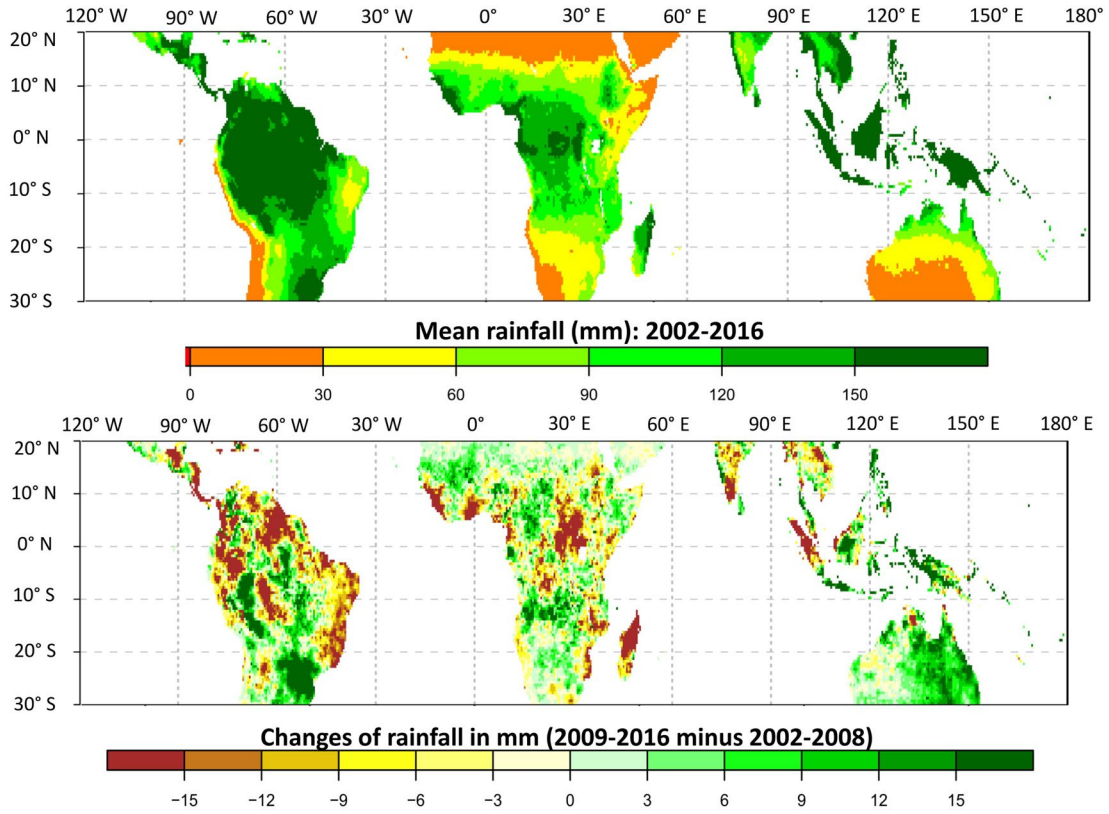

Figure 12. (top) The total mean rainfall from using TRMM and GPM for the 2002–2016 time period and (bottom) the difference in rainfall between the 2009–2016 and 2002–2008 time periods. GPM, Global Precipitation Measurement Monitor; TRMM, Tropical Rainfall Monitoring Mission.

between the gravity based and surface measurement-based ET, estimates indicate that more work is needed to quantify the seasonal ET across the tropics given its importance for quantifying tropical carbon and water feedbacks. New surface temperature measurements from the ECOsystem Spaceborne Thermal Radiometer Experiment on Space Station (ECOSTRESS), could help resolve these differences as their improved spatial resolution (~100 m) is more comparable to ground validation sites for the purpose of testing algorithms that can relate remote sensing observations of surface temperature to ET (e.g. Cawse-Nicholson et al., 2020; J. B. Fisher et al., 2020). However, a key drawback of ECOSTRESS is that its observations are only possible in non-cloudy conditions. Combining ECOSTRESS and other hydrologic observations with models to better understand variations in hydrologic variables that are not directly observed (e.g., soil moisture) or at times when observations are less plentiful (e.g., cloudy conditions) may be useful to fill these gaps (Purdy et al., 2018).

3.3. 21st Century Changes and Variability of Rainfall, Terrestrial Water Storage, and ET

Given the importance of inter-annual variations in rainfall and TWS in explaining NBE and GPP, we would expect that longer term changes in rainfall, water deficit, and soil moisture should have an impact on carbon dynamics, productivity, NBE, and stocks. Our primary approach for assessing these long-term changes through satellite measurements are from the Tropical Rainfall Monitoring Mission (TRMM), the Global Precipitation Measurement Monitor (GPM), and the GRACE mission (Appendix A.5). We therefore present and evaluate decadal scale changes in these observations and how these changes might affect tropical carbon balance. Figure 12 (top panel) shows the mean rainfall as calculated by the TRMM instrument and Figure 12 (bottom panel) shows the change in rainfall for the time periods between 2002–2008 and 2009–2016 using both TRMM And GPM data; we used these time periods due to the increase in La Nina periods beginning in 2008, which resulted in a marked decrease in fire emissions (Section 2). We do not attempt to separate how the observed changes in the tropical water cycle are related to ENSO versus decadal variability

19449208, 2021, 1, Downloaded from https://agupubs.onlinelibrary.wiley.com/doi/10.1029/2020RG000711, Wiley Online Library on [10/11/2025]. See the Terms and Conditions (https://onlinelibrary.wiley.com/terms-and-conditions) on Wiley Online Library for rules of use; OA articles are governed by the applicable Creative Commons License

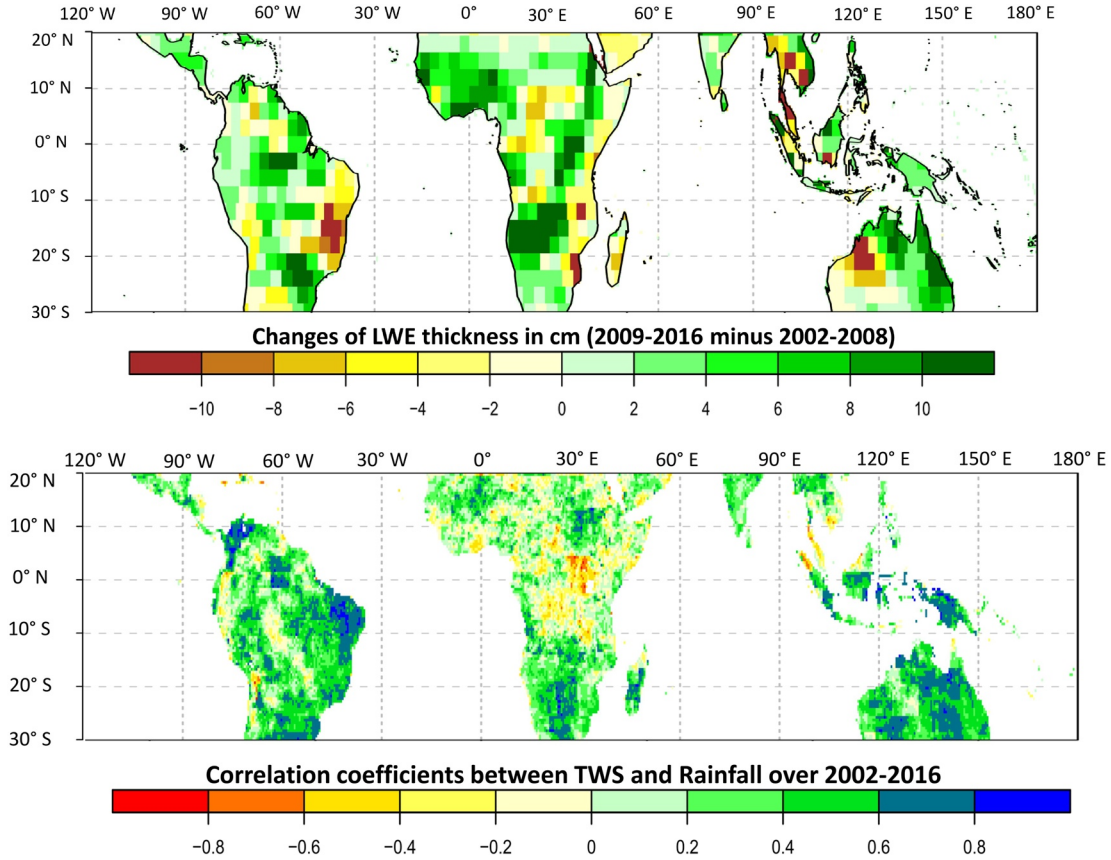

Figure 13. (top) The change in TWS from GRACE in cm for the same time periods as Figure 12. (bottom) The correlation between TWS and rainfall for the 2002–2016 time period. GRACE, Gravity Recovery and Climate Experiment; TWS, terrestrial water storage.

in oceanic temperatures or anthropogenic effects as the focus is on how these observed variations in water affect carbon and vice versa.

To better understand changes in the terrestrial water budget, rainfall data can be compared against the change in TWS as measured by the GRACE mission (Tapley et al., 2004). GRACE has been revolutionary in detecting subsurface water storage changes including in root zone soil moisture and groundwater that are critical for plant access to water during times of drought and little surface water and can help to reveal information on the concept of plant water use and drought resilience. A recent paper by Rodell et al. (2018) has highlighted global trends in TWS over the GRACE observational period, showing the impacts of combined climate variability, human use and water consumption, and potential signatures of climate change. Figure 13 (top panel) shows the changes in TWS from April 2002 to December 2016.

As with the rainfall data, Figure 12 (top) shows that there are both increases and decreases in TWS across the moist and dry tropics but with a net increase in TWS during this time period (Reager et al., 2016; Rodell et al., 2019), primarily as a result of increased rainfall from La Nina. Figure 13 (bottom panel) shows the correlation between the changes in TWS and rainfall for these time periods. While GRACE data also reflect changes in ET and river runoff (e.g., Swann & Koven, 2017), it is useful to compare GRACE and TRMM/GPM together because they reflect the primary input of moisture to the land and how much the land retains water for possible use by the biosphere. Correlations are largest in the dry tropics but surprisingly almost zero or even negative in many places in the wet tropics, which suggests that other factors such as a change in ET or capacity of soil to hold water and subsequent river run-off (the other primary water fluxes) may be affecting these correlations.

Based on the NBE/TWS comparisons in Figure 9, we might expect a net increase in carbon storage based on the net increase in tropical water storage or rainfall. Indeed, studies such as Song et al. (2018) show

19449208, 2021, 1, Downloaded from https://agupubs.onlinelibrary.wiley.com/doi/10.1029/2020RG000711, Wiley Online Library on [10/11/2025]. See the Terms and Conditions (https://onlinelibrary.wiley.com/terms-and-conditions) on Wiley Online Library for rules of use; OA articles are governed by the applicable Creative Commons License

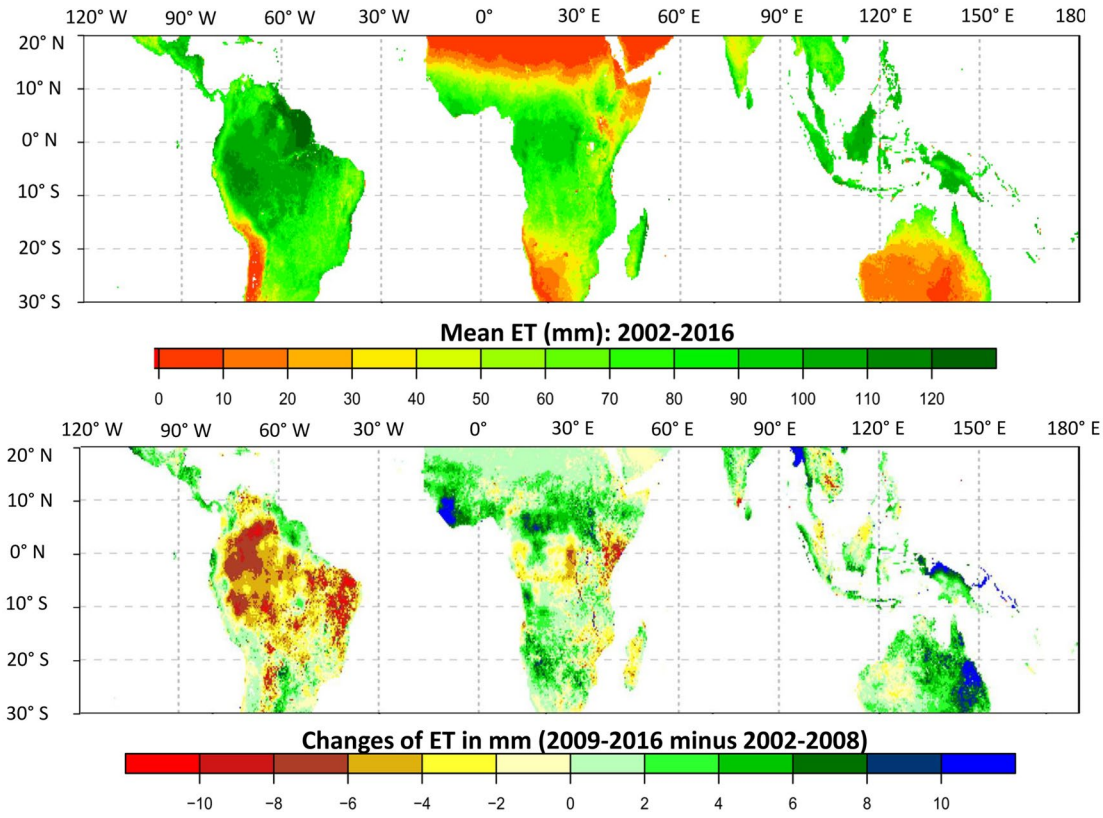

Figure 14. Same as Figure 12 but for evapotranspiration based on MODIS and re-analysis (Appendix A.6). MODIS, Moderate Resolution Imaging Spectroradiometer.

an increase in vegetation in the Northern African dry tropics, while Zhou et al. (2018) shows increased browning in the Congo associated with decreasing rainfall. However, as discussed in the next section there is evidence for regional changes in ET across the tropics, and these changes, along with those observed in TWS, should also have an impact on the tropical carbon balance due to the covariation between ET, SIF, and vegetation and these must be considered as additional evidence in the tropical carbon puzzle. Using the MODIS based ET estimates from J. B. Fisher et al. (2009), Figure 14 (top) shows an estimate of the mean ET for the 2002 to 2016 time period and the change in ET across the tropics for the same time period in the previous plots. A decline in the Amazon of about 8 mm/month for the Western Amazon or approximately 8% given the ET in this part of ~100 mm/month is observed. These data can be compared to ET estimates based on the residual of TWS, rainfall, and river runoff in which ET is derived for large basins (Maeda et al., 2017; Swann & Koven, 2017). ET estimates from these types of data also suggest a similar decline (Swann & Koven, 2017), a surprising result given that total TWS is increasing in this area. Two hypotheses are able to explain this behavior which are that GPP is declining or that water use efficiency (WUE) is increasing, both of which suggests that the Amazon is responding to changing climatic conditions such as changes in humidity or radiation (e.g., van der Sleen et al., 2014), or more frequent droughts (e.g., S. Saatchi et al., 2013). These differences may also be affected by the choice of starting dates as the ENSO events and corresponding droughts in 2010 and 2015 may have had a much bigger impact on the biosphere than the positive ENSO anomalies between 2002 and 2008.

The changes in rainfall, ET, and TWS for the wet tropics suggest a complex picture for the trajectories of water and carbon during 21st century. Reconciling our process understanding of how water flows through the atmosphere and soil against these observations will therefore be critical towards explaining carbon balance in the moist tropics. On the other hand, the dry tropics appear to show well behaved relationships: TWS and rainfall are well correlated and increases/decreases in ET are generally related to increases/

19449208, 2021, 1, Downloaded from https://agupubs.onlinelibrary.wiley.com/doi/10.1029/2020RG000711, Wiley Online Library on [10/11/2025]. See the Terms and Conditions (https://onlinelibrary.wiley.com/terms-and-conditions) on Wiley Online Library for rules of use; OA articles are governed by the applicable Creative Commons License

19449208, 2021, 1, Downloaded from https://agupubs.onlinelibrary.wiley.com/doi/10.1029/2020RG000711, Wiley Online Library on [10/11/2025]. See the Terms and Conditions (https://onlinelibrary.wiley.com/terms-and-conditions) on Wiley Online Library for rules of use; OA articles are governed by the applicable Creative Commons License

decreases in rainfall and TWS, suggesting that ET is responding to changing soil moisture and rainfall. However, it is unclear if the balance of ET and precipitation remains constant or is changing in response to increasing temperature, CO_2, or VPD or changes in forest structure. Understanding this response is important as increases/decreases in water balance (or ET-P) decreases/increases terrestrial soil moisture and subsequent uptake of CO_2 by forests (e.g. Fung et al., 2005, Gentine et al., 2019; Green et al., 2019). Changes in forest structure could also affect this balance; a decline in vegetation decrease transpiration, resulting in a decline in tropospheric humidity, but at the same time increase sensible heat which can draw in moisture (e.g. Risi et al., 2013; Llopart et al., 2014 and refs therein), mitigating the humidity decline. Increases in VPD, such as observed in the transition zone between the wet and dry tropics (Barkhordian et al., 2020) or increasing atmospheric CO_2, can also alter evapotranspiration characteristics. An increase in VPD can increase ET if the wet tropics is radiation limited or be a response to declining ET if the forest is water limited (e.g. Boese et al., 2017; Greene et al., 2020). On the other hand an increase in CO_2 likely increases the water use efficiency of plants because plants need less water to trade for CO_2, resulting in a corresponding decrease in transpiration (e.g. Eamus 1991; van der Sleen et al., 2014). The balance of these disparate effects in turn modulates the terrestrial water balance or ET-P. However, models are not yet equipped to easily integrate these new satellite observations for testing and then updating the process description that describes these feedbacks (e.g. Risi et al., 2013) and subsequent water balance. New approaches are therefore necessary to fully exploit the range of satellite data for quantifying carbon / water interactions as discussed in Section 5.

4. Other Uncertainties in Carbon and Water Processes, Reservoirs, and Cycling

As discussed previously, the satellite record, when combined with aircraft and in situ data, has greatly expanded our knowledge of the carbon and water cycles and how they interact. However, many puzzles remain that are critical toward quantifying the evolution of the terrestrial carbon and water cycles. One mystery is the role of temperature versus water in modulating terrestrial carbon cycling. As discussed in Section 3 and in Humphrey et al. (2018), CO_2 growth rates show a strong relationship with water storage as discuss in Section 3 and this contrasts with statistical analyses that find a strong relationship between the CO_2 growth rate and temperature variations (e.g., M. Jung et al., 2017; W. Wang et al, 2013). A multitude of factors explain these inconsistencies, but they are likely partially influenced by (a) compensating/cofounding processes acting on net fluxes, for example, increased drying is associated with increased temperature, (b) limited measurement capability for resolving spatial variations in drivers and processes below-ground such as soil moisture and roots in a vertically resolved manner, (c) errors in climatic drivers used in analyses, (d) coupling between these factors through land-atmosphere interactions, and (e) inability to directly estimate with remote sensing other components of the net carbon balance, such as autotrophic and heterotrophic respiration. The combination of these factors drive a multitude of uncertainties in specific pathways of carbon water coupling and confound our ability to predict the evolution of the tropical carbon cycle.

As discussed in Section 2, respiration remains one of the largest uncertainties in the carbon budget. However, quantifying respiration is challenging and currently only possible using remote sensing at very coarse scales as a residual of net carbon flux and GPP, such as discussed in Liu et al. (2017) and Bowman et al. (2018). For heterotrophic respiration in particular, there is large uncertainty in the effect of soil moisture and soil carbon with different models showing very different functional forms in the heterotrophic respiration, soil moisture relationship (Sierra et al., 2015). Consequently, heterotrophic respiration is the dominant source of uncertainty in soil carbon fluxes (Todd-Brown et al., 2013). Some progress has recently been made on better understanding these relationships (Bond-Lamberty et al., 2018; Yan et al., 2018), but this progress is still almost entirely based on in situ data from, with less than 25 sites distributed across the tropics. Konings et al. (2019) recently suggested heterotrophic respiration could be constrained with remote sensing by inverting the land surface carbon balance using the XCO_2, SIF, and fire data. However, uncertainties in the carbon balance components and the difficulty of disentangling autotrophic and heterotrophic respiration limit the precision of this method. Lastly, dissolved carbon in aquatic systems can be an important component necessary to close the carbon budget, and is likely particularly high in many of the streams

19449208, 2021, 1, Downloaded from https://agupubs.onlinelibrary.wiley.com/doi/10.1029/2020RG000711, Wiley Online Library on [10/11/2025]. See the Terms and Conditions (https://onlinelibrary.wiley.com/terms-and-conditions) on Wiley Online Library for rules of use; OA articles are governed by the applicable Creative Commons License

flowing from peatland areas in the tropics. However, these measurements are essentially unconstrained by current remote sensing.

The coupling between photosynthesis and water and their interactions belowground remains poorly understood. Root density and root water uptake is highly uncertain (Powell et al., 2013) but currently unobservable. Regions such as the Congo have shallow groundwater, but relatively few observations of belowground processes (Y. Fan et al., 2013). Little is also known about how rooting density varies with depth but this relationship is likely important for modulating drought stress (e.g. Giardina et al., 2018). Many tropical regions contain peatlands or standing water, but these are poorly mapped (Dargie et al., 2017). Furthermore, research in plant hydraulics has shown the need to account for movement of water within plants, and the close link between belowground processes and water uptake (Bonan et al., 2014; Kennedy et al., 2019) in order to correctly reproduce the seasonal cycle of GPP and ET in tropical rainforests (e.g. Powell et al., 2013; Anderegg et al., 2018). These poorly constrained processes likely contribute to the large differences between ET estimates, as discussed in this manuscript and many others (e.g., Fisher et al., 2020; S. Pan et al., 2020 and refs therein). They also underscore the importance of continuing to improve estimates of ET, as this quantity is critical for evaluating feedbacks between the plant and soil moisture and plant hydraulics in the carbon, water, and energy cycles.

Previous studies have also shown the importance of demographic composition globally, and thus presumably tropically (Friend et al., 2014) in modulating carbon and water balance. Demography-resolving models that can be trained on and tested against remote sensing data have become more capable of simulating tropical forests (R. A. Fisher et al., 2015; L. Xu et al., 2016), but so far these simulations largely remain confined to regional rather than pan-tropical studies. Above ground, large uncertainties remain in the role of vertical variations of light, humidity, CO_2, wind and temperature across the canopy and horizontally (Banerjee & Linn, 2018).

5. Quantifying Carbon and Water Processes and Reservoirs by Combining Satellite Data and Models

While there are ever increasing measurements of carbon, water, and energy states, and to some extent processes (e.g., SIF, deuterium), models are needed to relate these states to the overall tropical carbon and water budgets and to explain and forecast their future changes (e.g. Bonan et al., 2019 and refs therein). In doing so, the key challenge is to robustly combine the observational data, with its fundamental link to reality, to models that summarize our theoretical understanding and provide a framework. This process is illustrated in Figure 15 in which data, with its characterized uncertainties, and model parameters or state, with their own *a priori* uncertainties (e.g., Raupach et al., 2005; T. Schneider et al., 2017), are integrated together. Integration of model and data are typically informed with Bayes' theorem. Such approaches are known as data assimilation or model-data fusion methods. In this section, we introduce model-data fusion and discuss its benefits and challenges for reducing uncertainty in processes, fluxes, and reservoirs that control carbon and water cycling.

A number of model-data fusion efforts have focused on assimilating satellite observations into existing terrestrial biosphere models (e.g., Bacour et al., 2019; MacBean et al., 2016). Assimilating observations into these models can constrain fluxes (Macbean et al., 2018) and processes such as CO_2 fertilization (W. K. Smith et al., 2019). These models represent a large diversity of process and are therefore computationally highly intensive. To maintain computational tractability, these efforts tend to use Kalman filters and smoothers to optimally combine models and data, which have the benefit of being computationally tractable but require Gaussian assumptions about the uncertainties. Because of their large number of parameters, such model-data fusion approaches also remain susceptible to equifinality (Beven, 1993; MacBean et al., 2016), compensating errors between parameters and processes when the number of observed dimensions is less than the number of unknowns. Alternatively, if a carbon cycle model of intermediate complexity is used, then Markov Chain Monte Carlo approaches become computationally tractable, removing the need to assume a Gaussian distribution in model and observational uncertainties (Bloom et al., 2016). We note that new ESM's are being developed using these approaches with the goal of harnessing the satellite program of record and upcoming measurements (T. Schneider et al., 2017) for the purpose of quantifying biogeochemical processes and improving Earth system prediction.

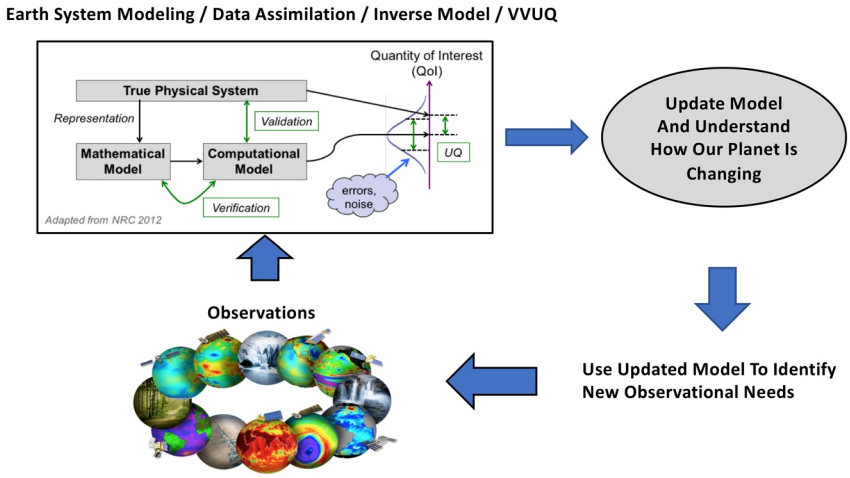

Figure 15. A notional schematic (courtesy Duane Waliser) of how observations are assimilated into an Earth System model to evaluate a quantity of interest (e.g., Soil Carbon, Water Use Efficiency), which can then be compared to validation data sets for the purpose of validation and uncertainty quantification. The updated model then helps inform our understanding of the Earth System and its evolution as well as provide information on which observations can be used to reduce uncertainty further in our knowledge of the Earth System.

We demonstrate this approach using an intermediate complexity model depicted in Figure 16, which simulates the dynamics of pools (reservoirs) of live and dead carbon (solid green boxes), according to various carbon processes, including fire and management (black edged green boxes), the dynamics of plant and soil moisture (blue boxes) according to hydrological fluxes (black edge blue boxes), the vertical structure of the ecosystem, and the critical processes that drive the dynamics of the carbon and water pools, and their coupling, such as photosynthesis and ET, using emulation of more complex modeling representations (e.g., Smallman et al., 2017, 2019). The model that we demonstrate also operates at a given pixel scale linked to resolution of satellite observations. Similar to Figure 1, observational data (orange boxes) provide con-

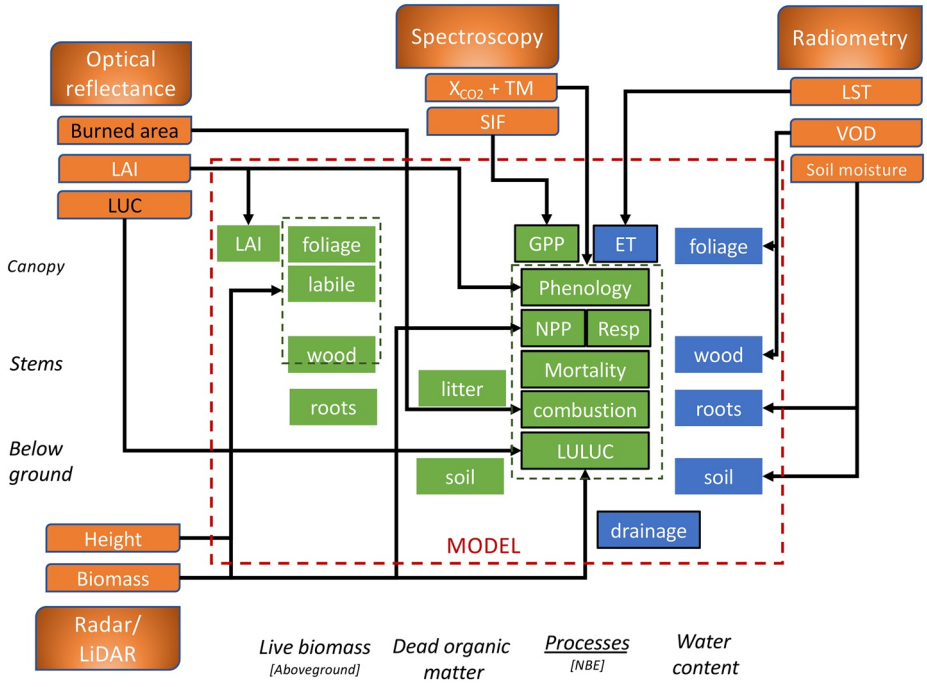

Figure 16. A schematic of a terrestrial carbon cycle model and how different satellite derived data sets can be used to inform different components of this model.

19449208, 2021, 1, Downloaded from https://agupubs.onlinelibrary.wiley.com/doi/10.1029/2020RG000711, Wiley Online Library on [10/11/2025]. See the Terms and Conditions (https://onlinelibrary.wiley.com/terms-and-conditions) on Wiley Online Library for rules of use; OA articles are governed by the applicable Creative Commons License

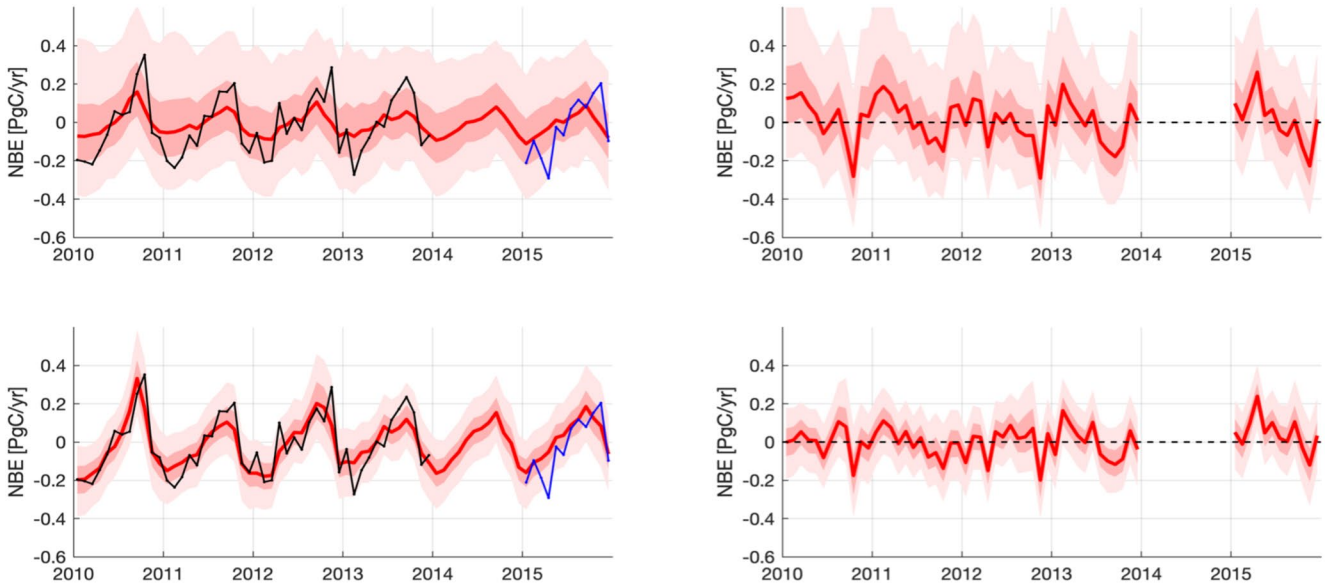

Figure 17. Monthly CARDAMOM NBE estimates (red = median, dark pink = 25th–75th percentile and light pink = 5th −95th percentile) over South America for 2010–2015. (top left) The CARDAMOM estimate and uncertainty (red shading) for NBE prior to assimilation of satellite data and (Top right) the difference between observed NBE and model (black data are from GOSAT and blue data are from OCO-2). (bottom left) CARDAMOM estimates after initial conditions and process parameters were constrained by 2010-13 GOSAT-derived CMS-Flux NBE (black line), as well as land surface data sets (biomass, leaf area, soil carbon and fluorescence) and atmospheric CO inversion data sets. The 2015 OCO-2-derived CMS-Flux NBE (blue line) was withheld from the assimilation for purposes of validation. (bottom right) Observed, Model after assimilation of data. The model and methodologies are described in Bloom et al. (2015 and 2016). CARDAMOM, Carbon Data Model Framework; CO, carbon monoxide; CMS, Carbon Monitoring System; GOSAT, Greenhouse Observation SATellite; NBE, net biosphere exchange.

straints on particular stocks and fluxes, or combinations of these (indicated by black lines). Optical data, such as from MODIS (Figure 1) provide a constraint on plant canopies and photosynthesis; spectroscopy constrains net fluxes through atmospheric observations; radiometry constrains energy balance and water cycling; radar/LIDAR data constrain biomass and vegetation structure.

Quantifying the various parameters (fluxes, reservoirs) in Figure 16 involves minimizing a cost function that depends on the observations and model so that under local environmental forcing, the model representation has the highest likelihood of representing local observations of carbon and water cycles and associated uncertainty. Errors in forcing and model structure will be probabilistic, spanning a parameter hypervolume dependent on the information content and number of observations. This fusion of model and data produces estimates of initial conditions at the start of the simulation period, and the parameters that describe the processes (e.g., rate constants) and their climate sensitivity (e.g., Bloom et al., 2016). A challenge in model-data fusion is to properly understand and propagate the uncertainty in the observations. Data need to be weighted by uncertainty and bias-corrected so that model tests and calibration are appropriate to the information content of the various observations. Connecting models and data also requires careful attention to the observation operator as sampling and resolution of the data must be accounted for in any model/data comparison. Furthermore, there is ongoing debate about whether frameworks should assimilate directly observed satellite quantities such as reflectance, or to assimilate their products, such as leaf area index (e.g., Quaife et al., 2008).

An example of the use of satellite data for constraining carbon balance and its sensitivity to temperature and TWS and other carbon processes is shown in Figure 17 for South America. For this analysis, satellite derived estimates of NBE, SIF, CO, TWS, LAI, fire emissions, and temperature, as discussed in previous sections, are assimilated into the Carbon Data Model Framework (CARDAMOM; e.g., Bloom et al., 2015; Y. Yin et al., 2020), which is similar in structure to Figure 16. 2020. A Markov Chain Monte Carlo (MCMC) approach is used to find the best solution for the model parameters shown in Figure 16. The top panels show the modeled and observed NBE estimates (top left) before assimilation and the difference between modeled and observed (right panel). The bottom panels show model and data after assimilation. OCO-2 data was not

19449208, 2021, 1, Downloaded from https://agupubs.onlinelibrary.wiley.com/doi/10.1029/2020RG000711, Wiley Online Library on [10/11/2025]. See the Terms and Conditions (https://onlinelibrary.wiley.com/terms-and-conditions) on Wiley Online Library for rules of use; OA articles are governed by the applicable Creative Commons License

19449208, 2021, 1, Downloaded from https://agupubs.onlinelibrary.wiley.com/doi/10.1029/2020RG000711, Wiley Online Library on [10/11/2025]. See the Terms and Conditions (https://onlinelibrary.wiley.com/terms-and-conditions) on Wiley Online Library for rules of use; OA articles are governed by the applicable Creative Commons License

included in the assimilation and withheld to evaluate the NBE estimate for the later time period. The updated model parameters are then used to project NBE to the time period covered by OCO-2 and shows that the model estimate and spread (based on the data constrained parameter uncertainty from assimilation step) can capture NBE seasonal timing and mean and reduce both the differences and calculated uncertainty of seasonal NBE in the prediction window with a reduction in the RMS of 0.12–0.096 PgC/y. Further analysis is needed to determine if the remaining differences are due to data or model error. Nevertheless, this example illustrates why the approach of integrating satellite data into a reduced complexity models shows promise for carbon cycle prediction over at least the time span of the assimilated data (e.g., Bloom et al., 2020), that is, using N years of assimilated satellite data allows for an update of the initial conditions and carbon/water processes such that the model can then predict ~N years of carbon fluxes.

6. Summary and Recommendations

An Earth System perspective is required to reduce uncertainties in tropical carbon balance and in turn improve estimates of the tropical carbon sink and its evolution. Mechanistically, this means using multiple different types of observations to disentangle carbon and water processes and their linkages, and by extension the links to the energy and nutrient cycles. Ideally these observations of different carbon, water, and energy states or fluxes are jointly used within an Earth System modeling framework to quantify the distribution of process controlling carbon balance and how these processes vary across the tropics. Based on the previous discussions we recommend the following:

6.1. Recommendation 1: Observations

There are several observables that we already know could transform our understanding of the tropical carbon cycle and its links to the Earth System. The effect of tropical vegetation change on the carbon cycle has mainly been assessed through an activity data. That approach should be replaced by direct estimation of forest biomass change requiring a new approach to the design of missions for satellite biomass which to date have aimed at static maps for a single point in time. Soil moisture, especially in the root zone, is thought to be a primary moderator of the tropical carbon sink based on data and models (e.g., Gentine et al., 2019; Green et al., 2019). Likely though, quantifying soil moisture will require use of multiple microwave and/or radar measurements in order to evaluate the profile of moisture from the canopy through the root zone. Correspondingly, improved estimates of ET and its subcomponents (transpiration, canopy evaporation, and soil evaporation) are needed to evaluate vegetation/atmosphere feedbacks, given the poor agreement in the ET estimates from moist forests using top-down approaches. Improved estimates of NBE, at finer temporal and spatial scales, are needed for attributing changes in carbon balance to climate variability and human activities and this will require greatly improved spatio-temporal sampling and accuracy of XCO_2 measurements, likely using spectrometers based in a geostationary orbit or a constellation of sounders. These sounders also typically measure SIF, a proxy for GPP, and which benefits from the improved sampling of these types of satellite configurations. This top-down view from satellites is optimized when combined with aircraft campaigns and surface networks; surface and aircraft data provide ground truthing of the satellite data and allow us to relate the top-down view to detailed process knowledge. Coordinated aircraft campaigns and surface networks with satellite missions are therefore critical toward quantifying biogeochemical processes at pan-tropical scales and fully leveraging the investment in these resources.

6.2. Recommendation 2: Process Estimation, Data Assimilation, and Modeling

Many Earth System models can assimilate satellite data for updating state parameters. However, we also need Earth System Models that can represent the range of processes controlling Carbon-Water-Energy interactions across the tropics and can also assimilate current and projected satellite data sets to quantify processes and feedbacks in a statistically robust manner. These models would also be useful for identifying current and new observations that are the most important for quantifying the evolution of the carbon sink. We recommend formulating new Earth System models so that the model parameters and uncertainties and their covariations are more easily quantified, structural errors are identified, and the model can learn (or parameters inverted from observations) from available satellite observations (e.g., T. Schneider et al., 2017;

M. J. Smith et al., 2014). Ideally such models should be formulated to take advantage up upcoming observations of vegetation at sub-kilometer scale from such as the ESA Copernicus Hyperspectral Imaging Mission (CHIME) and NASA Surface Biology – Geology (SBG) missions.

An alternative approach for quantifying carbon/climate feedbacks is through the use of the emergent constraint approach (e.g., Cox et al., 2013; Hall et al., 2019) which uses satellite data with multiple models to evaluate key processes controlling climate. However, use of satellite data for evaluating how carbon/climate feedbacks are distributed across the tropics and the globe are still in their beginning stages (e.g., Bowman et al., 2018) and it is unclear how these studies could be used to update the corresponding Earth System models for testing how different socio-economic pathways result in future climate states.

6.3. Recommendation 3: Address Land/Atmosphere Feedbacks

While much research has been focused on the direct effects of water cycling and temperature stress on forest composition and carbon balance, the satellite record points toward the increasing role of vegetation/atmosphere feedbacks in modulating the terrestrial carbon sink. Campaigns with an Earth System perspective are needed that integrate surface, aircraft, and satellite data; the detailed Processes Knowledge About Vegetation/Atmosphere Feedbacks and Aquatic Carbon from surface measurements can be evaluated against integrative (or top-down) aircraft and satellite observations to ensure the process distribution is also quantified.

Appendix: Description of data sets used in this review

Biomass

Two pan-tropical AGB maps (Baccini et al., 2012; S. S. Saatchi et al., 2011) have recently been developed at grid scales of 1 km and 500 m, respectively. Both use similar input data layers and are principally driven by the same (though re-analyzed) spaceborne LiDAR data set acquired by ICESat GLAS between 2003 and 2009. However, they use different ground data sets for calibration and different spatial modeling methodologies. As a result, there are significant regional differences between them, which tend to decrease when AGB estimates are aggregated to country or biome scale (Mitchard et al., 2013). The AGB and C calculations in this paper are based on an updated global version of the S. S. Saatchi et al. (2011) map. The global map is developed by making use of the ICES at GLAS measurements globally and existing regional algorithms for the global ecological zones from a literature review (Asner & Mascaro, 2014; Margolis et al., 2015; Mitchard et al., 2012; Mitchard et al., 2013; Neigh et al., 2013; Wu et al., 2009; Yu & Saatchi, 2016).

The map was developed originally at 100 m spatial resolution. We developed the spatial variations of canopy height of forests in the form of average Lorey's height (basal area weighted height) which is considered to have the most direct relationship to above ground biomass (Lefsky, 2010). The spatial modeling is performed using the Maximum Entropy estimation algorithm (MaxEnt) (S. J. Phillips et al., 2006; S. S. Saatchi et al., 2011; L. Xu et al., 2016). MaxEnt is a machine learning algorithm that make use of a Bayesian estimation approach to provide the probability of biomass range for each pixel of a map, defined by the GLAS derived biomass or height as training data. The probability maps were then combined to develop the height or biomass map and its pixel level uncertainty. Here, we used the GLAS based heights as samples and 12 remote sensing image layers (four Landsat visible reflectance, two ALOS PALSAR HH and HV polarizations, two SRTM metrics of mean and variance of elevation) as spatial layers for the machine learning algorithm. We randomly selected 80% of the Lorey's height samples (~4,600,000) as input for the model, and keep the remaining 20% for evaluating the fit. The height map at 100 m spatial resolution was further corrected for any systematic errors, particularly across high biomass density forests in tropics using a large data set of airborne scanning lidar (ALS) sampled across tropical forests in all three continents (Ferraz et al., 2018; Meyer et al., 2019; L. Xu et al., 2017). The height map was then used with height-biomass allometric models developed for different forest types across the globe using ground plots (44 biomass model) to estimate above ground live biomass (AGB) from height for each pixel. The biomass map was validated at the regional scale using a large number of ground plots acquired from national forest inventory data from northern temperate and boreal regions and a suite of research plots in tropical and sub-tropical regions. The below-ground

19449208, 2021, 1, Downloaded from https://agupubs.onlinelibrary.wiley.com/doi/10.1029/2020RG000711, Wiley Online Library on [10/11/2025]. See the Terms and Conditions (https://onlinelibrary.wiley.com/terms-and-conditions) on Wiley Online Library for rules of use; OA articles are governed by the applicable Creative Commons License

19449208, 2021, 1, Downloaded from https://agupubs.onlinelibrary.wiley.com/doi/10.1029/2020RG000711, Wiley Online Library on [10/11/2025]. See the Terms and Conditions (https://onlinelibrary.wiley.com/terms-and-conditions) on Wiley Online Library for rules of use; OA articles are governed by the applicable Creative Commons License

woody live biomass (BGB) was estimated using allometric models developed from root-to-shoot ratios for different forests types as recommended by the Intergovernmental Panel on Climate Change (IPCC) guidelines (IPCC, 2006; Mokany et al., 2006). We added AGB and BGB values and aggregated the biomass map to 1 km in order to reduce the uncertainty at finer spatial resolution. A factor of 0.47 was used to convert forest woody biomass to C content (McGroddy et al., 2004). The 1-km global data set is currently available from the JPL Carbon Monitoring System website (https://cmsun.jpl.nasa.gov) (Carreiras, Quegan, et al., 2017). The MaxeEnt machine learning algorithm produces probability distributions for the biomass ranges which we take as our uncertainties for this map. The uncertainties are shown in Figure 17.

Fire Emissions Based on Atmospheric CO

The basis for estimates of CO emissions from biomass burning sources shown in Figure 6 is a 15-year inversion analysis (Jiang et al., 2017) that uses the adjoint of the GEOS-Chem model (Henze et al., 2007) and MOPITT Version 6J multispectral CO observations (Deeter et al., 2014). This approach uses latitude bias-corrected MOPITT data (total CO columns and CO vertical profiles) averaged on the GEOS-Chem 5° longitude × 4° latitude grid to constrain model estimates of monthly CO fluxes in each grid cell from three primary source sectors: anthropogenic fossil fuel and biofuel, biomass burning and oxidation from BVOCs. CO from methane oxidation, ∼28% of the global CO budget (Haughlustaine et al., 2006), was estimated to be 877 Tg CO/yr as an aggregated global source. The Model of Emissions of Gases and Aerosols from Nature (MEGAN), version 2.0 (Guenther et al., 2006) was used to formulate the prior CO emissions from BVOCs. Biomass burning prior fluxes are from the Global Fire Emission Database (GFED3; van der Werf et al., 2010) and global prior fluxes for fossil fuel are from the Emission Database for Global Atmospheric Research (EDGAR 3.2FT2000; Olivier & Berdowski et al., 2001) with updated inventories for the northern hemisphere described in Jiang et al. (2017). The monthly, gridded CO flux estimates from Jiang et al. (2017) are then re-partitioned into sector CO emissions for biomass burning (BB), fossil fuels (FF) and biogenic non-methane VOC emissions (BIO) using a Bayesian inference approach that explicitly accounts for both a priori and posterior CO flux uncertainties (Bloom et al., 2015; J. R. Worden et al., 2017). This re-partitioning also allows the use of updated a priori estimates and here we applied emission factor uncertainties from GFED4 (van der Werf et al., 2017). As discussed in Jiang et al. (2013) and H. Worden et al. (2019), uncertainties for these emissions are calculated by comparing different emissions estimates using the different MOPITT CO products (profile, total column, and near-surface) as these are sensitive to different aspects of model chemistry and the emissions distributions; with this approach an uncertainty for any given grid box is approximately 23%.

Uncertainties in Carbon Emissions from Fires using BA and CO estimates

A recent paper by Yin (et al., 2020) assimilated CO and burned area estimates, as well as LAI and SIF into the CARDAMOM modeling/assimilation (Figure 18) framework for the purpose of quantifying NBE as a result of the recent fire decline. As shown in Figure 18, this analysis indicates that after assimilation CARDAMOM estimates a yearly uncertainty of ∼18% for tropical fire carbon emissions and both the burned area (based on GFED) and CO based estimates (from MOPITT) agree to within this uncertainty (Figure 19).

Gross Primary Production from Solar Induced Fluorescence

Although SIF has been retrieved from multiple satellites with nearly continuous global coverage since 1996, no single instrument offers a long term continuous running time series spanning multiple decades. Differences in instrument characteristics and retrieval methodology have challenged efforts to use multiple sensors to assess long term change, especially at sub-regional scale (Parazoo et al., 2019). OCO-2 currently offers the most accurate measurements at scales traceable to canopy level measurements, and currently spans a record beginning September 2014 (Magney et al., 2019; Parazoo et al., 2019). Monthly GPP is estimated from OCO-2 following the formalism of Parazoo et al. (2014). Grid scale GPP is inferred from a precision-weighted minimization of OCO-2 SIF, which is regressed against global GPP from upscaled flux tower data (e.g., Frankenberg et al., 2011; C. G. Jung et al., 2011), and is also subjected to a priori knowledge

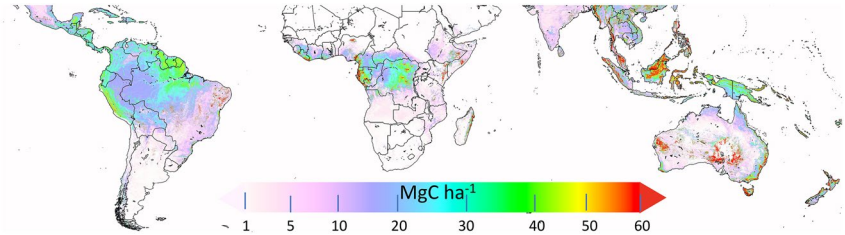

Figure 18. The uncertainy map for the above ground carbon shown in Figure 3. The uncertainty map is derived from a Bayesian approach described in Appendix A.1. The error is given at the 1-km pixel level (S. S. Saatchi et al., 2011).

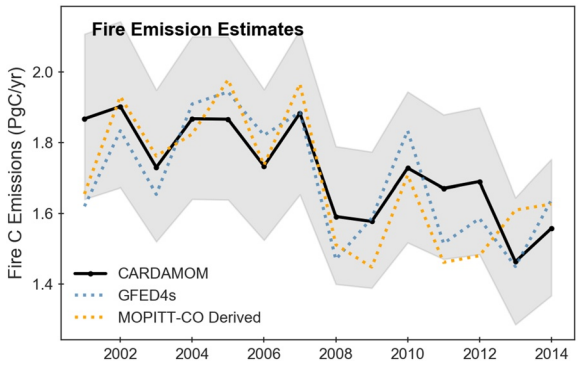

Figure 19. Estimate of tropical carbon emissions using the CO and burned area estimates assimilated into CARDAMOM (Section 4.2), adapted from Yin et al. (2019). CO, carbon monoxide.

of GPP derived from an ensemble of terrestrial ecosystem models (Sitch et al., 2015). SIF measurements are aggregated to 1 × 1° over a month. The precision of the estimate is estimated as the standard error, assuming a single sounding measurement error of 0.5 W m^{-2} um^{-1} sr^{-1} and divided by the square root of the number of observations for each grid. SIF measurements are scaled to GPP based upon biome specific scaling factors. The final GPP estimate is a balance between the prior and the SIF-derived GPP which is screened for clouds and scaled to daily average using cosine of solar zenith angle weighting. Figure 7 (bottom panel) show OCO-2 assessment of spatial and seasonal photosynthetic variability in the tropics.

XCO_2 and CO_2 fluxes

Net Biosphere Exchange (NBE) is optimized by assimilating GOSAT data (O'Dell et al., 2012) including v7.3 X_{CO2} retrievals and OCO-2 v7 retrievals into the CMS-Flux 4D-Var inversion framework (Bowman et al., 2017; Liu et al., 2014, 2017), which uses the GEOS-Chem adjoint model (Henze et al., 2007). GEOS-Chem (http://www.geos-chem.org) is a global chemical transport model (CTM) that uses GEOS (Goddard Earth Observing System) assimilated meteorological fields from the NASA Global Modeling Assimilation Office (GMAO) (Rienecker et al., 2008). We run the model at a horizontal resolution of 4° (latitude) 5° (longitude). The model has 47 vertical levels, with the top up to 0.01 hPa. The inversion covers 2010 to 2015. Due to changes of radiance calibration of GOSAT spectra in 2014, we only analyze 2010–2013 inversion results constrained by GOSAT, and 2015 constrained by OCO-2 column CO_2 observations. Fluxes are currently provided from 2010 through 2013 for the GOSAT time period and 2015 for the OCO-2 time period with updates to CO_2 fluxes soon to be available.

The estimates of NBE using top-down fluxes can have significant uncertainty, even at regional scales, they also vary significantly from region to region so that so that no one number adequately describes the NBE estimates. As a result, current studies (e.g., Bowman et al., 2017; Liu et al., 2017) attempt to aggregate NBE over longer time periods and regions and then quantify differences between time periods in order to reduce the error through averaging and then through potential bias subtraction. In the case of the Liu et al. (2017) paper, uncertainties are tested by quantifying the expected versus actual XCO_2 signal from the flux difference.

19449208, 2021, 1, Downloaded from https://agupubs.onlinelibrary.wiley.com/doi/10.1029/2020RG000711, Wiley Online Library on [10/11/2025]. See the Terms and Conditions (https://onlinelibrary.wiley.com/terms-and-conditions) on Wiley Online Library for rules of use; OA articles are governed by the applicable Creative Commons License

19449208, 2021, 1, Downloaded from https://agupubs.onlinelibrary.wiley.com/doi/10.1029/2020RG000711, Wiley Online Library on [10/11/2025]. See the Terms and Conditions (https://onlinelibrary.wiley.com/terms-and-conditions) on Wiley Online Library for rules of use; OA articles are governed by the applicable Creative Commons License

TRMM GPM and GRACE

The Tropical Rainfall Measuring Mission (TRMM) and Global Precipitation Monitoring (GPM) missions (e.g., Hou et al., 2014; Kummerow et al., 1998), have provided radar and microwave based estimates of rainfall from 1997 to the present. Uncertainties in this data set are well described in Rauniyar et al. (2017); different rainfall retrieval algorithms provide different estimates of rainfall with up to 100% differences for light rain and 30% differences for intermediate to heavy rain. While calibration of the data is therefore necessary to produce rainfall estimates from the observed radar and microwave signals and can vary depending on the approach used (e.g., Bookhagen & Burbank, 2010), the data can quantify interannual changes in monthly rainfall as determined through ground measurements (e.g., Almazroui, 2011). The TRMM mission stopped acquiring data in early 2015 but was followed by GPM that was launched in February 2014. In this paper we use a combined data set from the TRMM and GPM satellites (e.g., Huffman et al., 2007).

Monthly terrestrial water storage observations are now available from 2002 to 2017 and the ongoing GRACE follow-on mission (GRACE-FO). GRACE observations represent changes in the global gravity field as changes in equivalent water height with roughly 3-degrees of resolution and a precision of 1.5 cm water equivalent (Tapley et al., 2004). The monthly GRACE TWS uncertainty is estimated to be 25 mm/mo for an 800 km averaging radius (Rodell et al., 2004), approximately the same size of the selected basin groups in this study. We fill observation gaps and interpolate GRACE TWS to ensure temporal equivalence to P and R data sets, and calculate the arithmetic mean of these GRACE TWS retrievals (Sakumura et al., 2014).

Evapotranspiration

PT-JPL

The Evapotranspiration (ET) data shown here is retrieved by the PT-JPL algorithm (R. A. Fisher et al., 2008) using land surface properties from MODIS and atmospheric properties from MERRA. The algorithm has been widely validated throughout the literature as one of the top performing global remote sensing ET models (e.g., Y. Chen et al., 2014; Ershadi et al., 2014; Gomis-Cebolla et al., 2019; Jiménez et al., 2018; Michel & Seidling, 2016; Miralles et al., 2016; Polhamus et al., 2013; Purdy et al., 2018; Talsma et al., 2018; Vinukollu et al., 2011). Through eco-physiological constraint functions, PT-JPL retrieves actual ET by downscaling potential ET (PET) from the Priestley-Taylor equation (J. B. Fisher et al., 2011; Priestley & Taylor, 1972):

$$PET = \alpha \frac{\Delta}{\Delta + \gamma} R_n \tag{1}$$

where Δ is the slope of the saturation-to-vapor pressure curve, dependent on near surface air temperature (T_a) and water vapor pressure (e_a), γ is the psychrometric constant, R_n is net radiation (W m^{-2}), and α is the Priestley-Taylor coefficient of 1.26; PET is in units of W m^{-2}.

A series of scalar functions, based on atmospheric moisture, specifically vapor pressure deficit (D_a) and relative humidity (RH), and vegetation indices, including normalized difference and soil adjusted vegetation indices ($NDVI$ and $SAVI$), simultaneously reduce PET to actual ET, and partition total ET into three sources for canopy transpiration (ET_c), soil evaporation (ET_s), and interception evaporation (ET_i):

$$ET = ET_c + ET_s + ET_i \tag{2}$$

$$ET_c = \left(1 - f_{wet}\right) f_g f_T f_M \alpha \frac{\Delta}{\Delta + \gamma} R_{nc} \tag{3}$$

$$ET_s = \left(f_{wet} + f_{SM}\left(1 - f_{wet}\right)\right) \alpha \frac{\Delta}{\Delta + \gamma} \left(R_{ns} - G\right) \tag{4}$$

$$ET_i = f_{wet} \alpha \frac{\Delta}{\Delta + \gamma} R_{nc} \tag{5}$$

$$f_T = e^{-\left(\frac{T_a - T_{opt}}{T_{opt}}\right)^2} \quad (6)$$

$$T_{opt} = T_{max}\ at\ max\left(R_n T_a \frac{SAVI}{D_a}\right) \quad (7)$$

where f_{wet} is relative surface wetness (RH^4), f_g is green canopy fraction (f_{APAR} / f_{IPAR}) (Q. Zhang et al., 2005), f_T is a plant temperature constraint (Potter et al., 1993), f_M is a plant moisture constraint (f_{APAR} / $f_{APARmax}$) (Potter et al., 1993), and f_{SM} is a soil moisture constraint (RH^{Da}) [Bouchet, 1963; R. A. Fisher et al., 2008]. f_{APAR} is absorbed photosynthetically active radiation (PAR), f_{IPAR} is intercepted PAR, T_{opt} is the optimum temperature of plant phenology, and G is the soil heat flux (Purdy et al., 2016). R_{nc} and R_{ns} are R_n for the canopy and the soil, respectively, based on Leaf Area Index (LAI) derived from NDVI. PT-JPL is run globally and continuously in space and time with no need for calibration or site-specific parameters.

PT-JPL ET Uncertainty

The most recent validation of PT-JPL ET within ECOSTRESS demonstrates a normalized RMSE of 6%, bias of 8% and correlation of 0.88 for instantaneous retrievals (J. B. Fisher et al., 2020). In the tropical analysis of J. B. Fisher et al. (2009) in which comparisons of the PT-JPL ET estimates were compared against site data, the PT-JPL RMSE was 22.8 W m^{-2}, the bias was 7%, and the correlation was 0.91. At coarser spatiotemporal resolution analyses, such as discussed in this manuscript, accuracies improve substantially due to smoothing of noise and heterogeneity. Three independent evaluations (Y. Chen et al., 2014; Ershadi et al., 2014; Vinukollu et al., 2011) of PT-JPL, are highlighted here (e.g, McCabe et al., 2016; Michel et al., 2016; Miralles et al., 2016). These studies are noteworthy because all algorithms were run with common forcing data, the studies used an extensive set of validation data sets, and they represent independent groups from the US, Australia, and China. The Beijing/China study used the metrics of correlation coefficient (r^2) and slope of modeled regression against observed ET to determine that PT-JPL exhibited the highest r^2 and slope closest to 1.0 (Y. Chen et al., 2014), relative to other well-known ET models. Finally, the Australia study used the metrics of Nash-Sutcliffe Efficiency (NSE) and Root Mean Squared Difference (RMSD) to determine that PT-JPL exhibited the highest NSE and lowest RMSD (Ershadi et al., 2014).

ET Based on TWS, Rainfall and River Runoff

We estimate monthly total evapotranspiration across watersheds in the Amazon by using satellite observations of precipitation and terrestrial water storage (TWS), and ground-based measurements of river runoff (Maeda et al., 2017; Swann & Koven, 2017). Here, evapotranspiration is calculated as the monthly residuals between gridded precipitation estimates, in-situ runoff measurements, and the change of TWS:

$$\Delta W = P - R - ET$$

where ΔW is the change in sub-basin water storage, P is precipitation, and R is runoff. ΔW is estimated by using three Gravity Recovery and Climate Experiment (GRACE) TWS retrievals from Center for Space Research (CSR), GeoForschungsZentrum Potsdam (GFZ), and Jet Propulsion Laboratory (JPL). These three GRACE TWS retrievals are 1-degree land field products (each was downloaded from ftp://podaac-ftp.jpl.nasa.gov/allData/tellus/L3/land_mass/RL05/).

We fill observation gaps and interpolate GRACE TWS to ensure temporal equivalence to P and R data sets, and calculate the arithmetic mean of these GRACE TWS retrievals (Sakumura et al., 2014). Monthly runoff in each watershed is obtained from the Observation Service for the geodynamical, hydrological and biogeochemical control of erosion/alteration and material transport in the Amazon, Orinoco and Congo basins (SO-HYBAM) including in-situ river-gauge discharge measurements during 2003–2015. We use precipitation estimates from the Tropical Rainfall Measuring Mission (TRMM; 0.25 × 0.25° and 3-hourly

19449208, 2021, 1, Downloaded from https://agupubs.onlinelibrary.wiley.com/doi/10.1029/2020RG000711, Wiley Online Library on [10/11/2025]. See the Terms and Conditions (https://onlinelibrary.wiley.com/terms-and-conditions) on Wiley Online Library for rules of use; OA articles are governed by the applicable Creative Commons License

spatiotemporal resolutions; Huffman et al., 2007), Precipitation Estimation from Remotely Sensed Information derived from Artificial Neural Networks (PERSIANN) product (0.25 × 0.25° and daily spatiotemporal resolutions; Ashouri et al., 2015), and the Climate Research Unit (CRU) version 4 (0.5 × 0.5° and monthly spatiotemporal resolutions). We also calculate the arithmetic mean of the three precipitation products.

Uncertainty of ET using GRACE, runoff, and rainfall

The uncertainty of this ET product (σ_{ET}) is calculated as (Shi et al., 2019):

$$\sigma_{ET} = \sqrt{\sigma_{RAIN}^2 + \sigma_{GRACE}^2 + \sigma_{RUNOFF}^2}$$

where σ_{RAIN} is the uncertainty estimation from the three precipitation products, σ_{GRACE} is the uncertainty of GRACE TWS, and σ_{RUNOFF} is the uncertainty of runoff. We are not aware of any monthly runoff uncertainty estimates, and assume σ_{RUNOFF} is 10% of the runoff amount in each Amazonian sub-basin. Uncertainties for the GRACE and TRMM products are described in the previous section. However, for the rainfall estimates we assume the uncertainties are described by the RMS of the different rainfall estimates described above, which are informed by TRMM and GPM. At basin scale, ET uncertainties typically vary between 10% and 20%, and are limited by assumed uncertainty of the river runoff and rainfall.

Vapor Pressure Deficit (VPD)

Vapor Pressure Deficit is the difference between the saturation vapor content of air at temperature T, $e_s(T)$, and its actual vapor pressure, e_a (Seager et al., 2015). These are derived from the Atmospheric Infrared Sounder (AIRS/AMSU; Lambrigtsen & Lee, 2003) and can provide a record from 2002 through the present. To calculate VPD we use the following equation based on monthly near surface air temperature (T) and dew point (Td).

$$VPD = c_1 \times \exp\left(\frac{c_2 * T}{c_3 + T}\right) - c_1 \times \exp\left(\frac{c_2 * T_d}{c_3 + T_d}\right)$$

where, $c_1 = 0.611$ KPa, $c_2 = 17.5$, $c_3 = 240.978$°C. T and T_d are in °C and VPD is in KPa. The first and the second term in the above equation are the saturation vapor content of air T (e_s) and the actual vapor pressure (e_a), respectively.

Isotopic Composition of Lower Tropospheric Water Vapor

Satellite based measurements of the deuterium content of water vapor are typically obtained by inverting spectroscopically resolved radiances that are sensitive to HDO and H_2O molecular absorption at 1.6 (near infrared or NIR) and 8 microns (Thermal IR). Down-looking, Thermal IR based measurements are typically sensitive to the deuterium content of water vapor between 800 hPa and 300 hPa whereas near-IR based measurements are sensitive to the total column of water. Both data sets tend to have a precision ranging from 1%-4% with an accuracy of better than 1% (Frankenberg et al., 2013; A. Schneider et al., 2020; Worden et al, 2006, 2019), which is sufficient for resolving spatial and seasonal variations of the deuterium continent over tropical regions.

Data Availability Statement

The biomass data (Appendix A.1; S. S. Saatchi et al., 2011) can be found on the JPL CMS website cmsflux.jpl.nasa.gov. The OCO-2 SIF data (Appendix A.3) can be found here https://disc.gsfc.nasa.gov/datasets/OCO2_L2_Lite_SIF_8r/summary?keywords=oco2%20fluorescence. The NBE data (Liu et al., 2014; Appen-

19449208, 2021, 1, Downloaded from https://agupubs.onlinelibrary.wiley.com/doi/10.1029/2020RG000711, Wiley Online Library on [10/11/2025]. See the Terms and Conditions (https://onlinelibrary.wiley.com/terms-and-conditions) on Wiley Online Library for rules of use; OA articles are governed by the applicable Creative Commons License

dix A.4) are found on the JPL CMS web site cmsflux.jpl.nasa.gov. The CO emissions for fires (Jiang et al., 2017; Appendix A.2) can be found at the JPL CMS web site cmsflux.jpl.nasa.gov https://dashrepo.ucar.edu/data set/CO_Flux_Inversion_Attribution.html. https://doi.org/10.26024/r1r2-6620. The burned area data (van der Werf 2017; Appendix A.2) are from GFED4s: http://www.globalfiredata.org. TRMM and GPM data (Hou et al., 2014; Appendix A.5) can be found here: https://pmm.nasa.gov/trmm. The GRACE data (Sakumura et al., 2014; Appendix A.5) are from the following site https://grace.jpl.nasa.gov/data/get-data/. The ET data (J. B. Fisher et al., 2009; Appendix A.6) are on the following website http://josh.yosh.org/. The AIRS data used to derive VPD (Barkhordarian et al., 2017; Appendix A.7) are archived here: https://airs.jpl.nasa.gov/data/get_data. The Aura TES deuterium data (J. Worden et al., 2007; Appendix A.8) are from the Langley Atmospheric Research Center Data Archive https://eosweb.larc.nasa.gov/(NASA, 2019).

Acknowledgments
Part of this research was carried out at the Jet Propulsion Laboratory, California Institute of Technology, under a contract with the National Aeronautics and Space Administration. JBF was supported in part by NASA programs: ECOSTRESS, IDS, and SUSMAP. AAB, KWB, AGK, GRQ, and SSS were supported by NASA IDS program (NNH16ZDA001N-IDS). AGK and SSS were also supported by the NASA Carbon Cycle Science program (16-CARBON16-0130). MS was partly supported by the U.S. Department of Energy Office of Science Biological and Environmental Research as part of the Terrestrial Ecosystem Science Program through the Next-Generation Ecosystem Experiments (NGEE) Tropics project. PNNL is operated by Battelle Memorial Institute for the U.S. DOE under contract DE-AC05-76RLO1830. JRW and KB are partly supported by the NASA JPL TROPESS (Tropospheric Ozone and Precursors for Earth System Sounding) project. PG was supported by NASA grant 80NSSC18K0998.

References

Ahlström, A., Raupach, M. R., Schurgers, G., Smith, B., Arneth, A., Jung, M., et al. (2015). The dominant role of semi-arid ecosystems in the trend and variability of the land CO2 sink. *Science*, *348*(6237), 895–899. https://doi.org/10.1126/science.aaa1668

Almazroui, M. (2011). Calibration of TRMM rainfall climatology over Saudi Arabia during 1998–2009. *Atmospheric Research*, *99*(3–4), 400–414. https://doi.org/10.1016/j.atmosres.2010.11.006

Almeida, C. A. D., Coutinho, A. C., Esquerdo, J. C. D. M., Adami, M., Venturieri, A., Diniz, C. G., et al. (2016). High spatial resolution land use and land cover mapping of the Brazilian Legal Amazon in 2008 using Landsat-5/TM and MODIS data. *Acta Amazonica*, *46*(3), 291–302. https://doi.org/10.1590/1809-4392201505504

Anber, U., Gentine, P., Wang, S., & Sobel, A. H. (2015). Fog and rain in the Amazon. *Proceedings of the National Academy of Sciences*, *112*(37), 11473–11477. https://doi.org/10.1073/pnas.1505077112

Andela, N., Morton, D. C., Giglio, L., Chen, Y., Van Der Werf, G. R., Kasibhatla, P. S., & Bachelet, D. (2017). A human-driven decline in global burned area. *Science*, *356*(6345), 1356–1362. https://doi.org/10.1126/science.aal4108

Andela, N., Morton, D. C., Giglio, L., Paugam, R., Chen, Y., Hantson, S., et al. (2019). The Global Fire Atlas of individual fire size, duration, speed and direction. *Earth System Science Data*, *11*(2), 529–552. https://doi.org/10.5194/essd-2018-89

Andela, N., & van der Werf, G. R. (2014). Recent trends in African fires driven by cropland expansion and El Nino to La Nina transition. *Nature Climate Change*, *4*(9), 791–795. https://doi.org/10.1038/nclimate2313

Anderegg, W. R., Konings, A. G., Trugman, A. T., Yu, K., Bowling, D. R., Gabbitas, R., et al. (2018). Hydraulic diversity of forests regulates ecosystem resilience during drought. *Nature*, *561*(7724), 538.

Andreae, M. O., Rosenfeld, D., Artaxo, P., Costa, A. A., Frank, G. P., Longo, K. M., & Silva-Dias, M. A. F. D. (2004). Smoking rain clouds over the Amazon. *Science*, *303*(5662), 1337–1342. https://doi.org/10.1126/science.1092779

Aragão, L. E., Anderson, L. O., Fonseca, M. G., Rosan, T. M., Vedovato, L. B., Wagner, F. H., & Barlow, J. (2018). 21st Century drought-related fires counteract the decline of Amazon deforestation carbon emissions. *Nature Communications*, *9*(1), 1–12. https://doi.org/10.1038/s41467-017-02771-y

Arora, V. K., & Melton, J. R. (2018). Reduction in global area burned and wildfire emissions since 1930s enhances carbon uptake by land. *Nature Communications*, *9*(1), 1326. https://doi.org/10.1038/s41467-018-03838-0

Ashouri, H., Hsu, K. L., Sorooshian, S., Braithwaite, D. K., Knapp, K. R., Cecil, L. D., et al. (2015). PERSIANN-CDR: Daily precipitation climate data record from multisatellite observations for hydrological and climate studies. *Bulletin of the American Meteorological Society*, *96*(1), 69–83. https://doi.org/10.1175/BAMS-D-13-00068.1

Asner, G. P., & Mascaro, J. (2014). Mapping tropical forest carbon: Calibrating plot estimates to a simple LiDAR metric. *Remote Sensing of Environment*, *140*, 614–624. https://doi.org/10.1016/j.rse.2013.09.023

Babaeian, E., Sadeghi, M., Jones, S. B., Montzka, C., Vereecken, H., & Tuller, M. (2019). Ground, proximal and satellite remote sensing of soil moisture. *Reviews of Geophysics*, *57*(2), 530–616. https://doi.org/10.1029/2018RG000618

Baccini, A. G. S. J., Goetz, S. J., Walker, W. S., Laporte, N. T., Sun, M., Sulla-Menashe, D., et al. (2012). Estimated carbon dioxide emissions from tropical deforestation improved by carbon-density maps. *Nature Climate Change*, *2*(3), 182–185. https://doi.org/10.1038/nclimate1354

Bacour, C., Maignan, F., MacBean, N., Porcar-Castell, A., Flexas, J., Frankenberg, C., et al. (2019). Improving estimates of gross primary productivity by assimilating solar-induced fluorescence satellite retrievals in a terrestrial biosphere model using a process-based SIF model. *Journal of Geophysical Research: Biogeosciences*, *124*(11), 3281–3306. https://doi.org/10.1029/2019JG005040

Baker, N. R. (2008). Chlorophyll fluorescence: A probe of photosynthesis in vivo. *Annual Review of Plant Biology*, *59*, 89–113. https://doi.org/10.1146/annurev.arplant.59.032607.092759

Banerjee, T., & Linn, R. (2018). Effect of vertical canopy architecture on transpiration, thermoregulation and carbon assimilation. *Forests*, *9*(4), 1–18. https://doi.org/10.3390/f9040198

Barbosa, J. M., Broadbent, E. N., & Bitencourt, M. D. (2014). Remote sensing of aboveground biomass in tropical secondary forests: A review. *International Journal of Forestry Research*, *14*(1), https://doi.org/10.1155/2014/715796

Barkhordarian, A., Saatchi, S. S., Behrangi, A., Loikith, P. C., & Mechoso, C. R. (2019). A recent systematic increase in vapor pressure deficit over tropical South America. *Nature Publishing Group*, *9*(1), 1–12. https://doi.org/10.1038/s41598-019-51857-8

Bar-On, Y. M., Phillips, R., & Milo, R. (2018). The biomass distribution on Earth. *Proceedings of the National Academy of Sciences*, *115*(25), 6506–6511. https://doi.org/10.1038/pnas.1711842115

Beer, C., Reichstein, M., Tomelleri, E., Ciais, P., Jung, M., Carvalhais, N., et al. (2010). Terrestrial gross carbon dioxide uptake: Global distribution and covariation with climate. *Science*, *329*(5993), 834–838. https://doi.org/10.1126/science.1184984

Bennett, A. C., McDowell, N. G., Allen, C. D., & Anderson-Teixeira, K. J. (2015). Larger trees suffer most during drought in forests worldwide. *Nature Plants*, *1*(10), 15139.

Besnard, S., Carvalhais, N., Arain, M. A., Black, A., De Bruin, S., Buchmann, N., et al. (2018). Quantifying the effect of forest age in annual net forest carbon balance. *Environmental Research Letters*, *13*(12), 124018. https://doi.org/10.1088/1748-9326/aaeaeb

Beven, K. (1993). Prophecy, reality and uncertainty in distributed hydrological modeling. *Advances in Water Resources*, *16*(1), 41–51. http://www.sciencedirect.com/science/article/pii/030917089390028E

19449208, 2021, 1, Downloaded from https://agupubs.onlinelibrary.wiley.com/doi/10.1029/2020RG000711, Wiley Online Library on [10/11/2025]. See the Terms and Conditions (https://onlinelibrary.wiley.com/terms-and-conditions) on Wiley Online Library for rules of use; OA articles are governed by the applicable Creative Commons License

Bloom, A. A., Bowman, K., Liu, J., Konings, A. G., Worden, J., Parazoo, N. G., et al. (2020). Lagged effects dominate the inter-annual variability of the 2010-2015 tropical carbon balance. *Biogeosciences*, 1–49. https://doi.org/10.5194/bg-17-6393-2020

Bloom, A. A., Exbrayat, J. F., van der Velde, I. R., Feng, L., & Williams, M. (2016). The decadal state of the terrestrial carbon cycle: Global retrievals of terrestrial carbon allocation, pools, and residence times. *Proceedings of the National Academy of Sciences*, *113*(5), 1285–1290. https://doi.org/10.1073/pnas.1515160113

Bloom, A. A., & Williams, M. (2015). Constraining ecosystem carbon dynamics in a data-limited world: Integrating ecological common sense in a model–data fusion framework. *Biogeosciences*, *12*(5), 1299–1315. https://doi.org/10.5194/bg-12-1299-2015

Bonan, G. B. (2008). Forests and climate change: Forcings, feedbacks, and the climate benefits of forests. *Science*, *320*(5882), 1444–1449. https://doi.org/10.1126/science.1155121

Bonan, G. B., & Doney, S. C. (2018). Climate, ecosystems, and planetary futures: The challenge to predict life in Earth system models. *Science*, *359*(6375), 8328. https://doi.org/10.1126/science.aam8328

Bonan, G. B., Lombardozzi, D. L., Wieder, W. R., Oleson, K. W., Lawrence, D. M., Hoffman, F. M., & Collier, N. (2019). Model structure and climate data uncertainty in historical simulations of the terrestrial carbon cycle (1850–2014). *Global Biogeochemical Cycles*, *33*(10), 1310–1326. https://doi.org/10.1029/2019GB006175

Bonan, G. B., Williams, M., Fisher, R. A., & Oleson, K. W. (2014). Modeling stomatal conductance in the earth system: Linking leaf water-use efficiency and water transport along the soil-plant-atmosphere continuum. *Geoscientific Model Development*, *7*(5), 2193–2222. https://doi.org/10.5194/gmd-7-2193-2014

Bond-Lamberty, B., Bailey, V. L., Chen, M., Gough, C. M., & Vargas, R. (2018). Globally rising soil heterotrophic respiration over recent decades. *Nature*, *560*(7716), 80–83. https://doi.org/10.1038/s41586-018-0358-x

Bookhagen, B., & Burbank, D. W. (2010). Toward a complete Himalayan hydrological budget: Spatiotemporal distribution of snowmelt and rainfall and their impact on river discharge. *Journal of Geophysical Research*, *115*(F3). https://doi.org/10.1029/2009JF001426

Bowman, K. W., Cressie, N., Qu, X., & Hall, A. (2018). A hierarchical statistical framework for emergent constraints: Application to snow-albedo feedback. *Geophysical Research Letters*, *45*(23), 13–050. https://doi.org/10.1029/2018GL080082

Bowman, K. W., Liu, J., Bloom, A. A., Parazoo, N. C., Lee, M., Jiang, Z., et al. (2017). Global and Brazilian carbon response to El Niño Modoki 2011–2010. *Earth and Space Science*, *4*(10), 637–660. https://doi.org/10.1002/2016EA000204

Brando, P. M., Paolucci, L., Ummenhofer, C. C., Ordway, E. M., Hartmann, H., Cattau, M. E., et al. (2019). Droughts, wildfires, and forest carbon cycling: A pantropical synthesis. *Annual Review of Earth and Planetary Sciences*, *47*(1), 555–581. https://doi.org/10.1146/annurev-earth-082517-010235

Brandt, M., Wigneron, J. P., Chave, J., Tagesson, T., Penuelas, J., Ciais, P., et al. (2018). Satellite passive microwaves reveal recent climate-induced carbon losses in African drylands. *Nature ecology & evolution*, *2*(5), 827. https://doi.org/10.1038/s41559-018-0530-6

Brienen, R. J., Phillips, O. L., Feldpausch, T. R., Gloor, E., Baker, T. R., Lloyd, J., et al. (2015). Long-term decline of the Amazon carbon sink. *Nature*, *519*(7543), 344–348. https://doi.org/10.1038/nature14283

Carlson, K. M., Gerber, J. S., Mueller, N. D., Herrero, M., MacDonald, G. K., Brauman, K. A., & West, P. C. (2017). Greenhouse gas emissions intensity of global croplands. *Nature Climate Change*, *7*(1), 63–68. https://doi.org/10.1038/nclimate3158

Carreiras, J. M., Jones, J., Lucas, R. M., & Shimabukuro, Y. E. (2017). Mapping major land cover types and retrieving the age of secondary forests in the Brazilian Amazon by combining single-date optical and radar remote sensing data. *Remote Sensing of Environment*, *194*, 16–32. https://doi.org/10.1016/j.rse.2017.03.016

Carreiras, J. M., Quegan, S., Le Toan, T., Minh, D. H. T., Saatchi, S. S., Carvalhais, N., et al. (2017). Coverage of high biomass forests by the ESA BIOMASS mission under defnse restrictions. *Remote Sensing of Environment*, *196*, 154–162. https://doi.org/10.1016/j.rse.2017.05.003

Cassol, H. L. G., Carreiras, J. M. D. B., Moraes, E. C., Silva, C. V. D. J., Quegan, S., & Shimabukuro, Y. E. (2019). Retrieving secondary forest aboveground biomass from polarimetric ALOS-2 PALSAR-2 data in the Brazilian Amazon. *Remote Sensing*, *11*(1), 59. https://doi.org/10.3390/rs11010059

Cawse-Nicholson, K., Braverman, A., Kang, E. L., Li, M., Johnson, M., Halverson, G., et al. (2020). Sensitivity and uncertainty quantification for the ECOSTRESS evapotranspiration algorithm – DisALEXI. *International Journal of Applied Earth Observation and Geoinformation*, *89*, 102088. https://doi.org/10.1016/j.jag.2020.102088

Chazdon, R. L. (2008). Beyond deforestation: Restoring forests and ecosystem services on degraded lands. *Science*, *320*(5882), 1458–1460. https://doi.org/10.1126/science.1155365

Chen, Y., Morton, D. C., Andela, N., van der Werf, G. R., Giglio, L., & Randerson, J. T. (2017). A pan-tropical cascade of fire driven by El Niño/Southern Oscillation. *Nature Climate Change*, *7*(12), 906–911. https://doi.org/10.1080/0143116031000070283

Chen, Y., Randerson, J. T., Morton, D. C., Defries, R. S., Collatz, G. J., Kasibhatla, P. S., et al. (2011). Forecasting fire season severity in South America using sea surface temperature anomalies. *Science*, *334*(6057), 787–791. https://doi.org/10.1126/science.1209472

Chen, Y., Xia, J., Liang, S., Feng, J., Fisher, J. B., Li, X., et al. (2014). Comparison of satellite-based evapotranspiration models over terrestrial ecosystems in China. *Remote Sensing of Environment*, *140*, 279–293. https://doi.org/10.1016/j.rse.2013.08.045

Chuvieco, E., Lizundia-Loiola, J., Pettinari, M. L., Ramo, R., Padilla, M., Tansey, K., et al. (2018). Generation and analysis of a new global burned area product based on MODIS 250 m reflectance bands and thermal anomalies. *Earth System Science Data*, *10*(4), 2015–2031. https://doi.org/10.5194/essd-10-2015-2018

Cleveland, C. C., Houlton, B. Z., Smith, W. K., Marklein, A. R., Reed, S. C., Parton, W., et al. (2013). Patterns of new versus recycled primary production in the terrestrial biosphere. *Proceedings of the National Academy of Sciences of the United States of America*, *110*(31), 12733–12737. https://doi.org/10.1073/pnas.1302768110

Cleveland, C. C., Townsend, A. R., Taylor, P., Alvarez-Clare, S., Bustamante, M. M., Chuyong, G., et al. (2011). Relationships among net primary productivity, nutrients and climate in tropical rain forest: A pan-tropical analysis. *Ecology Letters*, *14*(9), 939–947. https://doi.org/10.1111/j.1461-0248.2011.01658.x

Cox, P. M., Pearson, D., Booth, B. B., Friedlingstein, P., Huntingford, C., Jones, C. D., & Luke, C. M. (2013). Sensitivity of tropical carbon to climate change constrained by carbon dioxide variability. *Nature*, *494*(7437), 341–344. https://doi.org/10.1038/nature11882

Dadap, N. C., Cobb, A. R., Hoyt, A. M., Harvey, C. F., & Konings, A. G. (2019). Satellite soil moisture observations predict fire vulnerability in Southeast Asian peatlands. *Environmental Research Letters*, *14*, 094014. https://doi.org/10.1088/1748-9326/ab3891

Dargie, G. C., Lewis, S. L., Lawson, I. T., Mitchard, E. T. A., Page, S. E., Bocko, Y. E., & Ifo, S. A. (2017). Age, extent and carbon storage of the central Congo Basin peatland complex. *Nature*, *542*(7639), 86–90. https://doi.org/10.1038/nature21048

Davidson, E. A., de Araújo, A. C., Artaxo, P., Balch, J. K., Brown, I. F., Bustamante, M. M., et al. (2012). The Amazon basin in transition. *Nature*, *481*(7381), 321–328. https://doi.org/10.1038/nature10717

19449208, 2021, 1, Downloaded from https://agupubs.onlinelibrary.wiley.com/doi/10.1029/2020RG000711, Wiley Online Library on [10/11/2025]. See the Terms and Conditions (https://onlinelibrary.wiley.com/terms-and-conditions) on Wiley Online Library for rules of use; OA articles are governed by the applicable Creative Commons License

Deeter, M. N., Martínez-Alonso, S., Edwards, D. P., Emmons, L. K., Gille, J. C., Worden, H. M., et al. (2014). The MOPITT version 6 product: Algorithm enhancements and validation. *Atmospheric Measurement Techniques*, *7*(11), 3623–3632. https://doi.org/10.5194/amt-7-3623-2014

Doughty, C. E., Metcalfe, D. B., Girardin, C. A. J., Amézquita, F. F., Cabrera, D. G., Huasco, W. H., et al. (2015). Drought impact on forest carbon dynamics and fluxes in Amazonia. *Nature*, *519*(7541), 78–80. https://doi.org/10.1038/nature14213

Dubayah, R. O., Sheldon, S. L., Clark, D. B., Hofton, M. A., Blair, J. B., Hurtt, G. C., & Chazdon, R. L. (2010). Estimation of tropical forest height and biomass dynamics using lidar remote sensing at La Selva, Costa Rica. *Journal of Geophysical Research*, *115*(G2). https://doi.org/10.1029/2009JG000933

Eamus, D. (1991). The Interaction of Rising Co2 and Temperatures with Water-Use Efficiency. *Plant, Cell & Environment*, *14*(8), 843–852. https://doi.org/10.1111/j.1365-3040.1991.tb01447.x

Eldering, A., Wennberg, P. O., Viatte, C., Frankenberg, C., Roehl, C. M., & Wunch, D. (2017). The orbiting carbon observatory-2: First 18 months of science data products. *Atmospheric Measurement Techniques*, *10*(2), 549–563. https://doi.org/10.5194/amt-2016-247

Englhart, S., Keuck, V., & Siegert, F. (2011). Aboveground biomass retrieval in tropical forests—The potential of combined X-and L-band SAR data use. *Remote Sensing of Environment*, *175*, 1260–1271. https://doi.org/10.1016/j.rse.2011.01.008

Ershadi, A., McCabe, M. F., Evans, J. P., Chaney, N. W., & Wood, E. F. (2014). Multi-site evaluation of terrestrial evaporation models using FLUXNET data. *Agricultural and Forest Meteorology*, *187*, 46–61. https://doi.org/10.1016/j.agrformet.2013.11.008

Exbrayat, J.-F., Liu, Y. Y., & Williams, M. (2017). Impact of deforestation and climate on the Amazon Basin's above-ground biomass during 1993–2012. *Scientific Reports*, *7*(1), 1–7. https://doi.org/10.1038/s41598-017-15788-6

Fan, Y., Li, H., & Miguez-Macho, G. (2013). Global patterns of groundwater depth. *Science*, *339*, 940–943. https://doi.org/10.1126/science.1229881

Fan, L., Wigneron, J. P., Ciais, P., Chave, J., Brandt, M., Fensholt, R., et al. (2019). Satellite-observed pantropical carbon dynamics. *Nature plants*, *5*(9), 1–8. https://doi.org/10.1038/s41477-019-0478-9

Ferraz, A., Saatchi, S., Xu, L., Hagen, S., Chave, J., Yu, Y., et al. (2018). Carbon storage potential in degraded forests of Kalimantan, Indonesia. *Environmental Research Letters*, *13*(9). https://doi.org/10.1088/1748-9326/aad782

Field, R. D., van der Werf, G. R., Fanin, T., Fetzer, E. J., Fuller, R., Jethva, H., et al. (2016). Indonesian fire activity and smoke pollution in 2015 show persistent nonlinear sensitivity to El Niño-induced drought. *Proceedings of the National Academy of Sciences*, *113*(33), 9204–9209. https://doi.org/10.1073/pnas.1524888113

Field, R. D., van der Werf, G. R., & Shen, S. S. P. (2009). Human amplification of drought-induced biomass burning in Indonesia since 1960. *Nature Geoscience*, *2*(3), 185–188. https://doi.org/10.1038/ngeo443

Fisher, J. B., Lee, B., Purdy, A. J., Halverson, G. H., Dohlen, M. B., Cawse-Nicholson, K., et al. (2020). ECOSTRESS: NASA's next generation mission to measure evapotranspiration from the international space station. *Water Resources Research 56*(4): 1–20. https://doi.org/10.1029/2019WR026058

Fisher, J. B., Malhi, Y., Bonal, D., Da Rocha, H. R., De Araujo, A. C., Gamo, M., et al. (2009). The land–atmosphere water flux in the tropics. *Global Change Biology*, *15*(11), 2694–2714. https://doi.org/10.1111/j.1365-2486.2008.01813.x

Fisher, J. B., Melton, F., Middleton, E., Hain, C., Anderson, M., Allen, R., et al. (2017). The future of evapotranspiration: Global requirements for ecosystem functioning, carbon and climate feedbacks, agricultural management, and water resources. *Water Resources Research*, *53*(4), 2618–2626. https://doi.org/10.1002/2016WR020175

Fisher, J. B., Whittaker, R. J., & Malhi, Y. (2011). ET come home: Potential evapotranspiration in geographical ecology. *Global Ecology and Biogeography*, *20*(1), 1–18. https://doi.org/10.1111/j.1466-8238.2010.00578.x

Fisher, R. A., Muszala, S., Verteinstein, M., Lawrence, P., Xu, C., McDowell, N. G., et al. (2015). Taking off the training wheels: The properties of a dynamic vegetation model without climate envelopes, CLM4. 5. *Geoscientific Model Development*, *8*(11), 3593–3619. https://doi.org/10.5194/gmd-8-3593-2015

Fisher, R. A., Williams, M., de Lourdes Ruivo, M., de Costa, A. L., & Meir, P. (2008). Evaluating climatic and soil water controls on evapotranspiration at two Amazonian rainforest sites. *Agricultural and Forest Meteorology*, *148*(6–7), 850–861. https://doi.org/10.1016/j.agrformet.2007.12.001

Flexas, J., Escalona, J. M., Evain, S., Gulías, J., Moya, I., Osmond, C. B., & Medrano, H. (2002). Steady-state chlorophyll fluorescence (Fs) measurements as a tool to follow variations of net CO2 assimilation and stomatal conductance during water-stress in C3 plants. *Physiologia Plantarum*, *114*(2), 231–240. https://doi.org/10.1034/j.1399-3054.2002.1140209.x

Forkel, M., Andela, N., Harrison, S. P., Lasslop, G., van Marle, M., Chuvieco, E., et al. (2019). Emergent relationships with respect to burned area in global satellite observations and fire-enabled vegetation models. *Biogeosciences*, *16*(1), 57–76. https://doi.org/10.5194/bg-16-57-2019

Frankenberg, C., Fisher, J. B., Worden, J., Badgley, G., Saatchi, S. S., Lee, J. E., & Yokota, T. (2011). New global observations of the terrestrial carbon cycle from GOSAT: Patterns of plant fluorescence with gross primary productivity. *Geophysical Research Letters*, *38*(17). https://doi.org/10.1029/2011GL048738

Frankenberg, C., Wunch, D., Toon, G., Risi, C., Scheepmaker, R., Lee, J. E., & Worden, J. (2013). Water vapor isotopologue retrievals from high-resolution GOSAT shortwave infrared spectra. *Atmospheric Measurement Techniques*, *6*(2), 263–274. https://doi.org/10.5194/amtd-5-6357-2012

Frankenberg, C., Yoshimura, K., Warneke, T., Aben, I., Butz, A., Deutscher, N., et al. (2009). Dynamic processes governing lower-tropospheric HDO/H2O ratios as observed from space and ground. *Science*, *325*(5946), 1374–1377. https://doi.org/10.1126/science.1173791

Friedlingstein, P., Cox, P., Betts, R., Bopp, L., von Bloh, W., Brovkin, V., et al. (2006). Climate–carbon cycle feedback analysis: Results from the C4MIP model intercomparison. *Journal of Climate*, *19*(14), 3337–3353. https://doi.org/10.1175/JCLI3800.1

Friedlingstein, P., et al. (2019). Global carbon budget 2019. *Earth System Science Data*, *11*(4), 1783–1838. https://doi.org/10.5194/essd-11-1783-2019

Friedlingstein, P., Meinshausen, M., Arora, V. K., Jones, C. D., Anav, A., Liddicoat, S. K., & Knutti, R. (2014). Uncertainties in CMIP5 climate projections due to carbon cycle feedbacks. *Journal of Climate*, *27*(2), 511–526. https://doi.org/10.1175/JCLI-D-12-00579.1

Friend, A. D., Lucht, W., Rademacher, T. T., Keribin, R., Betts, R., Cadule, P., et al. (2014). Carbon residence time dominates uncertainty in terrestrial vegetation responses to future climate and atmospheric CO2. *Proceedings of the National Academy of Sciences of the United States of America*, *111*(9), 3280–3285. https://doi.org/10.1073/pnas.1222477110

Fu, R., Yin, L., Li, W., Arias, P. A., Dickinson, R. E., Huang, L., et al. (2013). Increased dry-season length over southern Amazonia in recent decades and its implication for future climate projection. *Proceedings of the National Academy of Sciences*, *110*(45), 18110–18115. https://doi.org/10.1073/pnas.1302584110

19449208, 2021, 1, Downloaded from https://agupubs.onlinelibrary.wiley.com/doi/10.1029/2020RG000711, Wiley Online Library on [10/11/2025]. See the Terms and Conditions (https://onlinelibrary.wiley.com/terms-and-conditions) on Wiley Online Library for rules of use; OA articles are governed by the applicable Creative Commons License

Fung, I. Y., Doney, S. C., Lindsay, K., & John, J. (2005). Evolution of carbon sinks in a changing climate. *Proceedings of the National Academy of Sciences*, *102*(32), 11201–11206. https://doi.org/10.1073/pnas.0504949102
Galewsky, J., Steen-Larsen, H. C., Field, R. D., Worden, J., Risi, C., & Schneider, M. (2016). Stable isotopes in atmospheric water vapor and applications to the hydrologic cycle. *Reviews of Geophysics*, *54*(4), 809–865. https://doi.org/10.1002/2015RG000512
Ganesan, A. L., Schwietzke, S., Poulter, B., Arnold, T., Lan, X., & Rigby, M. (2019). Advancing scientific understanding of the global methane budget in support of the paris agreement. *Global Biogeochemical Cycles*, *9*(1), 53–38. https://doi.org/10.1029/2018GB006065
Gatti, L. V., Gloor, M., Miller, J. B., Doughty, C. E., Malhi, Y., Domingues, L. G., et al. (2014). Drought sensitivity of Amazonian carbon balance revealed by atmospheric measurements. *Nature*, *506*(7486), 76–80. https://doi.org/10.1038/nature12957
Gentine, P., Green, J. K., Guérin, M., Humphrey, V., Seneviratne, S. I., Zhang, Y., & Zhou, S. (2019). Coupling between the terrestrial carbon and water cycles—A review. *Environmental Research Letters*, *14*(8), 083003. https://doi.org/10.1088/1748-9326/ab22d6
Genty, B., Briantais, J. M., & Baker, N. R. (1989). The relationship between the quantum yield of photosynthetic electron transport and quenching of chlorophyll fluorescence. *Biochimica et Biophysica Acta (BBA) – General Subjects*, *990*(1), 87–92. https://doi.org/10.1016/S0304-4165(89)80016-9
Giardina, F., Konings, A. G., Kennedy, D., Alemohammad, S. H., Oliveira, R. S., Uriarte, M., & Gentine, P. (2018). Tall Amazonian forests are less sensitive to precipitation variability. *Nature Geoscience*, *11*(6), 405–409. https://doi.org/10.1111/nph.13646
Giglio, L., Randerson, J. T., & van der Werf, G. R. (2013). Analysis of daily, monthly, and annual burned area using the fourth-generation global fire emissions database (GFED4). *Journal of Geophysical Research*, *118*(1), 317–328. https://doi.org/10.1002/jgrg.20042
Gomis-Cebolla, J., Jimenez, J. C., & Sobrino, J. A. (2019). MODIS probabilistic cloud masking over the amazonian evergreen tropical forests: A comparison of machine learning-based methods. *International Journal of Remote Sensing*, *41*(1), 185–210. https://doi.org/10.1080/01431161.2019.1637963
Good, S. P., Noone, D., & Bowen, G. (2015). Hydrologic connectivity constrains partitioning of global terrestrial water fluxes. *Science*, *349*(6244), 175–177. https://doi.org/10.1126/science.aaa5931
Green, J. K., Konings, A. G., Alemohammad, S. H., Berry, J., Entekhabi, D., Kolassa, J., et al. (2017). Regionally strong feedbacks between the atmosphere and terrestrial biosphere. *Nature Geoscience*, *10*(6), 410–414. https://doi.org/10.1038/ngeo2957
Green, J. K., Seneviratne, S. I., Berg, A. M., Findell, K. L., Hagemann, S., Lawrence, D. M., & Gentine, P. (2019). Large influence of soil moisture on long-term terrestrial carbon uptake. *Nature*, *565*(7740), 476–479. https://doi.org/10.1038/s41586-018-0848-x
Guan, K., Pan, M., Li, H., Wolf, A., Wu, J., Medvigy, D., et al. (2015). Photosynthetic seasonality of global tropical forests constrained by hydroclimate. *Nature Geoscience*, *8*(4), 284–289. https://doi.org/10.1038/ngeo2382
Guenther, A., Karl, T., Harley, P., Wiedinmyer, C., Palmer, P. I., & Geron, C. (2006). Estimates of global terrestrial isoprene emissions using MEGAN (model of emissions of Gases and Aerosols from nature). *Atmospheric Chemistry and Physics*, *6*(11), 3181–3210. https://doi.org/10.5194/acpd-6-107-2006
Hall, A., Cox, P., Huntingford, C., & Klein, S. (2019). Progressing emergent constraints on future climate change. *Nature Climate Change*, *9*(4), 269–278. https://doi.org/10.1038/s41558-019-0436-6
Hancock, S., Armston, J., Hofton, M., Sun, X., Tang, H., Duncanson, L. I., et al. (2019). The GEDI simulator: A large-footprint waveform lidar simulator for calibration and validation of spaceborne missions. *Earth and Space Science*, *6*(2), 294–310. https://doi.org/10.1029/2018EA000506
Hansen, M. C., Potapov, P. V., Moore, R., Hancher, M., Turubanova, S. A. A., Tyukavina, A. ., & Kommareddy, A. (2013). High-resolution global maps of 21st-century forest cover change. *Science*, *342*(6160), 850–853. https://doi.org/10.1126/science.1244693
Hansen, M. C., Stehman, S. V., & Potapov, P. V. (2010). Quantification of global gross forest cover loss. *Proceedings of the National Academy of Sciences*, *107*(19), 8650–8655. https://doi.org/10.1073/pnas.0912668107
Hansis, E., Davis, S. J., & Pongratz, J. (2015). Relevance of methodological choices for accounting of land use change carbon fluxes. *Global Biogeochemical Cycles*, *29*(8), 1230–1246. https://doi.org/10.1002/2014GB004997
Harris, N. L., Brown, S., Hagen, S. C., Saatchi, S. S., Petrova, S., Salas, W., et al. (2012). Baseline map of carbon emissions from deforestation in tropical regions. *Science*, *336*(6088), 1573–1576. https://doi.org/10.1126/science.1217962
Harris, N. L., Goldman, E., Gabris, C., Nordling, J., Minnemeyer, S., Ansari, S., et al. (2017). Using spatial statistics to identify emerging hot spots of forest loss. *Environmental Research Letters*, *12*(2), 024012. https://doi.org/10.1088/1748-9326/aa5a2f
Hauglustaine, D. A., Hourdin, F., Jourdain, L., Filiberti, M. A., Walters, S., Lamarque, J. F., & Holland, E. A. (2004). Interactive chemistry in the Laboratoire de Météorologie Dynamique general circulation model: Description and background tropospheric chemistry evaluation. *Journal of Geophysical Research*, *109*(D4). https://doi.org/10.1029/2003JD003957
Henze, D. K., Hakami, A., & Seinfeld, J. H. (2007). Development of the adjoint of GEOS-Chem. *Atmospheric Chemistry and Physics*, *7*(9), 2413–2433. https://doi.org/10.5194/acpd-6-10591-2006
Hou, A. Y., Kakar, R. K., Neeck, S., Azarbarzin, A. A., Kummerow, C. D., Kojima, M., et al. (2014). The global precipitation measurement mission. *Bulletin of the American Meteorological Society*, *95*(5), 701–722. https://doi.org/10.1175/BAMS-D-13-00164.1
Houghton, R. A. (1999). The annual net flux of carbon to the atmosphere from changes in land use 1850–1990. *Tellus B: Chemical and Physical Meteorology*, *51*(2), 298–313. https://doi.org/10.3402/tellusb.v55i2.16764
Houghton, R. A. (2005). Aboveground forest biomass and the global carbon balance. *Global Change Biology*, *11*(6), 945–958. https://doi.org/10.1111/j.1365-2486.2005.00955.x
Houghton, R. A., Hall, F., & Goetz, S. J. (2009). Importance of biomass in the global carbon cycle. *Journal of Geophysical Research*, *114*(G2). https://doi.org/10.1029/2009JG000935
Houghton, R. A., & Nassikas, A. A. (2017). Global and regional fluxes of carbon from land use and land cover change 1850–2015. *Global Biogeochemical Cycles*, *31*(3), 456–472. https://doi.org/10.1002/2016GB005546
Houghton, R. A., Skole, D. L., Nobre, C. A., Hackler, J. L., Lawrence, K. T., & Chomentowski, W. H. (2000). Annual fluxes of carbon from deforestation and regrowth in the Brazilian Amazon. *Nature*, *403*(6767), 301–304. https://doi.org/10.1038/35002062
Huffman, G. J., Bolvin, D. T., Nelkin, E. J., Wolff, D. B., Adler, R. F., Gu, G., et al. (2007). The TRMM multisatellite precipitation analysis (TMPA): Quasi-global, multiyear, combined-sensor precipitation estimates at fine scales. *Journal of Hydrometeorology*, *8*(1), 38–55. https://doi.org/10.1175/JHM560.1
Humphrey, V., Zscheischler, J., Ciais, P., Gudmundsson, L., Sitch, S., & Seneviratne, S. I. (2018). Sensitivity of atmospheric CO 2 growth rate to observed changes in terrestrial water storage. *Nature*, *560*(7720), 628–631. https://doi.org/10.1038/s41586-018-0424-4
Ito, A., & Inatomi, M. (2012). Water-use efficiency of the terrestrial biosphere: A model analysis focusing on interactions between the global carbon and water cycles. *Journal of Hydrometeorology*, *13*(2), 681–694. https://doi.org/10.1175/JHM-D-10-05034.1
Jiang, Z., Jones, D. B. A., Worden, H. M., Deeter, M. N., Henze, D. K., Worden, J., (2013). Impact of model errors in convective transport on CO source estimates inferred from MOPITT CO retrievals. *Journal of Geophysical Research-Atmospheres*, *118*(4), 2073–2083. https://doi.org/10.1002/jgrd.50216

19449208, 2021, 1, Downloaded from https://agupubs.onlinelibrary.wiley.com/doi/10.1029/2020RG000711, Wiley Online Library on [10/11/2025]. See the Terms and Conditions (https://onlinelibrary.wiley.com/terms-and-conditions) on Wiley Online Library for rules of use; OA articles are governed by the applicable Creative Commons License

Jiang, Z., Worden, J. R., Worden, H., Deeter, M., Jones, D. B. A., Arellano, A. F., & Henze, D. K. (2017). A 15-year record of CO emissions constrained by MOPITT CO observations. *Atmospheric Chemistry and Physics*, *17*(7), 4565–4583. https://doi.org/10.5194/acp-17-4565-2017

Jiménez, C., Martens, B., Miralles, D. M., Fisher, J. B., Beck, H. E., & Fernández-Prieto, D. (2018). Exploring the merging of the global land evaporation WACMOS-ET products based on local tower measurements. *Hydrology and Earth System Sciences*, *22*(8), 4513–4533. https://doi.org/10.5194/hess-22-4513-2018

Jung, C. G., Shin, H. J., Park, M. J., Joh, H. K., & Kim, S. J. (2011). Evaluation of MODIS gross primary production (GPP) by comparing with GPP from CO 2 flux data measured in a mixed forest area. *Journal of the Korean Society of Agricultural Engineers*, *53*(2), 1–8. https://doi.org/10.5389/KSAE.2011.53.2.001

Jung, M., Reichstein, M., Schwalm, C. R., Huntingford, C., Sitch, S., Ahlström, A., et al. (2017). Compensatory water effects link yearly global land CO2 sink changes to temperature. *Nature*, *541*(7638), 516–520. https://doi.org/10.1038/nature20780

Kaiser, J. W., Heil, A., Andreae, M. O., Benedetti, A., Chubarova, N. Y., Jones, L., et al. (2012). Biomass burning emissions estimated with a global fire assimilation system based on observed fire radiative power. *Biogeosciences*, *9*(1), 527–554. https://doi.org/10.5194/bg-9-527-2012

Kennedy, D., Swenson, S., Oleson, K. W., Lawrence, D. M., Fisher, R., Carlos, A., & Gentine, P. (2019). Implementing plant hydraulics in the community land model, version 5. *Journal of Advances in Modeling Earth Systems*, *11*(2), 485–513. https://doi.org/10.1029/2018MS001500

Kent, R., Lindsell, J. A., Laurin, G. V., Valentini, R., & Coomes, D. A. (2015). Airborne LiDAR detects selectively logged tropical forest even in an advanced stage of recovery. *Remote Sensing*, *7*(7), 8348–8367. https://doi.org/10.3390/rs70708348

Kim, Y., Knox, R. G., Longo, M., Medvigy, D., Hutyra, L. R., Pyle, E. H., et al. (2012). Seasonal carbon dynamics and water fluxes in an a mazon rainforest. *Global Change Biology*, *18*(4), 1322–1334. https://doi.org/10.1111/j.1365-2486.2011.02629.x

Knorr, W., Jiang, L., & Arneth, A. (2016). Climate, CO2 and human population impacts on global wildfire emissions. *Biogeosciences*, *13*(1), 267–282. https://doi.org/10.5194/bg-13-267-2016

Konings, A. G., Bloom, A. A., Liu, J., Parazoo, N. C., Schimel, D. S., & Bowman, K. W. (2019). Global satellite-driven estimates of heterotrophic respiration. *Biogeosciences*, *16*(11), 2269–2284. https://doi.org/10.5194/bg-16-2269-2019

Krause, G. H., & Weis, E. (1991). Chlorophyll fluorescence and photosynthesis: The basics. *Annual Review of Plant Biology*, *42*(1), 313–349. https://doi.org/10.1146/annurev.pp.42.060191.001525

Kummerow, C., W. Barnes, T. K. O. A. and, 1998 (1998). The tropical rainfall measuring mission (TRMM) sensor package, *Journal of Atmospheric and Oceanic Technology*, *15*(3), 809–817, https://doi.org/10.1175/1520-0426

Kurz, W. A., Dymond, C. C., Stinson, G., Rampley, G. J., Neilson, E. T., Carroll, A. L., & Safranyik, L. (2008). Mountain pine beetle and forest carbon feedback to climate change. *Nature*, *452*(7190), 987–990. https://doi.org/10.1038/nature06777

Lambrigtsen, B. H., & Lee, S.-Y. (2003). Coalignment and synchronization of the AIRS instrument suite. *IEEE Transactions on Geoscience and Remote Sensing*, *41*(2), 343–351. https://doi.org/10.1109/TGRS.2002.808246

Le Quéré, C., Andrew, R. M., Friedlingstein, P., Sitch, S., Pongratz, J., Manning, A. C., et al. (2017). Global carbon budget 2017. *Earth System Science Data Discussions*, *10*(1), 1–79. https://doi.org/10.5194/essd-10-405-2018

Lee, J. E., Frankenberg, C., van der Tol, C., Berry, J. A., Guanter, L., Boyce, C. K., & Badgley, G. (2013). Forest productivity and water stress in Amazonia: Observations from GOSAT chlorophyll fluorescence. *Proceedings of the Royal Society B: Biological Sciences*, *280*(1761), 20130171. https://doi.org/10.2307/23478606

Lefsky, M. A. (2010). A global forest canopy height map from the Moderate Resolution Imaging Spectroradiometer and the Geoscience Laser Altimeter System. *Geophysical Research Letters*, *37*(15), https://doi.org/10.1029/2010GL043622

Lenton, T. M., Held, H., Kriegler, E., Hall, J. W., Lucht, W., Rahmstorf, S., & Schellnhuber, H. J. (2008). Tipping elements in the Earth's climate system. *Proceedings of the National Academy of Sciences*, *105*(6), 1786–1793. https://doi.org/10.1073/pnas.0705414105

Lewis, S. L., Brando, P. M., Phillips, O. L., van der Heijden, G. M., & Nepstad, D. (2011). The 2010 amazon drought. *Science*, *331*(6017), 554. https://doi.org/10.1126/science.1200807

Liu, J., Bowman, K. W., Lee, M., Henze, D. K., Bousserez, N., Brix, H., et al. (2014). Carbon monitoring system flux estimation and attribution: Impact of ACOS-GOSAT XCO2 sampling on the inference of terrestrial biospheric sources and sinks. *Tellus B: Chemical and Physical Meteorology*, *66*(1), 22486. https://doi.org/10.3402/tellusb.v66.22486

Liu, J., Bowman, K. W., Schimel, D. S., Parazoo, N. C., Jiang, Z., Lee, M., et al. (2017). Contrasting carbon cycle responses of the tropical continents to the 2015–2016 El Niño. *Science*, *358*(6360), eaam5690. https://doi.org/10.1126/science.aam5690

Llopart, M., Coppola, E., Giorgi, F., da Rocha, R. P., & Cuadra, S. V. (2014). Climate change impact on precipitation for the Amazon and La Plata basins. *Climatic Change*, *125*(1), 111–125. https://doi.org/10.1007/s10584-014-1140-1

MacBean, N., Peylin, P., Chevallier, F., Scholze, M., & Schürmann, G. (2016). Consistent assimilation of multiple data streams in a carbon cycle data assimilation system. *Geoscientific Model Development*, *9*(10), 3569–3588. https://doi.org/10.5194/gmd-9-3569-2016

Maeda, E. E., Ma, X., Wagner, F. H., Kim, H., Oki, T., Eamus, D., & Huete, A. (2017). Evapotranspiration seasonality across the amazon basin. *Earth System Dynamics*, *8*(2), 439–454. https://doi.org/10.5194/esd-8-439-2017

Maeda, E. E., Moura, Y. M., Wagner, F., Hilker, T., Lyapustin, A. I., Wang, Y., et al. (2016). Consistency of vegetation index seasonality across the Amazon rainforest. *International Journal of Applied Earth Observation and Geoinformation*, *52*, 42–53. https://doi.org/10.1016/j.jag.2016.05.005

Magney, T. S., Bowling, D. R., Logan, B., Grossmann, K., Stutz, J., & Blanken, P. (2019). Mechanistic evidence for tracking the seasonality of photosynthesis with solar-induced fluorescence. *Proceedings of the National Academy of Sciences*, *116*(24), 11640–11645. https://doi.org/10.1073/pnas.1900278116

Malhi, Y. (2012). The productivity, metabolism and carbon cycle of tropical forest vegetation. *Journal of Ecology*, *100*(1), 65–75. https://doi.org/10.1111/j.1365-2745.2011.01916.x

Malhi, Y., Silman, M., Salinas, N., Bush, M., Meir, P., & Saatchi, S. (2010). Introduction: Elevation gradients in the tropics: Laboratories for ecosystem ecology and global change research. *Global Change Biology*, *16*(12), 3171–3175. https://doi.org/10.1111/j.1365-2486.2010.02323.x

Marengo, J. A., & Bernasconi, M. (2015). Regional differences in aridity/drought conditions over northeast Brazil: Present state and future projections. *Climatic Change*, *129*(1–2), 103–115. https://doi.org/10.1007/s10584-014-1310-1

Marengo, J. A., Nobre, C. A., Tomasella, J., Oyama, M. D., Sampaio de Oliveira, G., De Oliveira, R., et al. (2008). The drought of Amazonia in 2005. *Journal of Climate*, *21*(3), 495–516. https://doi.org/10.1175/2007JCLI1600.1

Margolis, H. A., Nelson, R. F., Montesano, P. M., Beaudoin, A., Sun, G., Andersen, H. E., & Wulder, M. A. (2015). Combining satellite lidar, airborne lidar, and ground plots to estimate the amount and distribution of aboveground biomass in the boreal forest of North America. *Canadian Journal of Forest Research*, *45*(7), 838–855. https://doi.org/10.1139/cjfr-2015-0006

Marlier, M. E., DeFries, R. S., Voulgarakis, A., Kinney, P. L., Randerson, J. T., Shindell, D. T., et al. (2013). El Niño and health risks from landscape fire emissions in southeast Asia. *Nature Climate Change*, *3*(2), 131–136. https://doi.org/10.1038/nclimate1658

19449208, 2021, 1, Downloaded from https://agupubs.onlinelibrary.wiley.com/doi/10.1029/2020RG000711, Wiley Online Library on [10/11/2025]. See the Terms and Conditions (https://onlinelibrary.wiley.com/terms-and-conditions) on Wiley Online Library for rules of use; OA articles are governed by the applicable Creative Commons License

Massmann, A., Gentine, P., & Lin, C. (2019). When does vapor pressure deficit drive or reduce evapotranspiration? *Journal of Advances in Modeling Earth Systems*, *11*(10), 3305–3320. https://doi.org/10.1029/2019MS001790

McCabe, M. F., Ershadi, A., Jimenez, C., Miralles, D. G., Michel, D., & Wood, E. F. (2016). The GEWEX LandFlux project: evaluation of model evaporation using tower-based and globally gridded forcing data. *Geoscientific Model Development*, *9*(1), 283–305. https://doi.org/10.5194/gmd-9-283-2016

McGroddy, M. E., Daufresne, T., & Hedin, L. O. (2004). Scaling of C: N: P stoichiometry in forests worldwide: Implications of terrestrial redfield-type ratios. *Ecology*, *85*(9), 2390–2401. https://doi.org/10.1890/03-0351

Melack, J. M., Hess, L. L., Gastil, M., Forsberg, B. R., Hamilton, S. K., Lima, I. B., & Novo, E. M. (2004). Regionalization of methane emissions in the Amazon Basin with microwave remote sensing. *Global Change Biology*, *10*(5), 530–544. https://doi.org/10.1111/j.1365-2486.2004.00763.x

Meyer, V., Saatchi, S., Ferraz, A., Xu, L., Duque, A., García, M., & Chave, J. (2019). Forest degradation and biomass loss along the Chocó region of Colombia. *Carbon Balance and Management*, *14*(1), 2. https://doi.org/10.1186/s13021-019-0117-9

Meyer, V., Saatchi, S. S., Chave, J., Dalling, J. W., Bohlman, S., Fricker, G. A., et al. (2013). Detecting tropical forest biomass dynamics from repeated airborne lidar measurements. *Biogeosciences*, *10*(8), 1957–1992. https://doi.org/10.5194/bgd-10-1957-2013

Michel, A., & Seidling, W. (2016). *Forest condition in Europe: 2016 technical report of ICP forests: Report under the UNECE convention on long-range transboundary air pollution (CLRTAP)*. https://doi.org/10.13140/RG.2.2.35983.38566

Miralles, D. G., Jiménez, C., Jung, M., Michel, D., Ershadi, A., McCabe, M. F., et al. (2016). The WACMOS-ET project-Part 2: Evaluation of global terrestrial evaporation data sets. *Hydrology and Earth System Sciences*, *20*(2), 823–842. https://doi.org/10.5194/hessd-12-10651-2015

Mitchard, E. T., Saatchi, S. S., Baccini, A., Asner, G. P., Goetz, S. J., Harris, N. L., & Brown, S. (2013). Uncertainty in the spatial distribution of tropical forest biomass: A comparison of pan-tropical maps. *Carbon Balance and Management*, *8*(1), 10. https://doi.org/10.1186/1750-0680-8-10

Mitchard, E. T., Saatchi, S. S., White, L., Abernethy, K., Jeffery, K. J., Lewis, S. L., et al. (2012). Mapping tropical forest biomass with radar and spaceborne LiDAR in Lopé national park, Gabon: Overcoming problems of high biomass and persistent cloud. *Biogeosciences*, *9*(1), 179–191. https://doi.org/10.5194/bg-9-179-2012

Mohammed, G. H., Colombo, R., Middleton, E. M., Rascher, U., van der Tol, C., Nedbal, L., et al. (2019). Remote sensing of solar-induced chlorophyll fluorescence (SIF) in vegetation: 50 years of progress. *Remote Sensing of Environment*, *231*, 111177. https://doi.org/10.1016/j.rse.2019.04.030

Mokany, K., Raison, R. J., & Prokushkin, A. S. (2006). Critical analysis of root: Shoot ratios in terrestrial biomes. *Global Change Biology*, *12*(1), 84–96. https://doi.org/10.1111/j.1365-2486.2005.001043.x

Morel, A. C., Saatchi, S. S., Malhi, Y., Berry, N. J., Banin, L., & Burslem, R. (2011). *Estimating aboveground biomass in forest and oil palm plantation in Sabah, Malaysian Borneo using ALOS PALSAR data, Forest Ecology and Management*, 262, 1786–1798, https://doi.org/10.1016/j.foreco.2011.07.008

Moya, I., Camenen, L., Evain, S., Goulas, Y., Cerovic, Z. G., Latouche, G., et al. (2004). A new instrument for passive remote sensing: 1. Measurements of sunlight-induced chlorophyll fluorescence. *Remote Sensing of Environment*, *91*(2), 186–197. https://doi.org/10.1016/j.rse.2004.02.012

Myneni, R. B., Los, S. O., & Asrar, G. (1995). Potential gross primary productivity of terrestrial vegetation from 1982–1990. *Geophysical Research Letters*, *22*(19), 2617–2620. https://doi.org/10.1029/95GL02562

Myneni, R. B., Yang, W., Nemani, R. R., Huete, A. R., Dickinson, R. E., Knyazikhin, Y., et al. (2007). Large seasonal swings in leaf area of Amazon rainforests. *Proceedings of the National Academy of Sciences*, *104*(12), 4820–4823. https://doi.org/10.1073/pnas.0611338104

Neelin, J. D., Münnich, M., Su, H., Meyerson, J. E., & Holloway, C. E. (2006). Tropical drying trends in global warming models and observations. *Proceedings of the National Academy of Sciences*, *103*(16), 6110–6115. https://doi.org/10.1073/pnas.0601798103

Neigh, C. S., Nelson, R. F., Ranson, K. J., Margolis, H. A., Montesano, P. M., Sun, G., et al. (2013). Taking stock of circumboreal forest carbon with ground measurements, airborne and spaceborne LiDAR. *Remote Sensing of Environment*, *137*, 274–287. https://doi.org/10.1016/j.rse.2013.06.019

Nepstad, D., Lefebvre, P., Lopes da Silva, U., Tomasella, J., Schlesinger, P., Solórzano, L., et al. (2004). Amazon drought and its implications for forest flammability and tree growth: A basin-wide analysis. *Global Change Biology*, *10*(5), 704–717. https://doi.org/10.1111/j.1529-8817.2003.00772.x

Nobre, C. A., Sellers, P. J., & Shukla, J. (1991). Amazonian deforestation and regional climate change. *Journal of Climate*, *4*(10), 957–988. https://doi.org/10.1175/1520-0442(1991)004<0957:ADARCC>2.0.CO;2

O'Dell, C. W., Connor, B., Bösch, H., O'Brien, D., Frankenberg, C., & Castano, R. (2012). The ACOS CO_2 retrieval algorithm–Part 1: Description and validation against synthetic observations. *Atmospheric Measurement Techniques*, *5*(1), 99–121. https://doi.org/10.5194/amt-5-99-2012

Olivier, J. G. J., Berdowski, J. J. M., Peters, J. A. H. W., Bakker, J., Visschedijk, A. J. H., & Bloos, J. P. J. (2001). Applications of EDGAR. *Including a description of EDGAR*, *3*, 1970–1995. https://rivm.openrepository.com/handle/10029/9203

Ordway, E. M., & Asner, G. P. (2020). Carbon declines along tropical forest edges correspond to heterogeneous effects on canopy structure and function. *Proceedings of the National Academy of Sciences of the United States of America*, *117*(14), 7863–7870. https://doi.org/10.1073/pnas.1914420117

Palmer, P. I. (2018). The role of satellite observations in understanding the impact of El Niño on the carbon cycle: Current capabilities and future opportunities. *Philosophical Transactions of the Royal Society B: Biological Sciences*, *373*(1760). https://doi.org/10.1098/rstb.2017.0407

Palmer, P. I., Feng, L., Baker, D., Chevallier, F., Bösch, H., & Somkuti, P. (2019). Net carbon emissions from African biosphere dominate pan-tropical atmospheric CO2 signal. *Nature Communications*, *10*(1). https://doi.org/10.1038/s41467-019-11097-w

Pan, S., Pan, N., Tian, H., Friedlingstein, P., Stitch, S., Shi, H., et al. (2020). Evaluation of global terrestrial evapotranspiration using state-of-the-art approaches in remote sensing, machine learning and land surface modeling. *Hydrology and Earth System Sciences*, *24*(3), 1485–1509. https://doi.org/10.5194/hess-24-1485-2020

Pan, Y., Birdsey, R. A., Fang, J., & Houghton, R. (2011). A large and persistent carbon sink in the world's forests. *Science*, *333*(6045), 989–993. https://doi.org/10.1126/science.1201609

Parazoo, N. C., Bowman, K., Fisher, J. B., Frankenberg, C., Jones, D. B., Cescatti, A., et al. (2014). Terrestrial gross primary production inferred from satellite fluorescence and vegetation models. *Global Change Biology*, *20*(10), 3103–3121. https://doi.org/10.1111/gcb.12652

19449208, 2021, 1, Downloaded from https://agupubs.onlinelibrary.wiley.com/doi/10.1029/2020RG000711, Wiley Online Library on [10/11/2025]. See the Terms and Conditions (https://onlinelibrary.wiley.com/terms-and-conditions) on Wiley Online Library for rules of use; OA articles are governed by the applicable Creative Commons License

Parazoo, N. C., Frankenberg, C., Köhler, P., Joiner, J., Yoshida, Y., Magney, T., et al. (2019). Toward a harmonized long-term space-borne record of far-red solar-induced fluorescence. *Journal of Geophysical Research: Biogeosciences*, *124*(8), 2518–2539. https://doi.org/10.1029/2019JG005289

Parker, R. J., Boesch, H., McNorton, J., Comyn-Platt, E., Gloor, M., Wilson, C., et al. (2018). Evaluating year-to-year anomalies in tropical wetland methane emissions using satellite CH4 observations. *Remote Sensing of Environment*, *211*, 261–275. https://doi.org/10.1016/j.rse.2018.02.011

Pearson, T. R., Brown, S., Murray, L., & Sidman, G. (2017). Greenhouse gas emissions from tropical forest degradation: An underestimated source. *Carbon Balance and Management*, *12*(1). https://doi.org/10.1186/s13021-017-0072-2

Pechony, O., & Shindell, D. T. (2010). Driving forces of global wildfires over the past millennium and the forthcoming century. *Proceedings of the National Academy of Sciences*, *107*(45), 19167–19170. https://doi.org/10.1073/pnas.1003669107

Pechony, O., Shindell, D. T., & Faluvegi, G. (2013). Direct top-down estimates of biomass burning CO emissions using TES and MOPITT versus bottom-up GFED inventory. *Journal of Geophysical Research*, *118*(14), 8054–8066. https://doi.org/10.1002/jgrd.50624

Pelletier, J., Paquette, A., Mbindo, K., Zimba, N., Siampale, A., Chendauka, B., & Roberts, J. W. (2018). Carbon sink despite large deforestation in African tropical dry forests (miombo woodlands). *Environmental Research Letters*, *13*(9), 094017. https://doi.org/10.1088/1748-9326/aadc9a

Pfister, G., Hess, P. G., Emmons, L. K., Lamarque, J.-F., Wiedinmyer, C., Edwards, D. P., et al. (2005). Quantifying CO emissions from the 2004 Alaskan wildfires using MOPITT CO data. *Geophysical Research Letters*, *32*(11), 11809. https://doi.org/10.1029/2005GL022995

Phillips, O. L., Aragão, L. E., Lewis, S. L., Fisher, J. B., Lloyd, J., López-González, G., et al. (2009). Drought sensitivity of the Amazon rainforest. *Science*, *323*(5919), 1344–1347. https://doi.org/10.1126/science.1164033

Phillips, O. L., & Lewis, S. L. (2014). Evaluating the tropical forest carbon sink. *Global Change Biology*, *20*(7), 2039–2041. https://doi.org/10.1111/gcb.12423

Phillips, O. L., Van Der Heijden, G., Lewis, S. L., López-González, G., Aragão, L. E., Lloyd, J., et al. (2010). Drought–mortality relationships for tropical forests. *New Phytologist*, *187*(3), 631–646. https://doi.org/10.1111/j.1469-8137.2010.03359.x

Phillips, S. J., Anderson, R. P., & Schapire, R. E. (2006). Maximum entropy modeling of species geographic distributions. *Ecological Modelling*, *190*(3–4), 231–259. https://doi.org/10.1016/j.ecolmodel.2005.03.026

Pires, G. F., & Costa, M. H. (2013). Deforestation causes different subregional effects on the Amazon bioclimatic equilibrium. *Geophysical Research Letters*, *40*(14), 3618–3623. https://doi.org/10.1002/grl.50570

Polhamus, A., Fisher, J. B., & Tu, K. P. (2013). What controls the error structure in evapotranspiration models? *Agricultural and Forest Meteorology*, *169*, 12–24. https://doi.org/10.1016/j.agrformet.2012.10.002

Poorter, L., Bongers, F., Aide, T. M., Zambrano, A. M. A., Balvanera, P., Becknell, J. M., et al. (2016). Biomass resilience of Neotropical secondary forests. *Nature*, *530*(7589), 211–214. https://doi.org/10.1038/nature16512

Pöschl, U., Martin, S. T., Sinha, B., Chen, Q., Gunthe, S. S., Huffman, J. A. (2010). Rainforest Aerosols as Biogenic Nuclei of Clouds and Precipitation in the Amazon. *Science*, *29*(5998), 1513–1516.

Potter, C. S., Randerson, J. T., Field, C. B., Matson, P. A., Vitousek, P. M., Mooney, H. A., & Klooster, S. A. (1993). Terrestrial ecosystem production: A process model based on global satellite and surface data. *Global Biogeochemical Cycles*, *7*(4), 811–841. https://doi.org/10.1029/93GB02725

Powell, T. L., Galbraith, D. R., Christoffersen, B. O., Harper, A., Imbuzeiro, H. M. A., Rowland, L., et al. (2013). Confronting model predictions of carbon fluxes with measurements of Amazon forests subjected to experimental drought. *New Phytologist*, *200*(2), 350–365. https://doi.org/10.1111/nph.12390

Priestley, C. H. B., & Taylor, R. J. (1972). On the assessment of surface heat flux and evaporation using large-scale parameters. *Monthly Weather Review*, *100*(2), 81–92. https://doi.org/10.1175/1520-0493(1972)100<0081:OTAOSH>2.3.CO;2

Purdy, A. J., Fisher, J. B., Goulden, M. L., Colliander, A., Halverson, G., Tu, K., & Famiglietti, J. S. (2018). SMAP soil moisture improves global evapotranspiration. *Remote Sensing of Environment*, *219*, 1–14. https://doi.org/10.1016/j.rse.2018.09.023

Putz, F. E., & Redford, K. H. (2010). The importance of defining 'forest': Tropical forest degradation, deforestation, long-term phase shifts, and further transitions. *Biotropica*, *42*(1), 10–20. https://doi.org/10.1111/j.1744-7429.2009.00567.x

Quaife, T., Lewis, P. M. De K., Williams, M., Law, B. E., Disney, M., & Bowyer, P. (2008). Assimilating canopy reflectance data into an ecosystem model with an ensemble kalman filter. *Remote Sensing of Environment*, *111*, 1347–1364. https://doi.org/10.1016/j.rse.2007.05.020

Quegan, S., Le Toan, T., Chave, J., Dall, J., Exbrayat, J.-F., Minh, D. H. T., et al. (2019). The European Space Agency BIOMASS mission: Measuring forest above-ground biomass from space. *Remote Sensing of Environment*, *227*, 44–60. https://doi.org/10.1016/j.rse.2019.03.032

Rahul, P., Prasanna, K., Ghosh, P., Anilkumar, N., & Yoshimura, K. (2018). Stable isotopes in water vapor and rainwater over Indian sector of Southern Ocean and estimation of fraction of recycled moisture. *Scientific Reports*, *8*(1), 7552. https://doi.org/10.1038/s41598-018-25522-5

Rauniyar, S. P., Protat, A., & Kanamori, H. (2017). Uncertainties in TRMM-Era multisatellite-based tropical rainfall estimates over the Maritime Continent. *Earth and Space Science*, *4*(5), 275–302. https://doi.org/10.1002/2017EA000279

Raupach, M. R., Rayner, P. J., Barrett, D. J., Defries, R. S., Heimann, M., Ojima, D. S., et al. (2005). Model-data synthesis in terrestrial carbon observation: Methods, data requirements and data uncertainty specifications. *Global Change Biology*, *11*(3), 378–397. https://doi.org/10.1111/j.1365-2486.2005.00917.x

Reager, J. T., Gardner, A. S., Famiglietti, J. S., Wiese, D. N., Eicker, A., & Lo, M. H. (2016). A decade of sea level rise slowed by climate-driven hydrology. *Science*, *351*(6274), 699–703. https://doi.org/10.1126/science.aad8386

Restrepo-Coupe, N., da Rocha, H. R., Hutyra, L. R., da Araujo, A. C., Borma, L. S., Christoffersen, B., et al. (2013). What drives the seasonality of photosynthesis across the Amazon basin? A cross-site analysis of eddy flux tower measurements from the Brasil flux network. *Agricultural and Forest Meteorology*, *182*, 128–144. https://doi.org/10.1016/j.agrformet.2013.04.031

Richey, J. E., Melack, J. M., Aufdenkampe, A. K., Ballester, V. M., & Hess, L. L. (2002). Outgassing from Amazonian rivers and wetlands as a large tropical source of atmospheric CO_2. *Nature*, *416*(6881), 617–620. https://doi.org/10.1038/416617a

Rienecker, M. M., Suarez, M. J., Todling, R., Bacmeister, J., Takacs, L., Liu, H.-C., et al. (2008). *The GEOS-5 data assimilation system-documentation of versions 5.0.1 and 5.1.0, and 5.2.0*.

Risi, C., Bony, S., & Vimeux, F. (2008). Influence of convective processes on the isotopic composition (δ18O and δD) of precipitation and water vapor in the tropics: 2. Physical interpretation of the amount effect. *Journal of Geophysical Research*, *113*(D19). https://doi.org/10.1029/2008JD009943

Risi, C., Noone, D., Frankenberg, C., & Worden, J. (2013). Role of continental recycling in intraseasonal variations of continental moisture as deduced from model simulations and water vapor isotopic measurements. *Water Resources Research*, *49*(7), 4136–4156. https://doi.org/10.1002/wrcr.20312

19449208, 2021, 1, Downloaded from https://agupubs.onlinelibrary.wiley.com/doi/10.1029/2020RG000711, Wiley Online Library on [10/11/2025]. See the Terms and Conditions (https://onlinelibrary.wiley.com/terms-and-conditions) on Wiley Online Library for rules of use; OA articles are governed by the applicable Creative Commons License

Rodell, M., Famiglietti, J. S., Wiese, D. N., Reager, J. T., Beaudoing, H. K., Landerer, F. W., & Lo, M. H. (2018). Emerging trends in global freshwater availability. *Nature*, *557*(7707), 651–659. https://doi.org/10.1038/s41586-018-0123-1

Rodell, M., Famiglietti, J. S., Wiese, D. N., Reager, J. T., Beaudoing, H. K., Landerer, F. W., & Lo, M. H. (2019). Author Correction: Emerging trends in global freshwater availability. *Nature*, *565*(7739), E7. https://doi.org/10.1038/s41586-018-0831-6

Rosenfeld, D., Andreae, M. O., Asmi, A., Chin, M., de Leeuw, G., Donovan, D. P., et al. (2014). Global observations of aerosol-cloud-precipitation-climate interactions. *Reviews of Geophysics*, *52*(4), 750–808. https://doi.org/10.1002/2013RG000441

Rowland, L., da Costa, A. C. L., Galbraith, D. R., Oliveira, R. S., Binks, O. J., Oliveira, A. A. R., et al. (2015). Death from drought in tropical forests is triggered by hydraulics not carbon starvation. *Nature*, *528*(7580), 119. https://doi.org/10.1038/nature15539

Ryu, Y., Berry, J. A., & Baldocchi, D. D. (2019). What is global photosynthesis? History, uncertainties and opportunities, *Remote Sensiong of Environment*, *223*, 95–114. https://doi.org/10.1016/j.rse.2019.01.016

Saatchi, S., Asefi-Najafabady, S., Malhi, Y., Aragão, L. E., Anderson, L. O., Myneni, R. B., & Nemani, R. (2013). Persistent effects of a severe drought on Amazonian forest canopy. *Proceedings of the National Academy of Sciences*, *110*(2), 565–570. https://doi.org/10.1073/pnas.1204651110

Saatchi, S., Mascaro, J., Xu, L., Keller, M., Yang, Y., Duffy, P., et al. (2015). Seeing the forest beyond the trees. *Global Ecology and Biogeography*, *24*(5), 606–610. https://doi.org/10.1111/geb.12256

Saatchi, S., Ulander, L., Williams, M., Quegan, S., LeToan, T., Shugart, H., & Chave, J. (2012). Forest biomass and the science of inventory from space. *Nature Climate Change*, *2*(12), 826–827. https://doi.org/10.1038/nclimate1759

Saatchi, S. S., Harris, N. L., Brown, S., Lefsky, M., Mitchard, E. T., Salas, W., et al. (2011). Benchmark map of forest carbon stocks in tropical regions across three continents. *Proceedings of the National Academy of Sciences*, *108*(24), 9899–9904. https://doi.org/10.1073/pnas.1019576108

Sakumura, C., Bettadpur, S., & Bruinsma, S. (2014). Ensemble prediction and intercomparison analysis of GRACE time-variable gravity field models. *Geophysical Research Letters*, *41*(5), 1389–1397. https://doi.org/10.1002/2013GL058632

Salati, E., Dall'Olio, A., Matsui, E., & Gat, J. R. (1979). Recycling of water in the Amazon Basin: An isotopic study. *Water Resources Research*, *15*(5), 1250–1258. https://doi.org/10.1029/WR015i005p01250

Saleska, S. R., Miller, S. D., Matross, D. M., Goulden, M. L., Wofsy, S. C., Da Rocha, H. R., & Hutyra, L. (2003). Carbon in Amazon forests: Unexpected seasonal fluxes and disturbance-induced losses. *Science*, *302*(5650), 1554–1557. https://doi.org/10.1126/science.1091165

Saleska, S. R., Wu, J., Guan, K., Araujo, A. C., Huete, A., Nobre, A. D., & Restrepo-Coupe, N. (2016). Dry-season greening of Amazon forests. *Nature*, *531*(7594), E4–E9. https://doi.org/10.1038/nature16457

Santilli, M., Moutinho, P., Schwartzman, S., Nepstad, D., Curran, L., & Nobre, C. (2005). Tropical deforestation and the kyoto protocol. *Climatic Change*, *71*(3), 267–276. https://doi.org/10.1007/s10584-005-8074-6

Schimel, D., Stephens, B. B., & Fisher, J. B. (2015). Effect of increasing CO_2 on the terrestrial carbon cycle. *Proceedings of the National Academy of Sciences*, *112*(2), 436–441. https://doi.org/10.1073/pnas.1407302112

Schneider, A., Borsdorff, T., Aan de Brugh, J., Aemisegger, F., Feist, D. G., Kivi, R., et al. (2020). First data set of HDO columns from the tropospheric monitoring instrument (TROPOMI). *Atmospheric Measurement Techniques*, *13*(1), 85–100. https://doi.org/10.5194/amt-13-85-2020

Schneider, T., Lan, S., Stuart, A., & Teixeira, J. (2017). Earth system modeling 2.0: A Blueprint for models that learn from observations and targeted high-resolution simulations. *Geophysical Research Letters*, *44*(24), 12396–12417. https://doi.org/10.1002/2017GL076101

Seager, R., Hooks, A., Williams, A. P., Cook, B., Nakamura, J., & Henderson, N. (2015). Climatology, variability, and trends in the U.S. Vapor pressure deficit, an important fire-related meteorological quantity. *Journal of Applied Meteorology & Climatology*, *54*(6), 1121–1141. https://doi.org/10.1175/JAMC-D-14-0321.1

Sellers, P. J., Schimel, D. S., Moore, III, B., Liu, J., & Eldering, A. (2018). Observing carbon cycle–climate feedbacks from space. *Proceedings of the National Academy of Sciences of the United States of America*, *115*(31), 7860–7868. https://doi.org/10.1073/pnas.1716613115

Sena, E. T., Dias, M. A. F. S., Carvalho, L. M. V., & Dias, P. L. S. (2018). Reduced wet-season length detected by satellite retrievals of cloudiness over Brazilian Amazonia: A new methodology. *Journal of Climate*, *31*(24), 9941–9964. https://doi.org/10.1175/JCLI-D-17-0702.1

Shi, M., Liu, J., Worden, J. R., Bloom, A. A., Wong, S., & Fu, R. (2019). The 2005 Amazon drought legacy effect delayed the 2006 wet season onset. *Geophysical Research Letters*, *46*(15), 9082–9090. https://doi.org/10.1029/2019GL083776

Shindell, D. T., Faluvegi, G., Stevenson, D. S., Krol, M. C., Emmons, L. K., Lamarque, J. F., et al. (2006). Multimodel simulations of carbon monoxide: Comparison with observations and projected near-future changes. *Journal of Geophysical Research*, *111*(D19). https://doi.org/10.1029/2006JD007100

Sierra, C. A., Trumbore, S. E., Davidson, E. A., Vicca, S., & Janssens, I. (2015). Sensitivity of decomposition rates of soil organic matter with respect to simultaneous changes in temperature and moisture. *Journal of Advances in Modeling Earth Systems*, *7*(1), 335–356. https://doi.org/10.1002/2013MS000282

Skole, D., & Tucker, C. (1993). Tropical deforestation and habitat fragmentation in the Amazon: Satellite data from 1978 to 1988. *Science*, *260*(5116), 1905–1910. https://doi.org/10.1126/science.260.5116.1905

Smallman, T. L., Exbrayat, J. -F., Mencuccini, M., Bloom, A. A., & Williams, M. (2017). Assimilation of repeated woody biomass observations constrains decadal ecosystem carbon cycle uncertainty in aggrading forests. *Journal of Geophysical Research Biogeosciences*, *122*(3), 528–545. https://doi.org/10.1002/2016JG003520

Smallman, T. L., & Williams, M. (2019). Description and validation of an intermediate complexity model for ecosystem photosynthesis and evapotranspiration: ACM-GPP-ETv1. *Geoscientific Model Development*, *12*(6), 2227–2253. https://doi.org/10.5194/gmd-12-2227-2019

Smith, M. J., Palmer, P. I., Purves, D. W., Vanderwel, M. C., Lyutsarev, V., Calderhead, B., et al. (2014). Changing how earth system modeling is done to provide more useful information for decision making, science, and society. *Bulletin of the American Meteorological Society*, *95*(9), 1453–1464. https://doi.org/10.1175/BAMS-D-13-00080.1

Smith, W. K., Fox, A. M., MacBean, N., Moore, D. J. P., & Parazoo, N. C. (2019). Constraining estimates of terrestrial carbon uptake: New opportunities using long-term satellite observations and data assimilation. *New Phytologist*, *225*(1), 105–112. https://doi.org/10.1111/nph.16055

Song, X. P., Hansen, M. C., Stehman, S. V., Potapov, P. V., Tyukavina, A., Vermote, E. F., & Townshend, J. R. (2018). Global land change from 1982 to 2016. *Nature*, *560*(7720), 639–643. https://doi.org/10.1038/s41586-018-0411-9

Stephens, B. B., Gurney, K. R., Tans, P. P., Sweeney, C., Peters, W., Bruhwiler, L., et al. (2007). Weak northern and strong tropical land carbon uptake from vertical profiles of atmospheric CO_2. *Science*, *316*(5832), 1732–1735. https://doi.org/10.1126/science.1137004

Sun, Y., Frankenberg, C., Wood, J. D., Schimel, D. S., Jung, M., Guanter, L., et al. (2017). OCO-2 advances photosynthesis observation from space via solar-induced chlorophyll fluorescence. *Science*, *358*(6360), eaam5747. https://doi.org/10.1126/science.aam5747

19449208, 2021, 1, Downloaded from https://agupubs.onlinelibrary.wiley.com/doi/10.1029/2020RG000711, Wiley Online Library on [10/11/2025]. See the Terms and Conditions (https://onlinelibrary.wiley.com/terms-and-conditions) on Wiley Online Library for rules of use; OA articles are governed by the applicable Creative Commons License

Swann, A. L. S., & Koven, C. D. (2017). A direct estimate of the seasonal cycle of evapotranspiration over the Amazon basin. *Journal of Hydrometeorology*, *18*(8), 2173–2185. https://doi.org/10.1175/JHM-D-17-0004.1

Talsma, C., Good, S., Miralles, D., Fisher, J., Martens, B., Jimenez, C., & Purdy, A. (2018). Sensitivity of evapotranspiration components in remote sensing-based models. *Remote Sensing*, *10*(10), 1601. https://doi.org/10.3390/rs10101601

Tapley, B. D., Bettadpur, S., Ries, J. C., Thompson, P. F., & Watkins, M. M. (2004). GRACE measurements of mass variability in the Earth system. *Science*, *305*(5683), 503–505. https://doi.org/10.1126/science.1099192

Todd-Brown, K. E. O., Randerson, J. T., Post, W. M., Hoffman, F. M., Tarnocai, C., Schuur, E. A. G., & Allison, S. D. (2013). Causes of variation in soil carbon simulations from CMIP5 Earth system models and comparison with observations. *Biogeosciences*, *10*(3), 1717–1736. https://doi.org/10.5194/bg-10-1717-2013

van der, L.-L. I. T., van der Velde, I. R., Krol, M. C., Gatti, L. V., Domingues, L. G., Correia, C. S. C., et al. (2015). Response of the Amazon carbon balance to the 2010 drought derived with Carbon Tracker South America. *Global Biogeochemical Cycles*, *29*(7), 1092–1108. https://doi.org/10.1002/2014GB005082

van der Sleen, P., Groenendijk, P., Vlam, M., Anten, N. P. R., Boom, A., Bongers, F., et al. (2014). No growth stimulation of tropical trees by 150 years of CO2 fertilization but water-use efficiency increased. *Nature Geoscience*, *8*(1), 24–28. https://doi.org/10.1038/ngeo2313

van der Werf, G. R., Randerson, J. T., Giglio, L., Collatz, G. J., Mu, M., Kasibhatla, P. S., & van Leeuwen, T. T. (2010). Global fire emissions and the contribution of deforestation, savanna, forest, agricultural, and peat fires (1997–2009). *Atmospheric Chemistry and Physics*, *10*(23), 11707–11735. https://doi.org/10.5194/acp-10-11707-2010

van der Werf, G. R., Randerson, J. T., Giglio, L., van Leeuwen, T. T., Chen, Y., Rogers, B. M., et al. (2017). Global fire emissions estimates during 1997-2016. *Earth System Science Data*, *9*(2), 697–720. https://doi.org/10.5194/essd-9-697-2017

Vinukollu, R. K., Meynadier, R., Sheffield, J., & Wood, E. F. (2011). Multi-model, multi-sensor estimates of global evapotranspiration: Climatology, uncertainties and trends. *Hydrological Processes*, *25*(26), 3993–4010. https://doi.org/10.1002/hyp.8393

Wang, G., & Schimel, D. (2003). Climate change, climate modes, and climate impacts. *Annual Review of Environment and Resources*, *28*(1), 1–28. https://doi.org/10.1146/annurev.energy.28.050302.105444

Wang, W., Ciais, P., Nemani, R. R., Canadell, J. G., Piao, S., Sitch, S., et al. (2013). Variations in atmospheric CO2 growth rates coupled with tropical temperature. *Proceedings of the National Academy of Sciences*, *110*(32), 13061–13066. https://doi.org/10.1073/pnas.1219683110

Wei, Z., Yoshimura, K., Wang, L., Miralles, D. G., Jasechko, S., & Lee, X. (2017). Revisiting the contribution of transpiration to global terrestrial evapotranspiration. *Geophysical Research Letters*, *44*(6), 2792–2801. https://doi.org/10.1002/2016GL072235

Worden, J., Bowman, K., Noone, D., Beer, R., Clough, S., Eldering, A., et al. (2006). Tropospheric Emission Spectrometer observations of the tropospheric HDO/H2O ratio: Estimation approach and characterization. *Journal of Geophysical Research: Atmosphere*, *111*(D16). https://doi.org/10.1029/2005JD006606

Worden, J., Noone, D., Bowman, K., Beer, R., Eldering, A., Fisher, B., et al. (2007). Importance of rain evaporation and continental convection in the tropical water cycle. *Nature*, *445*(7127), 528–530. https://doi.org/10.1038/nature05508

Worden, J. R., Bloom, A. A., Pandey, S., Jiang, Z., Worden, H. M., Walker, T. W., & Röckmann, T. (2017). Reduced biomass burning emissions reconcile conflicting estimates of the post-2006 atmospheric methane budget. *Nature Communications*, *8*(1), 2227. https://doi.org/10.1038/s41467-017-02246-0

Worden, J. R., Kulawik, S. S., Fu, D., Payne, V., Lipton, A. E., Polonsky, I., et al. (2019). Characterization and evaluation of AIRS-based estimates of the deuterium content of water vapor. *Atmospheric Measurement Techniques*, *12*(4), 2331–2339. https://doi.org/10.5194/amt-12-2331-2019

Wright, J. S., Fu, R., Worden, J. R., Chakraborty, S., Clinton, N. E., Risi, C., et al. (2017). Rainforest-initiated wet season onset over the southern Amazon. *Proceedings of the National Academy of Sciences*, *114*(32), 8481–8486. https://doi.org/10.1073/pnas.1621516114

Wu, J., Albert, L. P., Lopes, A. P., Restrepo-Coupe, N., Hayek, M., Wiedemann, K. T., et al. (2016). Leaf development and demography explain photosynthetic seasonality in Amazon evergreen forests. *Science*, *351*(6276), 972–976. https://doi.org/10.1126/science.aad5068

Xu, L., Saatchi, S. S., Shapiro, A., Meyer, V., Ferraz, A., Yang, Y., et al. (2017). Spatial distribution of carbon stored in forests of the democratic republic of Congo. *Scientific Reports*, *7*(1), 15030. https://doi.org/10.1038/s41598-017-15050-z

Xu, L., Saatchi, S. S., Yang, Y., Myneni, R. B., Frankenberg, C., Chowdhury, D., & Bi, J. (2015). Satellite observation of tropical forest seasonality: Spatial patterns of carbon exchange in Amazonia. *Environmental Research Letters*, *10*(8), 084005. https://doi.org/10.1088/1748-9326/10/8/084005

Xu, L., Saatchi, S. S., Yang, Y., Yu, Y., & White, L. (2016). Performance of non-parametric algorithms for spatial mapping of tropical forest structure. *Carbon Balance and Management*, *11*(1), 18. https://doi.org/10.1186/s13021-016-0062-9

Yan, Z., Bond-Lamberty, B., Todd-Brown, K. E., Bailey, V. L., Li, S., Liu, C., & Liu, C. (2018). A moisture function of soil heterotrophic respiration that incorporates microscale processes. *Nature Communications*, *9*(1), 1–10. https://doi.org/10.1038/s41467-018-04971-6

Yang, X., Song, Z., Liu, H., Van Zwieten, L., Song, A., Li, Z., et al. (2018). Phytolith accumulation in broadleaf and conifer forests of northern China: Implications for phytolith carbon sequestration. *Geoderma*, *312*, 36–44. https://doi.org/10.1016/j.geoderma.2017.10.005

Yang, X., Tang, J., Mustard, J. F., Lee, J., & Rossini, M. (2015). Solar-induced chlorophyll fluorescence correlates with canopy photosynthesis on diurnal and seasonal scales in a temperate deciduous forest. *Geophysical Research Letters*, *42*(8), 2977–2987. https://doi.org/10.1002/2015GL063201

Yang, Y., Saatchi, S. S., Xu, L., Yu, Y., Choi, S., Phillips, N., et al. (2018). Post-drought decline of the Amazon carbon sink. *Nature Communications*, *9*(1), 1–9https://doi.org/10.1038/s41467-018-05668-6

Yin, L., Fu, R., Shevliakova, E., & Dickinson, R. E. (2013). How well can CMIP5 simulate precipitation and its controlling processes over tropical South America? *Climate Dynamics*, *41*(11–12), 3127–3143. https://doi.org/10.1007/s00382-012-1582-y

Yin, Y., Bloom, A. A., Worden, J., Saatchi, S., Yang, Y., Williams, M., et al. (2020). Fire decline in dry tropical ecosystems enhances decadal land carbon sink. *Nature Communications*, *11*(1). https://doi.org/10.1038/s41467-020-15852-2

Yin, Y., Chevallier, F., Ciais, P., Broquet, G., Fortems-Cheiney, A., Pison, I., & Saunois, M. (2015). Decadal trends in global CO emissions as seen by MOPITT. *Atmospheric Chemistry and Physics Discussions*, *15*(23). https://doi.org/10.5194/acp-15-13433-2015

Yin, Y., Ciais, P., Chevallier, F., Van der Werf, G. R., Fanin, T., Broquet, G., et al. (2016). Variability of fire carbon emissions in equatorial Asia and its nonlinear sensitivity to El Niño. *Geophysical Research Letters*, *43*(19), 10472–10479. https://doi.org/10.1002/2016GL070971

Yu, Y., & Saatchi, S. (2016). Sensitivity of L-band SAR backscatter to aboveground biomass of global forests. *Remote Sensing*, *8*(6), 522. https://doi.org/10.3390/rs8060522

Zemp, D. C., Schleussner, C. F., Barbosa, H., Hirota, M., Montade, V., Sampaio, G., et al. (2017). Self-amplified Amazon forest loss due to vegetation-atmosphere feedbacks. *Nature Communications*, *8*(1). https://doi.org/10.1038/NCOMMS14681

19449208, 2021, 1, Downloaded from https://agupubs.onlinelibrary.wiley.com/doi/10.1029/2020RG000711, Wiley Online Library on [10/11/2025]. See the Terms and Conditions (https://onlinelibrary.wiley.com/terms-and-conditions) on Wiley Online Library for rules of use; OA articles are governed by the applicable Creative Commons License

Zhang, Q., Xiao, X., Braswell, B., Linder, E., Baret, F., & Moore, B., III (2005). Estimating light absorption by chlorophyll, leaf and canopy in a deciduous broadleaf forest using MODIS data and a radiative transfer model. *Remote Sensing of Environment*, *99*(3), 357–371. https://doi.org/10.1016/j.rse.2005.09.009

Zhang, Y., Joiner, J., Alemohammad, S. H., Zhou, S., & Gentine, P. (2018). A global spatially contiguous solar-induced fluorescence (CSIF) dataset using neural networks. *Biogeosciences*, *15*(19), 5779–5800. https://doi.org/10.5194/bg-15-5779-2018

Zhang, Y., Xiao, X., Wu, X., Zhou, S., Zhang, G., Qin, Y., & Dong, J. (2017). *A global moderate resolution dataset of gross primary production of vegetation for 2000–2016*. Scientific Data, 4(1), 1–13. https://doi.org/10.1038/sdata.2017.165

Zhao, M., Heinsch, F. A., Nemani, R. R., & Running, S. W. (2005). Improvements of the MODIS terrestrial gross and net primary production global data set. *Remote Sensing of Environment*, *95*(2), 164–176. https://doi.org/10.1016/j.rse.2004.12.011

Zhou, X., Peng, C., Dang, Q. L., Chen, J., & Parton, S. (2005). Predicting forest growth and yield in northeastern Ontario using the process-based model of TRIPLEX1. 0. *Canadian Journal of Forest Research*, *35*(9), 2268–2280. https://doi.org/10.1139/x05-149

Zhou, L., Tian, Y., Myneni, R. B., Ciais, P., Saatchi, S., Liu, Y. Y., et al. (2014). Widespread decline of Congo rainforest greenness in the past decade. *Nature*, *509*(7498), 86–90. https://doi.org/10.1038/nature13265

Zubkova, M., Boschetti, L., Abatzoglou, J. T., & Giglio, L. (2019). Changes in fire activity in Africa from 2002 to 2016 and their potential drivers. *Geophysical Research Letters*, *46*(13), 7643–7653. https://doi.org/10.1029/2019GL083469

19449208, 2021, 1, Downloaded from https://agupubs.onlinelibrary.wiley.com/doi/10.1029/2020RG000711, Wiley Online Library on [10/11/2025]. See the Terms and Conditions (https://onlinelibrary.wiley.com/terms-and-conditions) on Wiley Online Library for rules of use; OA articles are governed by the applicable Creative Commons License